How studying the interaction of Sir4 with a subset of Nups uncovered a new chromatin bound complex

by

Diego Lomnitzer Lapetina

A thesis submitted in partial fulfillment of the requirements for the degree of

Doctor of Philosophy

Department of Cell Biology
University of Alberta

Abstract

The nucleus is the defining feature of eukaryotic cells and its major function is to house the cell's genome and segregate it from the surrounding cytoplasm. The membranes encapsulating the nucleus constitute the nuclear envelope (NE). The interactions between the NE and chromatin facilitate the spatial organization of chromosomes. Moreover, chromatin positioning inside the nucleus can modulate transcriptional status. The peripheral localization of chromatin is usually associated with gene repression (heterochromatin), and the central regions of the nucleus are often populated by transcriptionally active genes (euchromatin). Yeast have proven to be an important model system for studying the interactions of heterochromatin with the NE membrane, specifically the interaction of telomeres with the inner nuclear membrane proteins. In this study, we expanded on previous observations that nuclear pore complexes (NPCs) are required for telomere tethering and gene silencing. We showed that four proteins involved in chromatin regulation (Nup170, Siz2, Sir4, and Esc1) physically and functionally interact with one another. Furthermore, these proteins also physically interact with nucleoporins present at the NPC core scaffold. Importantly, the structure formed by the NPC core scaffold, Sir4, Esc1 and Siz2 lacks Nups present in other NPC sub-complexes. We termed this structure as the Sir4 associated Nups complex (Snups).

The detection of proteins involved in telomere positioning suggested that Snup complexes function in the tethering of telomeres to the NE. In our analysis of this complex, we observed that SUMO ligase, Siz2, was bound to proteins from the Snup complex. This observation was intriguing as SUMOylation, and specifically Siz2, has been implicated in tethering telomeres to the NE. Given the importance of Siz2 in telomere tethering, we decided to better characterize its cellular distribution and protein stability. Previous observations suggested that Siz2 is present through out the nucleoplasm. However, we observed that Siz2 was also detectable at the NE, consistent with the physical association we observed between Siz2 and proteins from the Snup complex. We also observed a robust recruitment of Siz2 to the NE during mitosis, coinciding with its phosphorylation. We identified the sites of phosphorylation in Siz2 and constructed point mutants that block Siz2 phosphorylation. Using these mutants, we show that the recruitment of Siz2 to the NE during mitosis is required for the proper association of telomeres with the NE.

Dedication

To my golden hearted wife, Juliana Capitanio…

…to Dimas and Neiva for their unconditional support…

and to the few and brave friends that helped me during this long journey.

Acknowledgements:

I am truly honoured to have worked under the supervision of Dr. Richard W. Wozniak. The journey through the maze we call science can be a daunting task; but I am certain that under the guidance and wisdom of Dr. Wozniak my path was as easy as it could be. I am certain that the time spent in his laboratory made me not just a better scientist, but it also helped to shape me as a human being. I learnt through my years in the Wozniak's laboratory that constant attention to details and an inquisitive mind are usually the key elements behind an impressive list of publication. I am, and I always will be, grateful for his help to improve myself.

I was fortunate to be surrounded by many bright scientists. This impressive group of researcher instructed me during the phase of experimental design, and helped me interpreting my (often not so obvious) results. I have great admiration for the scientific knowledge of Dr. Tadashi Makio and Dr. Christopher Ptak, two people that provided their valuable time to make me a better scientist. Also, I am also grateful for the help provided by past lab members Dr. Christopher Neufeld, Dr. David Van de Vosse, Dr. Jana Mitchel, Dr. Lucas Cairo, Dr. Neil Adams, and Dr. Nogi Park. Finally, I am certain that under the guidance of Dr. Wozniak's the new graduate students Brett Roughhead, Natasha Saik, and Ulyss Roesner will shine and filled our scientific community with amazing discoveries.

Every evening, once I was over with my work in the lab, I drove to the place that calmed my mind and sharpened my body. My journey in Brazilian Jiu Jitsu was parallel to the work developed in the laboratory. I always had a good training partner to train, which helped me to let go the bad days that we all have in science. I am truly grateful to mine BJJ family.

I am sure that my friends and family were great part of my success. I am especially thankful to MSc. Tucaaue Alvares, a true friend that always shared his knowledge about life. We definitely had a great time together and I'm appreciate the fact that you were always there when I needed. I have also been blessed with two amazing role models named Neiva and Dimas Capitanio. Their unconditional support and love eased the pain of been away from Brazil.

Usually we leave the best for the last and here it is no exception. I could not have finish this journey without the support and encouragement of my gifted wife Juliana Capitanio. We shared the privilege to work together in the laboratory, and during this time she was always there to help me. Juliana is probably the smartest person that I have meet during my (not so) brief journey in earth. Juliana's impeccable work ethic and curious mind inspired me to be a better scientist and person. I will always be grateful for your love and support.

Table of Contents

List of tables:

List of figures:

List of symbols or abbreviations:

µ	micro
µm	microns/micrometre
µg	microgram
µL	microliter
℃	degrees Celsius
bp	base pairs
CCD	charge-coupled device
ChIP	chromatin immunoprecipitation
d	days
DNA	deoxyribonucleic acid
ECL	enhanced chemiluminescence
EM	electron microscopy
FG	phenylalanine glycine
Fig.	figure
G	gram
G1	gap 1 phase
G2	gap 2 phase
GAP	GTPase activating protein
GDP	guanosine-5’-diphosphate
GEF	guanine nucleotide exchange factor
eGFP	enhanced green fluorescent protein
GST	glutathione-S-transferase

GTP	guanosine-5’-triphosphate
GTPase	guanosine-5’-triphosphate hydrolase
h	hours
HA	hemagglutinin
PrA	protein A
HML	hidden *MAT* left
HMR	hidden *MAT* right
IgG	immunoglobulin G
INM	inner nuclear membrane
IRC	inner ring complex
IRM	inner ring membrane
kDa	kilodalton
kap	karyopherin
LacI	lactose repressor
LacO	lactose operator
m	milli
M	molarity/mega
MAT	mating-type locus
mCherry	monomeric cherry
MDa	megadalton
mg	milligram
mg	miligrams
min	minutes
mL	millilitre
mRNA	messenger ribonucleic acid

n	nano
NAD	nicotimamide adenine dinucleotide
NE	nuclear envelope
NES	nuclear export signal
NLS	nuclear localization signal
NPC	nuclear pore complex
NTF	nuclear transport factor
Nup	nucleoporins
OD	optical density
ONM	outer nuclear membrane
ORC	outer ring complex
ORF	open read frame
PCR	polymerase chain reaction
PMT	post translational modification
Pom	pore membrane protein
rDNA	ribosomal DNA
RFP-T	red fluorescent protein-t
RNA	ribonucleic acid
RNP	ribonucleoprotein
SAC	spindle assembly checkpoint
SBM	sumo binding motif
SC	synthetic complete media
SDS-PAGE	sodium dodecyl sulfate polyacrylamide gel eletrophoresis
sec	seconds
SIM	sumo interacting motif

SPB	spindle pole body
TCA	trichloroacetic acid
Tel	telomere
TPE	telomere positioning effect
WT	wild type
YPD	yeast extract peptone dextrose media

Epigraph

“Some people never go crazy. What truly horrible lives they must lead.”

Charles Bukowski

1. Introduction

1.1 Preface

During the course of cellular evolution, the incremental increase in the cellular volume observed in eukaryotes created a necessity for specialized compartmentalization (Fichtman et al., 2010). This compartmentalization was achieved by enveloping specific metabolic pathways by membranes and the corresponding development of transport mechanisms that allowed communication between compartments. The nucleus is one of such compartments. The nucleus is responsible for housing the nuclear genome and all DNA metabolic processes. The membrane system defining this organelle is referred to as the nuclear envelope (NE) (Hetzer et al., 2005). The NE is formed by two membranes separated by a lumen, and several transmembrane proteins. The NE membrane exposed to the cytoplasmic face is contiguous to the endoplasmic reticulum and it is called the outer nuclear membrane (ONM), while the membrane facing the nucleoplasm is called the inner nuclear membrane (INM).

The NE facilitates genome organization by providing anchorage sites for chromosomes (Czapiewski et al., 2016). However, the presence of the NE restricts the communication between the nuclear interior (nucleoplasm) and exterior (cytoplasm). Concomitant with the segregation of the genetic material, eukaryotic cells developed large proteinaceous structures termed nuclear pore complexes (NPCs) (Wente, 2000). Since

the discovery of the NPC, several research groups have aimed to expand the understanding of this structure. Advancements in the fields of microscopy and biochemistry have allowed for more refined modeling of the NPC (Alber et al., 2007a; Alber et al., 2007b; Lin et al., 2016; Rout et al., 2000; Stuwe et al., 2015). To date, studies depict NPC as an eight-fold symmetrical channel formed by multiple copies of ~30 different proteins named nucleoporins (Nups). The channels created by the NPCs function as gatekeepers for all nuclear-cytoplasmic transport. While ions and small metabolites can diffuse freely through the central channel, the transport of large macromolecules requires soluble transport factors known as karyopherins (Kaps) (Aitchison and Rout, 2012; Wente, 2000).

In addition to the nucleocytoplasmic transport mediated by NPCs, individual Nups have been implicated in biological processes ranging from chromosome segregation to transcriptional regulation (Palancade and Doye, 2008; Ptak et al., 2014). The large amount of proteins composing the NPC, combined to present experimental limitation have imposed major challenges in elucidating the molecular links between NPC and chromatin. Nevertheless, identifying such biological processes is paramount to understand how NPCs influence genome organization and gene transcription.

1.2 Nuclear Envelope

The nucleus is a defining feature of eukaryotic cells. The NE defines its perimeter and establishes a barrier responsible for the separation of the cytoplasm and the nucleoplasm (Hetzer, 2010). The NE is formed by two closely apposed lipid bilayers; the INM and ONM. The ONM is contiguous with the peripheral endoplasmic reticulum and both share protein complexes, including the attached ribosomes. However, several proteins are found exclusively at the ONM (Kvam and Goldfarb, 2006; Lombardi and Lammerding, 2011). While the ONM faces the cytoplasm, the INM is in direct contact with the nucleoplasm, and contains proteins involved in intranuclear signaling, chromosome segregation, and genome organization. (Czapiewski et al., 2016; Hetzer, 2010; Taddei et al., 2010a; Zimmer and Fabre, 2011). Higher eukaryotic cells, such as mammalian, also contain a meshwork of filaments termed lamina (Dechat et al., 2008). The lamina is connected to the INM through its interaction with proteins present in the INM and NPCs. The nuclear lamina is required for proper nuclear morphology and provides docking sites for chromatin. Despite the lack of detectable lamina in lower eukaryotes, such as budding yeast, several proteins convey lamina-like functions (Andrulis et al., 2002; Taddei et al., 2004a).

Cargo transport across the NE occurs through pores formed through the fusion of the INM and ONM. The pore membrane requires a specific subset of proteins to stabilize the sharp membrane curvatures.

These integral proteins interact with and consequently anchor the nuclear pore complexes to the NE. The NPCs are large macromolecular assemblies responsible for regulating nucleocytoplasmic transport.

1.3 Nuclear Pore Complex

In order to overcome the physical barrier created by the NE, eukaryotic cells evolved pores to allow the exchange of molecules between the cytoplasm and nucleoplasm (Doye and Hurt, 1997). The first description of nuclear pores was reported in 1950. Callan and Tomlin used an electron microscope to study the nucleus of the amphibian oocyte and described electron-dense structures that extended across the ONM and INM and were distributed in an irregular pattern along the nuclear surface (Callan and Tomlin, 1950). In 1959, Watson proposed the term “pore complex” to describe the electron-dense structures that extended across the NE (Kabachinski and Schwartz, 2015; Watson, 1959). In the years following the first description of nuclear pores, a massive amount of work focused on defining the structure of the NPC. The improvement in the resolution of the electron microscope made it possible to better visualize NPCs (Rout et al., 2000; Stoffler et al., 1999). Observations that emerged from electron micrographs revealed the NPC as an octagonal structure, composed of repetitive units symmetrically arranged around the central transport channel. The NPC plays an essential role in regulating nuclear-

cytoplasmic transport and it is well-conserved throughout divergent species, such as *Saccharomyces cerevisiae* and humans. Studies have shown that the overall structure, morphology, composition, and function are of pore complexes remarkably similar across eukaryotes (Kabachinski and Schwartz, 2015). However, technological advances allowed a more empirical approach to studying these structures, thus revealing subtle differences in the NPC size and morphology (D'Angelo and Hetzer, 2008; Fernandez-Martinez and Rout, 2009). While the vertebrate NPC is ~130 nm in diameter and ~80 nm in height, the yeast counterpart is slightly smaller ~100 nm in diameter by ~40 nm in height. Moreover, reflecting observed differences in NPC composition, proteomic analyses estimated that vertebrate NPC molecular weight might range from ~60 to ~125 MDa, and the yeast NPCs molecular weight might range from ~50 to ~66 MDa.

Recently, by combining multitude experimental approaches with the power of computational analysis, researchers created a spatial map predicting the localization of each nucleoporin inside the NPC (Figure 1.1) (Knockenhauer and Schwartz, 2016; Lin et al., 2016; Stuwe et al., 2015). To date, the preferred model depicts the NPC as a doughnut shape structure formed by groups of proteins symmetrically arranged into spokes and rings (Fig1-1). The fundamental symmetry unit at the NPC core is known as the "spoke" subunit (Alber et al., 2007a; Alber et al., 2007b). Grouping the proteins into spokes yields a structure with nearly identical nucleoplasmic and cytoplasmic halves. Each NPC comprises eight spokes

arranged perpendicular to the central channel and conjoined at the NPC equator. The core of the NPC contains the inner/outer rings, and is called the core scaffold. The core scaffold is a cylindrical structure encircling the NPC central channel, and is attached to the NE through its interaction with pore membrane proteins (Poms). Interacting with the core scaffold are the linker nucleoporins. These proteins are responsible for linking the NPC core to the FG-Nups. The FG-Nups contain large unstructured regions formed by the repetition of Phenylalanine-Glycine aminoacids. These unstructured regions create a semi-permeable barrier that prohibits the unspecific traffic of molecules greater than ~10nm (Kabachinski and Schwartz, 2015; Lin et al., 2016; Rout et al., 2000; Strambio-de-Castillia and Rout, 2002; Stuwe et al., 2015). Finally, the cytoplasmic and nucleoplasmic faces of the NPC contain filamentous proteins that are attached to the core scaffold. On the cytoplasmic side, emanating from the NPC, the cytoplasmic Nups are responsible for several biological processes, such as initiating or terminating cytonuclear transport (Strambio-De-Castillia et al., 2010). On the opposite face of the NPC, facing the nucleoplasm, eight filaments extend from the core scaffold and distally conjoin to form a structure named the nuclear basket (Figure 1.1). Studies have suggested that in addition to their function in transport, Nups forming the nuclear basket are involved in a diverse range of biological processes (Lewis et al., 2007; Palancade and Doye, 2008).

A

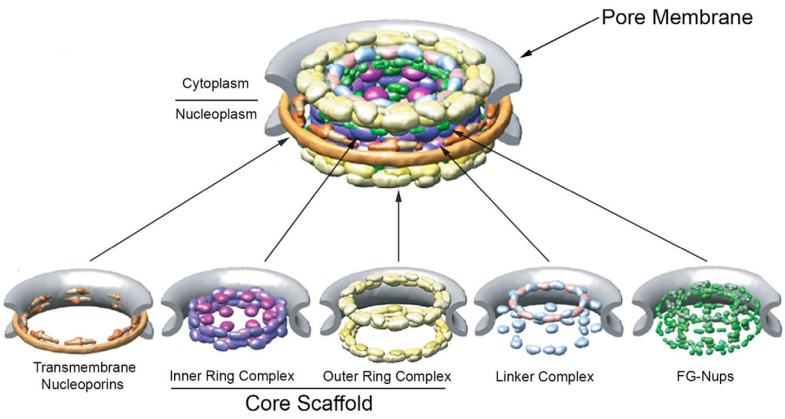

B

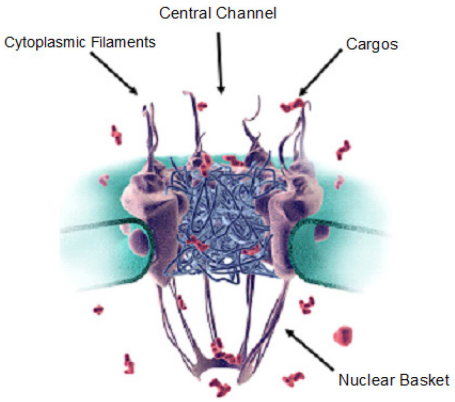

Figure 1-1. The nuclear pore complex structure and sub-complexes

A) A graphical representation displaying the NPC and its major sub-complexes embedded into the NE. The nucleoporins are grouped accordingly to their predicted localization within the NPC. The NPC is embedded at the NE (gray), and anchored to the pore membrane through the lumen ring (dark orange) and transmembrane nucleoporins (light orange). The core scaffold is composed of the inner ring complex (purple) and outer ring complex (yellow). The linker Nups (cyan/pink) attach to the core scaffold and anchor the FG-Nups (green) *Adapted from Alber et al. 2007b*. B) A cross section through the NPC representing the central channel, cytoplasmic filaments, nuclear basket, and cargos. *Adapted from (Patel et al., 2007).*

The nucleoporins populating the nucleoplasmic face, such as the proteins comprising the nuclear basket and features of the NPC core, can mediate interactions with chromatin and, in higher eukaryotes, the nuclear lamina (Cairo et al., 2013b; Palancade and Doye, 2008; Ptak et al., 2014; Van de Vosse et al., 2013; Van de Vosse et al., 2011). In addition, due to their localization, these structures provide docking sites for multiple NPC-associated proteins involved in regulating a diverse range of nuclear processes, such as post-translational modifications, genome stability, chromosome segregation, and transcriptional regulation.

1.4 Nucleoporins:

Using the yeast model researchers identified several of the NPC components. The combination of yeast genetics and biochemical techniques led to the identification of approximately 30 different proteins, referred to as nucleoporins or Nups (Doye and Hurt, 1997; Rout et al., 2000). Further studies revealed that nucleoporins are largely conserved from yeast to human (Table 1.1).

The nucleoporins are divided into different complexes based on their structure and function (Aitchison and Rout, 2012). The first group contains the integral protein of the pore membrane, also termed Poms (Onischenko et al., 2009). The second group includes Nups from the NPC structural core scaffold (Beck and Hurt, 2017; Lin et al., 2016). The core scaffold is sub-divided into outer and inner nuclear rings. The inner ring

contains Nup170, Nup157, Nup188, and Nup192, while the outer ring contains Nup84, Nup85, Nup120, Nup133, Nup145p, Seh1, and Sec13 (Aitchison et al., 1995; Kelley et al., 2015; Lin et al., 2016; Stuwe et al., 2015). The third group contains the linker proteins Nup82 and Nic96 (Alber et al., 2007a; Alber et al., 2007b). The fourth group contains several nucleoporins containing large segments of unstructured repeats of phenylalanine-glycine; this group is also identified as FG-Nups (Strawn et al., 2004). The fifth group contains nucleoporins that are asymmetrically distributed in the NPC. The cytoplasm face contains the cytoplasmic filaments, while the nucleoplasm contains the nuclear basket (Alber et al., 2007a; Alber et al., 2007b; Kabachinski and Schwartz, 2015; Lin et al., 2016).

The assembly of a complex structure, such as the NPC, with its surprisingly small variety of proteins and the observed symmetry is only possible because a single NPC contains multiple copies of each nucleoporin (Mi et al., 2015; Rout et al., 2000; Stuwe et al., 2015). Several studies have suggested that nucleoporins exist mainly in 16 copies per NPC, with some exceptions that contain either eight or 32 copies. Thus, a fully assembled NPC contains in average ~500 nucleoporins. The sheer size of this large proteinaceous assembly, combined with its flexible and dynamic nature, hinders the ability to resolve such structures by X-ray crystallography. To overcome these difficulties, researchers have used the "divide-and-conquer" approach, thus allowing the determination of

Table 1-1. Nucleoporins

Mammalian	*S. cerevisiae*	Nup category
Nup 358 (RabBP2)	-	FG
Nup214	Nup159	FG
Nup153	Nup1/Nup2/Nup60	FG
Nup98	Nup145-N/Nup100/Nup116	FG
Nup62	Nsp1	FG
Nup58/Nup4	Nup49	FG
Nup54	Nup57	FG
Nup53 (Nup35)	Nup53/Nup59	FG
Nup50	Nup2	FG
NLP1 (hCG1)	Nup42	FG
Nup205	Nup192	Non-FG
Nup188	Nup188	Non-FG
Nup160	Nup120	Non-FG
Nup155	Nup157/Nup170	Non-FG
Nup133	Nup133	Non-FG
Nup107	Nup84	Non-FG
Nup96	Nup145-C	Non-FG
Nup93	Nic96	Non-FG
Nup88	Nup82	Non-FG
Nup85 (Nup75)	Nup85	Non-FG
Nup43	-	Non-FG
Nup37	-	Non-FG
ALADIN	-	Non-FG
Gle1	Gle1	Non-FG
RAE1 (Gle2)	Gle 2	Non-FG
Sec13	Sec13	Non-FG
Seh1	Seh1	Non-FG
Tpr	Mlp1/Mlp2	Non-FG
Pom121	-	Pom
gp210	-	Pom
NDC1	Ndc1	Pom
-	Pom33	Pom
-	Pom34	Pom
-	Pom152	Pom

**Adapted from D'Angelo and Hetzer, et al., 2008*.

individual domains, proteins, and even sub-complexes at an atomic resolution (Kelley et al., 2015; Lin et al., 2016; Stuwe et al., 2015). These structural studies have revealed that nucleoporins have a relatively simple structure, and are formed by a few types of protein-folding domains, a transmembrane domain, a β-propeller, and α-solenoid.

1.4.1 Pore membrane proteins

The integral membrane proteins, Poms, in the membrane ring play a major role in recruiting and anchoring soluble NPC components to the NE (Aitchison and Rout, 2012; Kabachinski and Schwartz, 2015; Onischenko et al., 2009). In yeast, the membrane ring is composed of three different proteins, Pom34, Pom152, and Ndc1. In addition to the previously described Poms, a recent study identified a potential fourth transmembrane protein, Pom33 (Chadrin et al., 2010). However, despite the role of Pom33 in the correct distribution of the NPC around the NE and its interaction with several NPC components, its transient association with the NPC has raised questions about its classification as a member of the Pom protein family .

All Poms share a transmembrane helix, which mediates NPC attachment to the NE. In addition to the presence of α-helices, these proteins have large regions spanning the lumen and the pore side of the membrane. In budding yeast, the Ndc1 and Pom34 position are slightly skewed towards the pore portion of the membrane, while the Pom152 is

predominantly buried in the nuclear envelope lumen (Onischenko et al., 2009; Wozniak et al., 1994). The *POM34* and *POM152* are not essential, suggesting these genes share some degree of functional redundancy among themselves. This theory is supported by the similar genetic interactions shared by these genes. *NDC1* is the only essential and evolutionary conserved Pom in yeast (Onischenko et al., 2009). Several observations have suggested that *NDC1* plays an essential role in NPC assembly and maintenance. A study probing for the functions of Poms in yeast isolated Ndc1 in a complex with Pom152 and Pom34, and the Nup53 and Nup59. Because Nup53 and Nup59 interact with the core scaffold nucleoporins Nup170 and Nup157 and the transmembrane nucleoporin Ndc1, it has been suggested that Nup53 and Nup59 are involved in the NPC anchoring to the pore membrane (Alber et al., 2007a; Alber et al., 2007b; Lin et al., 2016; Stuwe et al., 2015). The importance of the Poms interaction with Nups is supported by a study demonstrating that NPC assembly is blocked in when cells are depleted of Pom34 in addition to deletion of the *NUP53* and *NUP59* genes. Similarly, the depletion of Nup59 in cells carrying *pom34Δpom152Δ* leads to severe ultrastructural defects of the NPC (Onischenko et al., 2009).

Studies in vertebrates also show that Poms play an essential role in NPC assembly. In cells going through open mitosis, the Poms not only have a role in *de novo* NPC assembly, but also provide a platform for NPC re-assembly upon nuclear envelope breakage. Using the nuclear envelope

assembly assay in *Xenopus laevis* egg extract, a study revealed that early chromatin interaction with the Nup107-Nup160 complex initiated NPC assembly. This discrete NPC structure recruits the Pom121 and Ndc1, thus facilitating the incorporation of Nup155 and Nup53 into what will become a mature NPC (D'Angelo et al., 2006). This is evidence that Poms have an essential role in NPC assembly and NPC anchoring to the nuclear envelope through their interactions with the core scaffold.

1.4.2 Core scaffold Nups

The structural core of the NPC is termed the core scaffold (Alber et al., 2007a; Alber et al., 2007b; Lin et al., 2016; Stuwe et al., 2015). The nucleoporins forming the core scaffold stabilize and anchor the NPC to the nuclear envelope, and facilitate the curvature observed at the pore membrane. While the Nups located closer to the central channel interact with the linker Nups and FG-Nups, the Nups closer to the NE interact with poms (Rout et al., 2000). In budding yeast, biochemical studies suggest that the core scaffold is composed of three abundant complexes, Nup84 complex, Nup170 complex and Nic96 complex (Alber et al., 2007b). The center of the core scaffold is composed of the inner ring membrane (IRM) or Nup170 complex. The peripheral region contains the outer ring membrane (ORM) or the Nup84 complex, and, finally, facing the central channel is found the Nic96 complex or linker Nups complex (Aitchison and

Rout, 2012; Kabachinski and Schwartz, 2015; Lin et al., 2016; Stuwe et al., 2015).

Structurally, the nucleoporins present in the inner ring complex (IRC) are mainly composed of α-solenoids-like, and β-propellers (Devos et al., 2006). While Nup188 and Nup192 are primarily formed by α-solenoid-like domains, Nup170 and Nup157 contain a β-propeller domain followed by a α-solenoid-like domain. Moreover, the broad distribution of the α-solenoid domain throughout the Nups belonging to IRC favors the formation of flexible protein-protein interactions, possibly explaining the significant degree of flexibility observed in the NPC.

As expected for their core localization, the inner ring proteins establish several protein-protein interactions (Alber et al., 2007a; Alber et al., 2007b; Lin et al., 2016). In the IRC side facing the NE, Nup170 and Nup53 strongly interact with Ndc1, and to a lesser extent with Pom152, thus providing a platform for attaching the NPC to the NE. In the IRC side facing the central channel, the interaction between Nup192 and Nic96 is responsible for the correct insertion of the FG-Nups Nup49, Nup57, and Nsp1 into the NPC central channel. Several studies presented strong evidence that the Nup145N is responsible for bridging the interaction between the inner and outer rings. Another study suggested that the connection between the inner and outer ring can be mediated by the interaction between Nup157 and Nup120

The outer ring membrane, also known as the Nup84 complex, has been the subject of several studies. The Nup84 complex is the largest and the best characterized protein complex in the NPC with a molecular weight of around 0.5-0.75 MDa. The outer ring nucleoporins are composed mainly by β-propeller and α-solenoid-like domains (Alber et al., 2007a; Devos et al., 2006). Among the nucleoporins that are primarily composed of the β-propeller chains are Seh1 and Sec13. The α-solenoid-like domain is present in Nup85, Nup84, and Nup145C. Finally, the combination of the N-terminal β-propeller followed by the C-terminal α-solenoid-like domain is present in Nup133 and Nup120 (Aitchison and Rout, 2012). Interestingly, these types of protein folds are also found in the coat complex for vesicular transport, leading to the hypothesis that the outer ring complex and the vesicle coating complex evolved from a "protocoatamer" (Kampmann and Blobel, 2009). Electron microscopy has been used to define that outer ring complex proteins are arranged in a Y format, with Nup145C/Sec13 forming the long arm and Nup120/Nup133 and Nup84/Nup85/Seh1 forming the two shorter arms, respectively. This heptameric complex is arranged so that the globular domains, formed by the rigid β-propeller, are exposed at the ends of each arm and stem while the thinner connecting segment is formed by the more flexible α-solenoid domain (Kelley et al., 2015). It has also been suggested that due to a high affinity for curved membranes the outer ring complex facilitated the pore

formation and stabilization, eventually prompting the recruiting of the remaining nucleoporins (Aitchison and Rout, 2012).

1.4.3 FG-Nucleoporins

While the NPC core is formed by the interaction of several structural nucleoporins present in the NPC scaffold, the central channel is comprised of a group of unstructured nucleoporins (Floch et al., 2014; Kabachinski and Schwartz, 2015; Knockenhauer and Schwartz, 2016). These unstructured nucleoporins are called FG-Nups because they contain long stretches of highly repetitive phenylalanine-glycine dipeptides repeats (Tetenbaum-Novatt et al., 2012). Early studies estimated that FG-Nups account for nearly one-third of all cataloged nucleoporins, and for more than 30% of the total mass of the yeast NPC (Aitchison and Rout, 2012; Rout et al., 2000). Usually, the FG-Nups contain a small structured coiled-coil domain present at the C-terminus, which establishes an interaction with the NPC scaffold allowing it to be correctly inserted into the NPCs (DeGrasse et al., 2009). The FG stretches can contain up to 48 repeats of FxFG, GLFG, SxFG, or PxFG. Moreover, spacers of variable sizes are responsible for separating the FG repeats, thus creating protein domains that might comprise 150-700 amino acids (Strawn et al., 2004). Considering that each NPC contains more than 200 FG-Nups, it is easy to envision those long unstructured filaments filling the central channel, and consequently creating a physical plug that will restrict the cytonuclear

transport (Figure 1.1). This physical barrier created by the FG repeats is the NPC region responsible for regulating nuclear-cytoplasmic transport. As previously mentioned, while cargos smaller than ~10 nm can freely diffuse through the NPC, large macromolecules have to associate with nuclear transport factors (NTF) to overcome the entropic barrier created by an intertwined collection of unstructured FG filaments (Knockenhauer and Schwartz, 2016; Wente and Rout, 2010). To transport cargos across the NPC central channel, the NTF-cargo complexes establish transient low-affinity interaction with several FG-repeats distributed throughout the central channel.

Despite extensive studies investigating the mechanism by which cargos are transported through the NPC, the nucleocytoplasmic transport still represents a big challenge in the field. Initial studies proposed that the presence of asymmetrical FG-Nups could explain the vectorial movement through the central channel, with the FG-Nups containing the highest affinity for NTF asymmetrically distributed at the NPC periphery (Zeitler and Weis, 2004). However, a study using a series of different FG-Nup mutants suggested that asymmetrical FG-Nups are not required for efficient nuclear-cytoplasm transport (Strawn et al., 2004; Zeitler and Weis, 2004). This study highlighted the high degree of functional redundancy present in the FG-Nups. Consistent with the idea of FG functional redundancy, researchers were able to delete over 50% of all the FG repeats without affecting cargo transport. This study also suggested

that despite the absence of a significant amount of FG repeats, the remaining domains were able to redistribute and compensate for those deleted motifs (Strawn et al., 2004). This observation might not be surprising given the fact that the central channel is highly populated by FG-Nups, which together display thousands of individual FG motifs.

Both the cytoplasmic and nucleoplasmic faces of the NPC contain asymmetrical FG-Nups (Walther et al., 2002). On the cytoplasmic face of the NPC, eight symmetrically distributed cytoplasmic fibrils stretch toward the cytoplasm. In yeast, these cytoplasmic fibrils are made of Nup159, Nup82, and Nsp1 (Gaik et al., 2015). The cytoplasmic fibrils are involved in several biological processes such as regulating cargo transport, mRNA transport and nuclear segregation (Taddei et al., 2010a; Wente, 2000). On the opposite side facing the nucleoplasm, yeast NPCs contain Nup60, Nup2, and Nup1. The nucleoplasmic FG-Nups have been implicated in SUMOylation, gene regulation and cell cycle regulation (Niepel et al., 2013; Ptak et al., 2014).

1.5 Nuclear transport

The major function of the NPC is to mediate nuclear-cytoplasmic transport. Molecular sorting and shuffling through the NPC rely mainly on two principles. The first principle is the ability to regulate transport through size exclusion. The physical plug created by the FG-Nups restricts the unspecific nucleocytoplasmic transport of macromolecules larger than ~10

nm (Kabachinski and Schwartz, 2015; Tetenbaum-Novatt et al., 2012). The second principle is the ability to actively regulate the nucleocytoplasmic transport of cargos interacting with NTF. To be carried across the NPC, proteins must contain a specific amino acid sequence, either a nuclear localization signal (NLS) or a nuclear export signal (NES), which is used to signal protein accumulation in the nucleus or cytoplasm, respectively (Wente and Rout, 2010).

In addition to the FG-Nups, the proteins from the core scaffold also contribute to the barrier created by the NPC, as deletion of *NUP170* and *NUP188* dilate the central channel of the NPC (Sampathkumar et al., 2013; Theerthagiri et al., 2010). Despite recent efforts to understand the molecular steps required for the cargo translocation through the NPC, the precise mechanism for nucleocytoplasmic transport remains unclear. The complex and dynamic nature of nucleocytoplasmic transport has led to the proposal of different transport models. These models will be discussed in detail in the following sections.

1.5.1 Karyopherins and nuclear transport sequences:

As previously mentioned, large macromolecules, such as proteins, tRNAs, ribosomal subunits and viral particles, must associate with soluble NTF to overcome the physical barrier present in the central channel of the NPC. Studies probing the elasticity (i.e. constriction and dilation) of the central channel revealed that cargos up to 39 nm in diameter could

translocate through the NPC (Lezon et al., 2009). Moreover, EM studies showed that the ~50 nm mRNP particles assumed a rod-like structure of ~25 nm when associated with the NPC, suggesting that macromolecules larger than the central channel go through structural rearrangement to be transported through the NPC. (Oeffinger and Zenklusen, 2012; Panté and Kann, 2002).

In order to gain access to the central channel, cargo must carry either an NLS or NES, amino acid sequences required to correctly associate the cargo with its NTF (Suntharalingam and Wente, 2003; Wente, 2000; Wente and Rout, 2010). Despite a few well characterized NLS/NES sequences, such as the classical Nuclear Localization Sequence (cNLS) which contains five amino acids (KKKRK), the field still lacks the consensus sequence for the vast majority of transport factors. Several transport factors that recognize the NLS/NES sequences are part of a protein group named karyopherins (Melchior, 2001; Ribbeck and Görlich, 2001). The karyopherin family is divided into two sub-groups, β-karyopherins, and α-karyopherins. In *S. cerevisiae,* the karyopherin family is composed of 14 α-karyopherins and one β-karyopherins (Chook and Süel, 2011; Kobayashi and Matsuura, 2013; Stewart, 2007). This protein family can recognize and bind to a large spectrum of nuclear transport sequence and FG-repeats, and consequently mediate the cargo transport. While the β-karyopherins directly bind to the cargos and FG-repeats to mediate the transport, the α-karyopherin, Kap60, has to interact with a

cNLS containing protein and Kap95 for its transport through the NPC. (Wente and Rout, 2010). The β-karyopherins proteins are typically acidic with a molecular size ranging from 95 to 130 kDa. Despite sharing a low sequence identity (< 20% sequence identity), these proteins have as a hallmark the presence of approximately 20 HEAT repeats (amphipathic helix-loop-helix motifs) (Ström and Weis, 2001). The tandem HEAT-repeats are formed by antiparallel helices connected by a short turn, forming a large helical solenoid domain containing significant structural flexibility. This structural flexibility is essential for the β-karyopherins functions, as it allows these proteins to interact with a vast array of molecules (Chook and Süel, 2011; Wente and Rout, 2010).

Due to the complex and essential role of nucleocytoplasmic transport in eukaryotic cells, some level of redundancy is expected to maximize cellular viability. Corroborating such a hypothesis, studies have demonstrated that karyopherins have the ability to compensate for one another, thus binding to molecules with some degree of promiscuity (Strawn et al., 2004; Wente, 2000; Wente and Rout, 2010). For example, in the absence of Kap123p, Kap121p can interact with and transport cargos that are primarily clients of Kap123p.

1.5.2 Cargo transport directionality

As previously mentioned, NPCs limit unspecific nucleocytoplasmic cargo exchange by creating a physical plug at the central channel. This

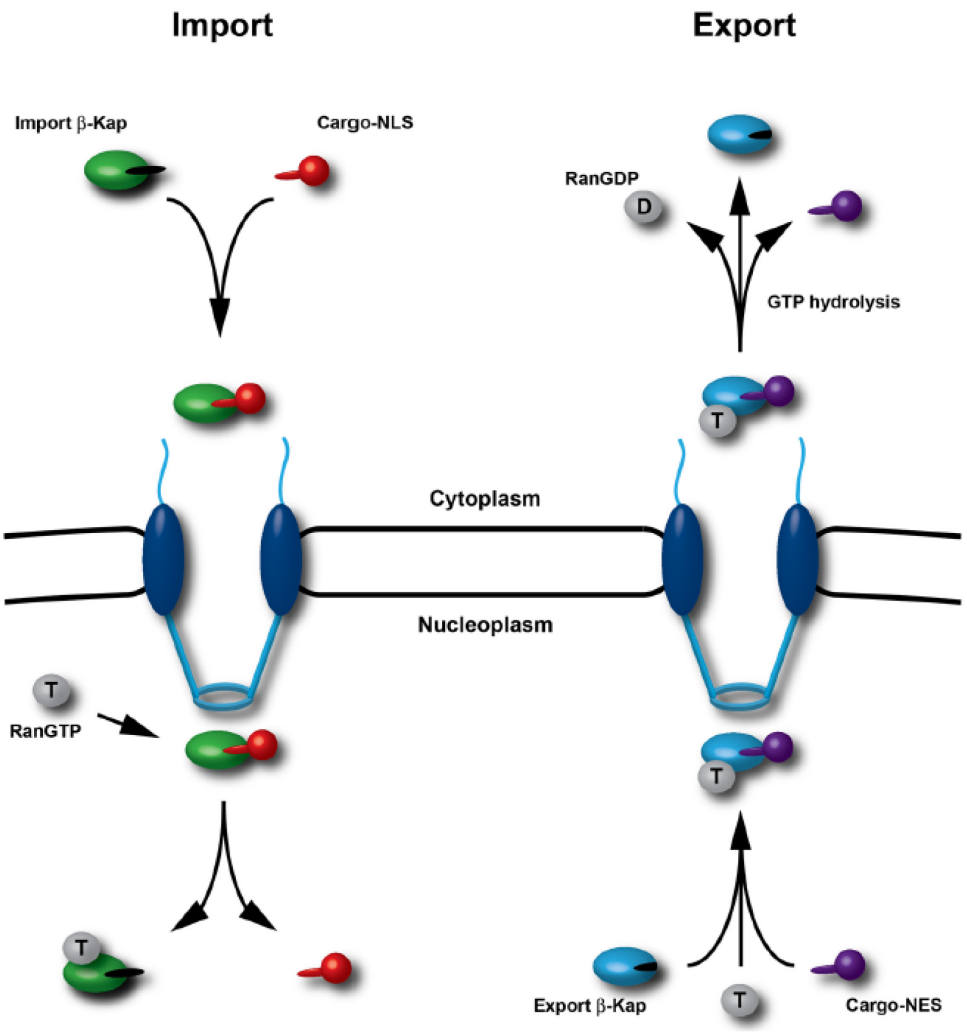

Figure 1-2. The nucleocytoplasmic transport cycle for import/export mediated by Kaps.

The karyopherin-mediated import of cargos (Red) is initiated by the interaction of the cargo's nuclear localization sequence (NLS) and the import Kap (Green). Following the complex formation between the karyopherin facilitates the cargo transport through the central channel. Upon entry into the nucleoplasm GTP-bound Ran (RanGTP, gray) binds to the Kap, thus inducing a conformational change and consequently releasing the cargo. Conversely, cargo export (purple) requires the interaction between the cargo's nuclear export sequence (NES) and an export Kap (blue). The RanGTP present in the nucleoplasm mediates the formation of cargo/kap complex, thus forming a trimeric complex Kap/cargo/RanGTP. Once the trimeric cargo complex reaches the cytoplasm it encounters RanGAP, which hydrolysis the GTP and dissociated the export complex.

physical process is devoid of energy consumption. However, the accumulation of cargos in a given nuclear compartment relies on the formation and maintenance of a differential concentration of Ran-GTP, also known as the Ran-GTP gradient (Macara, 2001). The physical interaction between cargos and karyopherins is regulated by RanGTP association with the amino-terminal portion of karyopherin. In yeast, the nuclear presence of the Ran guanine nucleotide exchange factor or RanGEF, favors the formation and enrichment of Ran-GTP. In contrast, the cytoplasm is enriched with the Ran GTPase-activating protein or RanGAP, thus favoring the accumulation of Ran-GDP (Wente and Rout, 2010).

The Ran-GTP interaction with karyopherins plays distinct roles in import and export. During import, the karyopherin involved in protein import to the nucleus recognizes and binds to its cargo in the cytoplasm environment (Kalab and Heald, 2008; Melchior, 2001). Next, the karyopherin establishes transient interactions with the FG-Nups at the central channel, thus mediating the cargo transport through the NPC (Corbett and Silver, 1997). When the cargo-karyopherin arrives in the nucleus, the high concentration of RanGTP favors the dissociation of the cargo-karyopherin complex. The karyopherin associated with RanGTP is quickly recycled back to the cytoplasm, where RanGAP stimulates GTP hydrolysis in RanGDP, thus vacating the karyopherin to another cycle of transport. Conversely, the high concentration of RanGTP in the nucleus

increases the cargo affinity for karyopherin involved with protein export. Ran-GTP facilitates the formation of a trimeric complex, and consequently its export through the NPC. Once the trimeric complex reaches the cytoplasm, RanGAP hydrolyses RanGTP, releasing the cargo (Kabachinski and Schwartz, 2015; Knockenhauer and Schwartz, 2016; Suntharalingam and Wente, 2003; Wente, 2000; Wente and Rout, 2010).

Given that the Ran gradient is essential for efficient nucleocytoplasmic transport, and that each cycle of transport requires at least one molecule of RanGTP, it is easy to imagine the requirement for an auxiliary pathway to replenish the nuclear levels of Ran. In yeast, Ran transport is performed by Ntf2, a protein that binds to RanGDP with high affinity. Once the RanGDP-Ntf2 complex reaches the nucleus, the RanGEF leads to the formation of RanGTP, and consequently the dissociation from Ntf2p (Aitchison and Rout, 2012).

1.5.3 Nucleocytoplasmic transport models

To date, we still do not entirely understand the precise molecular mechanism required to transport cargos through the NPC. Recent studies demonstrated that the natively unfolded FG repeats extend toward the central channel, creating a physical barrier capable of restricting the transport of unspecific cargos. (Floch et al., 2014; Wente and Rout, 2010). In budding yeast, the FG-Nups located at the central channel of the NPC establish quick and transient interactions with the NTF mediating the cargo

shuffling through the central channel. Despite the characterization of several proteins involved in nucleocytoplasmic transport, the biophysical principals behind this process are still a subject of debate (Strawn et al., 2004; Tetenbaum-Novatt et al., 2012). Over the past 50 years, theories ranging from mechanical iris to affinity gradient have been used to explain cargo transport, but the recent combination of genetic and biochemical data started to shed light on possible mechanisms. Currently, the most accepted theories are the selective phase/hydrogel model, virtual gate/polymer brush model, and forest model (Floch et al., 2014).

The selective phase model predicts that the inter and intra FG-repeat interactions would form a hydrogel plug responsible for controlling cargo transport through the central channel (Frey and Görlich, 2007). This model suggests that in order to translocate cargos through the central channel, the NTF can disrupt the FG-repeat meshwork creating a local and temporal entry access into the gel, thus leading to the cargo shuffling between the nucleus and cytoplasm. This model has been supported by studies demonstrating that FG-Nups are required for proper NPC selectivity, and that *in vitro* the high concentrations of FG-repeat spontaneously form a compact form of a hydrogel (Frey and Görlich, 2007; Ribbeck and Görlich, 2001). However, the reductionist views of this theory about the FG-Nups molecular nature, in addition to the observation that under physiological conditions the FG repeats do not form hydrogel, strongly argues against this model (Weis, 2007).

Unlike the selective phase model, the virtual gate model is based on the repulsive forces created by the FG repeats in addition to thermodynamic concepts (Rout et al., 2003). Considering that large molecules must be shuttled through channels containing over 100 copies of unfolded FG-Nups, it is reasonable to predict this as an entropically unfavorable process. The virtual gate model suggests that NPCs regulate the nucleocytoplasmic transport by decreasing the amount of energy necessary to initiate the transport process. To translocate large macromolecules across the NPC, cargos must form a complex with NTF. The cargo-NTF complex has higher affinity for the FG-Nups, thus decreasing the entropic barrier created by the FG-Nups (Li et al., 2016). The observation that deletion of FG-Nups, individually or in combination, influenced only particular transport factors further supports this model (Strawn et al., 2004).

The polymer-brush model suggests that unfolded FG repeats extend towards the nucleoplasm and cytoplasm and act as a molecular brush to repeal cargos not bound to NTF (Ma et al., 2012). However, after the formation of a cargo-NTF complex the FG-Nups surrounding the NPC entrance would collapse and consequently drag the potential cargos into the central channel (Yang, 2011).

The forest model employs parts of both the selective phase and virtual gate models. This theory was developed based on observations that FG-Nups can adopt either a collapsed globular conformation

(resembling shrubs), or an extended coil conformation (resembling trees) (Moussavi-Baygi et al., 2011; Wälde and Kehlenbach, 2010; Yang, 2011). This model foresees that similarly to the selective phase model the central region of the NPC channel is populated by extended coil formations that form several inter and intra molecular interactions, while the peripheral regions of the NPC channel are enriched with globular FG-Nups responsible for creating an entropic exclusion barrier, similar to the one described in the virtual gate model (Powers and Forbes, 2012).

1.6 NPC assembly and stoichiometry

As previously discussed, individual NPCs contain multiple copies of ~30 different nucleoporins (Rout et al., 2000). These nucleoporins are divided into sub-groups that will eventually work as building blocks for creating a mature NPC (Alber et al., 2007a; Alber et al., 2007b). The assembly of such structures represents a major challenge for cells, and it requires an intricate series of protein-protein interactions to correctly form and insert the NPC into the double membrane of the NE (Kabachinski and Schwartz, 2015; Knockenhauer and Schwartz, 2016). Similar to other cellular structures the NPCs are, during their lifespan, subjected to a dynamic process of assembling/disassembly during cell cycle progression (Aitchison and Rout, 2012; Antonin et al., 2008; Hetzer and Wente, 2009; Kabachinski and Schwartz, 2015). Studies have demonstrated that the NPC number doubles during the interphase to compensate for the

increase in the nuclear volume observed before cell division. NPCs can be assembled by two different mechanisms: the first occurs during open mitosis concomitantly with nuclear envelope breakdown, and the second mechanism of NPC assembly occurring along interphase, in which the NPCs are incorporated into the NE through *de novo* synthesis (D'Angelo and Hetzer, 2008; Hetzer and Wente, 2009).

1.6.1 NPC assembly and disassembly during open mitosis

Nuclear envelope permeabilization is paramount as eukaryotic cells evolve into multicellular organisms. Nuclear envelope breakdown occurs during the transition between prophase and prometaphase, and it completely disrupts nuclear integrity and compartmentalization (Hetzer, 2010). During NE retraction, the NPCs are disassembled quickly, thus making it difficult to precisely stipulate the order in which Nups are detached from NPCs (D'Angelo and Hetzer, 2008). However, microscopic studies suggest that NPC disassembly is highly synchronous and differs from the sequence observed during NPC assembly. By following the subcellular distribution of Nups representing different NPC subcomplexes, it was observed that peripheral Nups are the first to dissociate from NPCs, followed by the structural Nups (Dultz et al., 2008). It is believed that NPC disassembly is triggered by phosphorylation (Laurell et al., 2011). The phosphorylation of gp210 and members of the Nup107/106 complex is involved in the initiation of NPC disassembly. Mounting evidence suggests

that dissociated Nups might have specific functions during mitosis, with several NPC components accumulating at kinetochores or regulating chromosome separation (D'Angelo and Hetzer, 2008; Hetzer, 2010).

NPC assembly occurs after mitosis concomitantly with NE formation around the recently segregated chromosomes (Burke and Ellenberg, 2002; Maul, 1977). During this stage, the anaphase-promoting complex (APC) inactivates the mitotic kinase Cyclin Dependent Kinase 1 (CDK1), reducing the overall levels of nuclear phosphorylation and possibly triggering the NPC assembly process (Güttinger et al., 2009). In order to assemble and correctly insert the NPC into the newly formed membrane, several nucleoporins directly interact with chromatin, thus forming the structures known as pre-pores (Gillespie et al., 2007). Studies have suggested that the Nup ELYS/Mel28 interaction with chromatin is required for the recruitment of the structural complex Nup107-160 into the pre-pores followed by the deposition of minute fractions of Nup153 and Nup50 (Walther et al., 2003). As the membranes start reassembly around chromatin, accumulation of the transmembrane nucleoporin Pom121 is observed in chromatin regions enriched for Nup107-160 (Franz et al., 2007). Moreover, depletion of either Pom121 or the Nup107-160 complex impairs the correct formation of the NE or NPC, respectively. After the formation of the Pom121-Nup107-Nup160 complex, the Nup93 and then the Nup62 complexes are associated with the pre-pores, yielding a partially functional NPC (D'Angelo and Hetzer, 2008; Hetzer and Wente,

2009; Suntharalingam and Wente, 2003). A study has suggested that the Nup93 complex plays a major role in establishing the exclusion limit of NPC, suggesting that the Nup93 complex plays a major structural role in the process of NPC maturation (Theerthagiri et al., 2010). Briefly, after the Nup93 complex associates with the NPC the FG-Nups from the Nup62 complex are attached to the NPC central channel. The last steps in NPC assembly are inserting the proteins Nup215 and Tpr, in addition to major pools of Nup153, Nup50, and Gp210.

1.6.2 NPC assembly in closed mitosis

NPC biogenesis is prominent during cell proliferation and differentiation; studies have indicated that NPC density can nearly double during interphase (Winey et al., 1997). The mechanism by which NPCs are assembled during interphase is still not completely elucidated and several hypotheses have been suggested. Recent observations indicate that NPC assembly during interphase occurs through *de novo* mechanism (Aitchison and Rout, 2012).

Despite the fact that the cellular division process differs significantly between vertebrate cells and budding yeast, NPC assembly during interphase appears to be partially conserved throughout eukaryotes. Using the cell-free insertion assay, D'Angelo and colleagues determined that NPC components are recruited from both sides of the NE, in a process requiring RanGTP, Kaps, and the Nup107-160 complex (D'Angelo et al.,

2006). Since the integrity of yeast nuclei is maintained throughout the cellular division NPCs must be exclusively assembled via *de novo* synthesis, thus making budding yeast an ideal organism model to study this biological process. An electron microscopic study suggests that yeast cells continuously assemble NPCs through the cell cycle with density peaking in late anaphase with an average of ~15.6 NPCs/mm^2 (Winey et al., 1997). Determining the steps involved in the process of NPC assembly is challenging, as mutations of individual Nups can result in phenotypes ranging from the formation of NPC clusters to herniations of the NE towards the cytoplasm (Aitchison and Rout, 2012; Makio et al., 2013; Makio et al., 2009; Strambio-de-Castillia and Rout, 2002)Aitchison and Rout, 2012; Makio et al., 2013; Makio et al., 2009; Strambio-de-Castillia and Rout, 2002). However, the development of new tools such as repressible promoters to regulate gene expression has improved our understanding of NPC formation.

By tagging nucleoporins with the photoconvertible fluorescent protein Dendra, it was shown that symmetrical Nups accumulate on both sides of the NE (Onischenko et al., 2009), suggesting that pre-assembled sub-complexes might initiate the formation of mature NPCs. In addition, nucleocytoplasmic transport is also required for NPC assembly, as a mutation disrupting the Ran gradient or blocking the transport factors Ntf2 and Kap95 failed to correctly form NPCs (Ryan et al., 2007). Another transport factor implicated in NPC assembly is Kap121, which facilitates

Nup53 targeting to the NPC, where it will associate with the inner ring protein Nup170 (Lusk et al., 2002). Apart from nucleocytoplasmic transport, the core scaffold has an important role during the early steps of NPC assembly. It has been shown that overexpression of the C-terminal region of Nup170 generates structures resembling NPC intermediates in the cytoplasm and at the NE (Fernandez-Martinez and Rout, 2009). This phenotype is also observed in strains containing gene deletions of *NUP53/NUP59* or *POM152/POM34* in addition to the depletion of Nup170 (Onischenko et al., 2009).

The correct assembly of NPCs and their concomitant insertion into the NE requires proteins involved in membrane molding and restructuring. In yeast, the reticulons Rtn1/Rtn2 and their interacting partner Yop1 facilitate membrane curvature and are transiently enriched in regions populated by NPCs (Aitchison and Rout, 2012). The absence of these reticulons and its interacting partner Yop1 in mature NPC suggests a transient role of these proteins during early stages of NPC assembly.

In summary, considering the available literature related to NPC assembly, it is feasible to speculate the steps involved in the assembly and insertion of newly synthesized NPCs into NE during interphase (Aitchison and Rout, 2012; Fernandez-Martinez and Rout, 2009; Strambio-de-Castillia and Rout, 2002). The first step in NPC assembly requires the transmembrane nucleoporins (Poms), and proteins responsible for stabilizing membrane curvature such as reticulons. Next, transmembrane

nucleoporins recruit the inner ring complex in both faces of the NE, which consequently recruits the outer ring complex thus enhancing the membrane curvature, and further stabilizing the pore membrane. After the formation of the NPC core scaffold further association of FG-Nups and the nuclear basket would finalize the process of NPC assembly. Finally, despite our present knowledge, there is still much to be learned about NPC assembly in yeast, and it is important to clearly state that this described model is based on speculations using the available literature.

1.6.3 NPC turnover

The maintenance of functional NPCs is imperative considering the detrimental effects associated with nucleocytoplasmic transport defects. A mechanism to repair NPC has not been identified in cells, despite the critical function of NPC in cellular viability. Recent publications have suggested that to maintain NPC integrity, cells are constantly exchanging nucleoporins (D'Angelo et al., 2009). Another mechanism used to ensure the correct nucleocytoplasmic transport is the substitution of old and presumably ill-functional NPCs by newly synthesized ones. Finally, the redundancy observed among some nucleoporins could also be viewed as a possible mechanism to ensure NPC integrity (D'Angelo and Hetzer, 2008).

The turnover rate of mammalian nucleoporins varies from seconds for peripheral and FG-Nups to weeks for core nucleoporins (Toyama and

Hetzer, 2013). Interestingly, studies revealed that scaffold nucleoporins are extremely stable and that their expression levels are significantly down-regulated following cellular differentiation (D'Angelo et al., 2012; Ori et al., 2013). Conversely, the peripheral nucleoporins are less stable than scaffold nucleoporins, but their expression levels are not altered after cellular differentiation. Based on these observations it is possible to speculate that while the peripheral nucleoporins are dynamically associated with NPCs, the scaffold nucleoporins are stably connected to NPCs (D'Angelo et al., 2009; Ori et al., 2013). The nucleoporin turnover rates have not been studied in greater detail in budding yeast. However, studies using repressible promoters have demonstrated that protein stability varies greatly among the different NPC complexes (Makio et al., 2013; Makio et al., 2009). Moreover, fluorescent microscopy also shown that FG-Nups are highly mobile in budding yeast. Importantly, these observations agree with the findings for mammalian cells, suggesting that eukaryotic cells might share common NPC turnover mechanisms

1.6.4 NPC stoichiometry

Despite efforts to elucidate NPC organization, Nups stoichiometry is still not fully elucidated. The dynamic nature in combination with the large number of proteins present in a single NPC represents a major challenge for researchers in this field. Over the last 50 years different research groups have focused on determining the NPC composition, and by their

combined effort have provided a clear list of nucleoporins and subcellular localization (Gaik et al., 2015; Kelley et al., 2015; Lin et al., 2016; Rout et al., 2000; Stuwe et al., 2015). Despite these elegant approaches to identifying nucleoporins and establishing their distribution, to date, our knowledge of NPC stoichiometry is based on semi-quantitative methods that estimate the signal emitted by tagged nucleoporins. While this approach provides valuable information, the inherent experimental difficulties such as epitope recognition, and problems with expression of tagged nucleoporins impose major hurdles to further improving our knowledge about the molecular arrangement of the NPC.

Early attempts to address NPC stoichiometry established that nucleoporins could be mainly divided into three clusters (Rout et al., 2000). The low abundance cluster is formed by nucleoporins that are present exclusively on a single NPC side. The middle abundance cluster contains most of the nucleoporins. Finally, the high abundance cluster includes only a few specific Nups. However, these experiments did not address the possible biological variability of Nups expression among cells and even NPCs. It is important to remember that NPCs can present a heterogeneous configuration, such as the NPC lacking the nuclear basket found adjacent to the nucleolar region (Niepel et al., 2013). Even though the functions of such protein complexes, or the mechanisms responsible for creating such variability are still not fully elucidated, it is important to consider such factors when trying to assess NPC stoichiometry. The

possible existence of distinct NPCs represents an intriguing concept that would further explain how NPCs are involved in such a variety of biological processes.

Recent advancements in the microscopy and proteomics fields are improving our ability to further resolve the NPC structure as well as nucleoporin stoichiometry. Such improvements have allowed researchers to address how protein complexes are remodeled in different cell types and during distinct stages of the cell cycle (Fernandez-Martinez and Rout, 2009; Hetzer, 2010; Hetzer and Wente, 2009). A recent study using a combination of super-resolution microscopy and targeted proteomics found that while structural Nups, such as those present in the NPC scaffold, are stably expressed across different mammalian cell types, the protein levels of non-structural Nups are subject to significant differences in human tissues (Ori et al., 2013). These observations led the authors to propose that different mammalian cells might contain specialized populations of NPCs. These observations suggest that distinct NPC arrangements could influence several cellular mechanisms mediated by NPCs, such as nucleocytoplasmic transport and chromatin organization.

Corroborating the hypothesis that cells contain a heterogeneous population of NPCs, another study examined the stoichiometry of individual NPCs in the yeast model (Mi et al., 2015). To address this question, researchers measured the fluorescence emitted by different Nup-GFP fusions using a combination of photobleaching and super-

resolution microscopy. While this study further corroborates the stoichiometry previously described for several Nups, it highlighted that at least eight Nups are present in different number than previously described in the literature.

Improvements in cell biology techniques will offer exciting possibilities to increase our understanding of the NPC structure. Such advancements might help to address the observed NPC plasticity, and possibly lead to the identification and characterization of different NPC populations. Finally, it is reasonable to expect that NPCs containing a different set of Nups might possess different functions, thus eventually reconciling the broad, and at times divergent range of functions attributed to the NPC structure.

1.7 Non-canonical NPC functions

Despite the well-established function of NPC in cargo transport, nucleoporins have also been implicated in a diverse range of nuclear processes, such as DNA repair, SUMOylation, chromatin anchoring and silencing (Cairo et al., 2013b; Palancade and Doye, 2008; Ptak et al., 2014; Ptak and Wozniak, 2016; Van de Vosse et al., 2013). The non-transport related functions of the NPCs can be attributed to the interactions of individual Nups with proteins outside the NPCs, or to the fact that NPCs share proteins with other structures such as spindle pole bodies (SPBs). In budding yeast, Ndc1 is an example of a protein shared

between the SPBs and NPCs (Onischenko et al., 2009). Ndc1 was originally described as an essential protein for SPB duplication. However, microscopy and biochemical approaches characterized Ndc1 as a transmembrane pore protein (POM) essential for the NPC assembly. Other proteins representing the functional link between NPC and SPB are Mad1 and Mad2 (Cairo et al., 2013a). These proteins are necessary to activate the spindle assembly checkpoint (SAC) and are capable of dynamically associating with the nuclear basket in eukaryotic cells. It has been shown that Mad1 is recruited to kinetochores after the activation of the SAC checkpoint. This recruitment relies on the recognition of the Mad1 NES by the karyopherin Xpo1, and subsequently targeting of Mad1 to kinetochores in a process analogous to nuclear export. Other non-transport functions linked to the NPC, such as chromatin regulation, DNA repair, and post-translational modification, will be discussed in further detail in the following sections.

1.7.1 NPC and chromatin organization

Electron micrographs suggested a role for NPC in chromatin regulation, as the regions adjacent to the NPCs were enriched for euchromatin, a form of lightly packed chromatin (Hetzer, 2010; Ptak et al., 2014). Furthermore, these observations also detected chromatin fibers extending towards the NE and attaching to regions containing NPCs, an assumption based on the classical eight-fold radial symmetry morphology

of the NPC. The precise mechanism by which the NPC regulates chromatin is still the subject of intense research, and will be further explored in the following paragraphs, while the chromatin structure will be the main topic in Chapter 1.8.

As previously mentioned, several studies have indicated that the NPC shares a few proteins with another chromatin landmark, such SPBs (Cairo et al., 2013a; Meseroll and Cohen-Fix, 2016; Taddei and Gasser, 2012). Recently, in a study published by our research group, the NPC was linked with telomeres, another chromosomal landmark. In this study, we observed that the inner nuclear ring components *NUP170*, and to a lesser extend *NUP157*, regulate the expression of genes adjacent to telomeres (Van de Vosse et al., 2013). Another example of nucleoporins linking NPC and telomeres is the Nup84 complex (Therizols et al., 2006). A study has demonstrated that the Nup84 complex is required to properly repair DNA breaks occurring at telomeres.

In yeast, telomeres are usually clustered into three to eight foci that often localize adjacent to the NE. It is broadly accepted that telomere tethering to the NE facilitates silencing of genes present in this region, an effect known as telomere positioning effect (TPE) (Taddei et al., 2010a). In order to tether chromatin to the NE, chromatin-associated proteins have to interact with proteins present in the inner nuclear membrane. Telomere anchoring to the nuclear periphery relies on the interaction between telomeric proteins such as the Silent Information Regulator (SIR) family,

yKU and Rap1 and proteins present in the INM such as Esc1 and Mps3 (Taddei et al., 2004b; Taddei et al., 2010a). Telomere tethering to the NE is regulated through cell cycle progression, and it has been proposed that alterations in the interactions between telomeric and INM proteins mediate telomere recruitment during G1-phase, as well as release during late S-phase (Kupiec, 2014). Studies have suggested that interaction between Esc1 and Sir4p is mainly responsible for telomere anchoring during the G1-phase (Taddei et al., 2010b). As the cells progress to S-phase, the anchoring process is mediated by the Mps3 interaction with the yKu family and telomerase. More recently, using a vast array of proteomics, genomics, and microscopy approaches, we showed that Nup170 interacts with Sir4, thus facilitating telomere tethering to the nuclear envelope (Van de Vosse et al., 2013). Similar to Esc1, Nup170 affected telomere tethering mainly during G1-phase, possibly linking these proteins to a common pathway.

1.7.2 NPC and SUMOylation

Another biological process linked to the NPC is SUMOylation, a post-translational modification (PTM) that mainly modifies nuclear proteins (David, 2010; Geiss-Friedlander and Melchior, 2007; Mahajan et al., 1997; Matunis et al., 1996; Wilkinson and Henley, 2010). Briefly, the SUMOylation process in yeast requires the attachment of the ubiquitin-like protein, Smt3, onto a target protein (Tatham et al., 2009). First, E1

activator enzymes (Aos1/Uba2) activate Smt3. After peptide activation, an E2 conjugating enzyme (Ubc9) conjugates SMT3 to the target protein. In the final step, E3 ligase enzymes (Siz1, Siz2, Mms21, and Cts9) catalyze the formation of an isopeptide bond between the SUMO peptide and the acceptor lysine present in the target protein. Importantly, SUMOylation can be reversed through the action of the deSUMOylation enzymes Ulp1 and Ulp2. SUMOylation will be discussed in greater detail in Chapter 1.10. The goal of this section is to explore the links between NPC and SUMOylation.

The NPC was initially linked to SUMOylation through its interaction with Ulp1 (Palancade and Doye, 2008). Early studies suggested that the correct nuclear localization of Ulp1 was dependent on its interaction with the NPC's nuclear basket proteins Nup60, Mlp1p, and Mlp2p. Later studies showed that Ulp1's association with NPCs depends on its recognition by Kap121 and Kap60-95 (Makhnevych et al., 2007). Another group of nucleoporins involved in SUMOylation is the outer nuclear ring complex, also known as the Nup84 complex (Palancade et al., 2007b). Similar to what was described for mutations in the nuclear basket, deleting nucleoporins from the Nup84 complex altered ability of Ulp1 to interact with NPC, and also reduced its expression levels. Furthermore, NUP84 genetically and physically interacts with the SUMO-Targeted ubiquitin ligase (STUbL) proteins SLX5/SLX8 (Nagai et al., 2008). The observed pathway redundancy to correctly target Ulp1 to NPCs indicated the crucial importance of this biological process.

1.8 Chromatin

In 1871, F. Miescher published the first report about nucleic acid, and by 1880 W. Flemming named the structure containing DNA "chromatin" (Olins and Olins, 2003; Passarge, 1979). The subsequent evolution in the field of microscopy allowed Emil Heitz in 1928 to describe the presence of at least two different types of chromatin: one that was constitutive and highly-condensed (heterochromatin), and another that presented the ability to decondense during interphase (euchromatin).

The significant advancements observed in the field of genetics during the first half of the twentieth century revealed gene theory, and later the better characterization of proteins forming chromatin (Gilbert, 1978). In order to fit inside the nucleus DNA must be highly organized and packed. The highly condensed chromatin regions are not accessible to the transcriptional machinery, thus creating stretches of genome that are often transcriptionally silenced (Czapiewski et al., 2016; Ptak and Wozniak, 2016; Zimmer and Fabre, 2011). Conversely, the loosely packed euchromatin is more accessible to the transcriptional machinery, thus increasing the probability of gene expression. To accomplish such a degree of organization/compaction, chromatin is subjected to several layers of compaction. In the first order of compaction, the DNA associates with a group of proteins named histones. The association of ~147 base pairs with a histone octamer forms the nucleosome. Each histone octamer

is formed by two H2A-H2B dimers and a core H3-H4 tetramer (Olins and Olins, 2003). Furthermore, yeast encodes histone variants to provide diversity. For example, the histone Cse4 and Htz1 are present exclusively at centromeres (Verdaasdonk and Bloom, 2011). The second layer of compaction is achieved through nucleosome oligomerization to form a 30-nm fiber. In the last layer of compaction nucleosome fibers organize into a poorly defined form of chromatin structure (Woodcock and Ghosh, 2010). The layers involved in forming chromatin, and in regulating the DNA accessibility to transcription factors, are sensitive to subtle changes in the interaction between chromatin binding proteins and histone modifying enzymes.

The chromatin boundary regions are found in the interface of opposing chromatin states. These regions have the ability to regulate the spreading of either euchromatin or heterochromatin. The boundary regions are dynamic in nature, and the flexible tails of histones present in these areas are substrates of different epigenetic marks, such as acetylation, methylation, phosphorylation, ubiquitination, ADP-ribosylation, glycosylation, and SUMOylation (Olins and Olins, 2003; Woodcock and Ghosh, 2010).

The combination of different histone modifications can regulate chromatin accessibility to modifiers and transcription factors, leading to the proposal of the “histone code hypothesis” (Calo and Wysocka, 2013). The histone code hypothesis postulates that different patterns of PTM can be

read like a molecular bar code, and consequently recruit non-histone proteins to regulate chromatin state (Chi et al., 2010; Rothbart and Strahl, 2014). Despite a large amount of information supporting this hypothesis, the molecular details of how these non-histone proteins regulate chromatin dynamics are not fully elucidated. Deciphering the histone code will certainly require an extraordinary amount of work, considering that to date well over 100 different histone modifications have been described.

1.8.1 Chromatin silencing

The continuous effort to further characterize mechanisms of chromatin silencing during the past several decades has improved our understanding of heterochromatin structure (Olins and Olins, 2003; Woodcock and Ghosh, 2010). Despite the observation that budding yeast lacks heterochromatin hallmarks such as H3K9me3, studies have detected chromatin regions in yeast that contain a remarkable similarity with the heterochromatin found in higher eukaryotes (Jin et al., 2005; Morrison and Shen, 2009). These heterochromatin-like regions are exemplified by the mating-type loci, rDNA, centromeres, and telomeres. The mechanisms to establish chromatin silencing show subtle variations across the yeast genome. For example, while Sir4 recruitment by Rap1 initiates the silencing at telomeric regions, the silencing at mating-type loci relies on a redundant pathway containing different silencer elements -

Rap1, Abf1, and ORC (Luo et al., 2002; Meister et al., 2010; Rudner et al., 2005; Taddei et al., 2004b; Taddei et al., 2010b).

As briefly mentioned, silencing at a telomere is initiated by the interaction between Sir4 and Rap1 (Enomoto et al., 1994; Hardy et al., 1992; Moretti et al., 1994; Palladino et al., 1993). Sir4 recruitment to telomeric regions initiates the recruitment of the remaining SIR proteins, Sir2 and Sir3. After loading the SIR complex onto telomeric chromatin, Sir2 deacetylates histones H3 and H4, especially histone H4K16. The deacetylation of histone H4K16 generates a strong affinity binding site to Sir3, which subsequently recruits Sir4 (Zimmer and Fabre, 2011). Multiple rounds of SIR complex loading onto chromatin, followed by histone deacetylation creates compact and highly structured chromatin. Similarly, the silencing at mating-type loci, HML and HMR, requires the recruitment of Sir4, and consequently the SIR complex (Buck and Shore, 1995; Moretti and Shore, 2001; Rine and Herskowitz, 1987). However, the initial Sir4 recruitment to the HM loci is slightly different from the telomeric region. The mating type loci are bracketed by two silencer elements, E (Essential) and I (Important). These elements provide binding sites for Rap1, Abf1, and ORC, which subsequently act as nucleation sites for the SIR complex. While Rap1 binds to Sir4 directly, Abf1 interacts with Sir3, and ORC recruits Sir1, the only Silent Information Regulator present exclusively at the HM loci. Finally, after Sir4 recruitment, the following steps of histone

deacetylation and SIR complex spreading are similar to those observed at telomeres (Taddei and Gasser, 2012; Taddei et al., 2010b).

1.9 Telomeres

Telomeric DNA plays an essential role in genome integrity, as telomeres avoid the recruitment of machinery responsible for DNA damage repair at chromosome ends, thus avoiding the activation of the DNA repair checkpoint (Marcomini and Gasser, 2015). Telomeres are well-conserved across eukaryotic cells, and the budding yeast model has been used to further understand the functions of this chromatin structure (Duina et al., 2014; Kupiec, 2014). Telomeres form foci of transcriptionally silenced chromatin that are often anchored to the nuclear envelope. Since the first report of telomeres in the during the 1980's, several groups have worked to improve our understanding of telomere biology, including telomere structure and function (Shampay and Blackburn, 1988). However, despite all these efforts we still have several questions about the molecular steps involved in the establishment of telomeric gene silencing.

1.9.1 Telomere structure

In budding yeast, telomeres are formed by 300 ± 75 bp of simple $C_{1-3}A$ / TG_{1-3} repeats. At the telomere end, extending from the 3', is a G-rich single stranded tail containing 10-15 nucleotides (Wellinger and

Zakian, 2012). This G-rich overhang is extended during telomere replication in late S-phase providing a template for telomerase, an RNA-based enzyme responsible for maintaining telomere length (Osterhage and Friedman, 2009). By maintaining the G-rich tail present at the chromosome ends, telomerase is the biological answer to the "end replication problem" (Ellahi et al., 2015; Gilson and Géli, 2007; Gilson et al., 1993). Telomerase can be divided into two subunits; the subunit containing the proteins Est1, Est2 and Est3, and the Tlc1 subunit which serves as the RNA moiety template for the TG repeat extension (Wellinger and Zakian, 2012). Telomerase recruitment to telomeres is mediated by Cdc13, a protein that binds to G-rich single stranded DNA. Cdc13 is part of an essential protein complex named CST (Cdc13/Stn1/Ten1) telomere-capping complex. Deletion of any of the proteins in the complex results in telomere degradation and eventual activation of the DNA damage checkpoint (Rice and Skordalakes, 2016). Also, telomerase can be recruited to telomeres by the yKu family members, yKu70 and yKu80 (Taddei et al., 2010a).

Rap1 interacts with telomeric double-stranded DNA. Biochemical experiments determined that one molecule of Rap1 interacts with 18 bps of DNA, suggesting that each telomere could contain 16 to 20 molecules of Rap1. The presence of the Rap1 at telomeres prevents nucleosome formation at the chromosome ends, and its interaction with other proteins plays a crucial role in the maintenance of telomere length

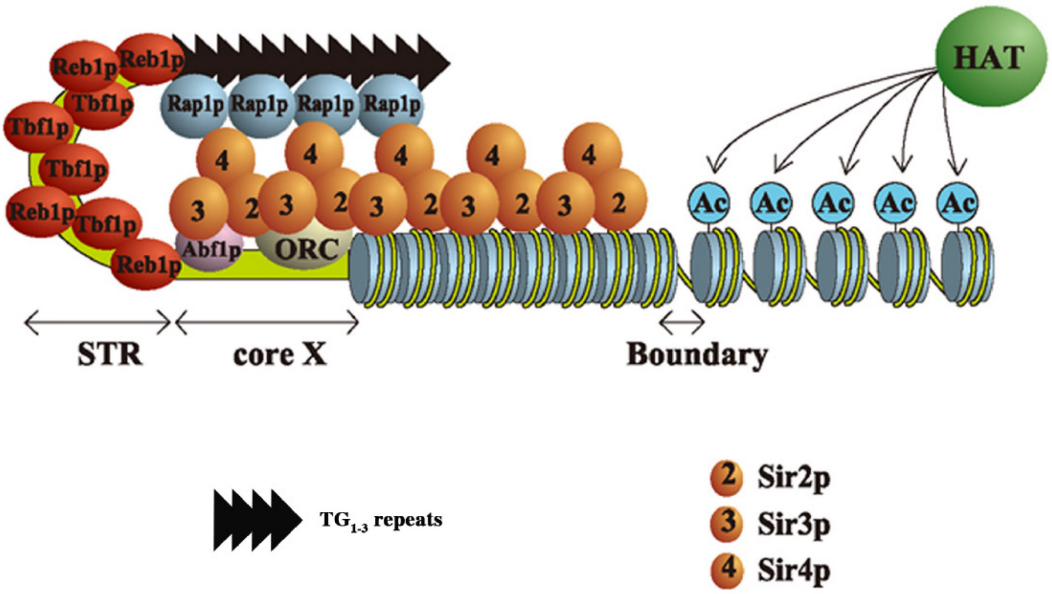

Figure 1-3. Schematic is representing the telomeric and subtelomeric gene silencing in S. cerevisiae.

The nucleation of silencing at telomeric and subtelomeric regions is initiated by the Rap1 interaction with Sir4. The Sir4 loaded onto telomeres recruits the remainder proteins of the SIR complex, Sir2, and Sir3. The heterochromatin spreading through telomere relies on the Sir2-mediated deacetylation, which enhances the histone affinity for Sir4 and Sir3. The repetitive cycles of binding followed by histone deacetylation facilitate the SIR complex spreading towards the centromeric region. As effect of Sir4 spreading, extra bind sites for Rap1 are created causing telomeres to fold over, thus enhancing the sub-telomeric gene silencing. Furthermore, subtelomeric repeat elements also regulate telomeric and subtelomeric silencing. The Abf1 and ORC elements present in the X element (core X) enhances the Sir Complex binding, while the Tbf1 and Reb1 present in the subtelomeric repeats (STR) inhibit the SIR complex recruitment. *Adapted from (Sun et al., 2011)*

(Gotta et al., 1996; Laroche et al., 2000; Luo et al., 2002; Moretti et al., 1994; Moretti and Shore, 2001; Strahl-Bolsinger et al., 1997).

The high concentration of Sir4 at telomeres provides abundant interaction sites for Rap1, leading to the proposal that telomeres fold over itself, thus enhancing the silencing across the entire telomeric region (Kupiec, 2014). However, a recent study challenges this concept as it shows that the SIR complex has a patchy distribution across telomeric and sub-telomeric regions (Ellahi et al., 2015). The mapping of the SIR complex landscape shows that SIR proteins are highly enriched at telomeric repeats and at the subtelomeric element (STE) core X, however, SIR-mediated silencing is not widespread as previously postulated. By using a combination of chromatin immunoprecipitation followed by DNA sequencing (ChIP-Seq) and RNA sequencing (RNA-seq), it has been proposed that SIR complex proteins only silence ~6% of subtelomeric genes.

These findings further support the importance of STE in budding yeast. The STEs are located adjacent to $C_{1-3}A$ / TG_{1-3} repeats and are classified as X and Y elements. While all telomeres contain a core X element containing binding sites for Abf1 and ORC, the Y element is not present in all telomeres, and it contains the anti-silencer elements Tbf1 and Reb1. In conclusion, the establishment of telomeric silencing is finely

tuned by the interplay between cis- and trans- acting factors found across telomeres (Wellinger and Zakian, 2012).

1.9.2 Telomere anchoring to the NE

In *Saccharomyces cerevisiae*, telomeres are usually anchored to the nuclear periphery. This peripheral localization enhances the silencing of the telomeric gene in an effect named TPE. The telomere tethering is accomplished by two partially redundant pathways, one mediated by the SIR complex and mediated by the yKu heterodimer (Kupiec, 2014; Taddei et al., 2010a). To anchor telomeres to the NE, telomeric proteins interact with proteins associated with the INM. Importantly, telomere anchoring is dynamically regulated during the cell cycle. Telomere tethering to the NE during G1-phase relies on the Sir4 interaction with either Esc1, Nup170 or Mps3, and during S-phase on the yKu heterodimer and telomerase with Mps3 (Taddei and Gasser, 2012; Taddei et al., 2010a).

During G1-phase, Sir4 mediated anchoring relies on the interaction of the Partitioning and Anchoring Domain (PAD; aa 950-1262) of Sir4 with the NE associated Esc1 (Andrulis et al., 2002; Taddei et al., 2004a). As the cells progress through the cell cycle, Sir4 and yKu80 interact with Mps3, thus establishing telomere anchoring during S-phase (Bupp et al., 2007; Schober et al., 2009). Also, observation that yKu70/yKu80 is required for Sir4 loading onto telomeres indicates that Mps3 and yKu pathways might be interconnected

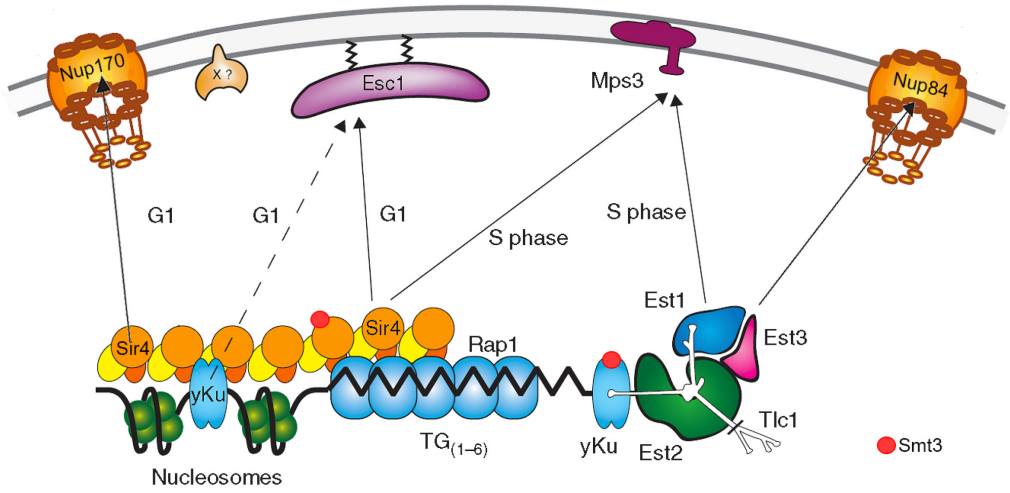

Figure 1-4. Schematic representing telomeric and subtelomeric gene silencing in S. cerevisiae.

Telomere tethering to the NE is mediated through partially redundant mechanisms. Telomere tethering to the NE relies on the transient interaction between proteins bound to the chromatin and INM components. During G1-phase, telomere anchoring is mediated through yKu interaction with Esc1, or through Sir4 interaction with Esc1 and/or Nup170. During S-phase, telomere tethers predominantly through Sir4 interaction with Mps3, or through the yKu-telomerase complex interaction with Mps3. Moreover, components of the NPC (the Nup84 complex and the nuclear basket components Mlp1/Mlp2) have also been implicated in telomere recruitment to the NE. Finally, SUMOylation of the telomeric proteins Sir4 and yKu also promote telomere tethering. *Adapted from (Taddei et al., 2010a)*

(Horigome et al., 2011; Luo et al., 2002). Moreover, the yKu80 interaction with telomerase facilitates telomere tethering during S-phase through its interaction with Mps3.

It has also been suggested that an unknown protein might be involved in telomere tethering during the G1-phase. This hypothesis is based on the observation that the yKu heterodimer is capable of mediating telomere anchoring during the G1-phase in cells lacking the Esc1 protein, while Mps3 has been implicated in telomere tethering exclusively during the S-phase (Taddei et al., 2010a).

Other factors have also been shown to contribute to telomere function, including components of the NPC. Initial studies identified the myosin-like protein Mlp2, a nuclear basket component, as a regulator of telomere tethering to the NE and gene silencing (Feuerbach et al., 2002; Galy et al., 2000). However, these results proved controversial, as the observations did not appear to be reproducible (Hediger et al., 2002). Subsequent work showed that the Nup84 complex, a component of the NPC core, also played a role in tethering, gene silencing, and DNA repair (Therizols et al., 2006). Finally, our group has shown that a different NPC core scaffold protein, Nup170, also regulates gene silencing at subtelomeric regions. These effects appear to be direct, as Nup170 associates with telomeres and co-purifies with Sir4. Furthermore, the loss of Nup170, while reducing telomere tethering, also reduces the Sir4 association with telomeres, suggesting a direct role in heterochromatin

assembly (Van de Vosse et al., 2013). These links between Nups and telomere regulation suggest a role for NPCs in these processes. However, such a role conflicts with the distinction between chromatin types observed at the nuclear periphery in yeast, where the silenced telomeres and subtelomeric heterochromatin are tethered with the INM, while transcriptionally active chromatin foci are anchored to the NPCs.

A potential mechanism to reconcile the different roles played by NPCs in chromatin organization comes from another recent study showing that telomeric proteins are subject to SUMOylation, a post-translational modification long linked to NPCs (Palancade and Doye, 2008). Even though SUMOylation effects on telomere localization are still not fully elucidated, initial reports have demonstrated that the SUMO E3 ligase Siz2p is required for the SUMOylation of the telomeric proteins Sir4, yKu70, and yKu80 (Denison et al., 2005; Wohlschlegel et al., 2004).

Furthermore, while the role that SUMOylation plays in the Sir4 biology is not clear, the absence of SUMOylation affects the telomere tethering mediated by the yKu pathway (Ferreira et al., 2011).

1.10 SUMOylation

SUMOylation is a PTM in which the ubiquitin-like protein SUMO is conjugated to a target protein (David, 2010; Hannich et al., 2005; Hwang et al., 2011; Impens et al., 2014; Palancade and Doye, 2008). Since its discovery in mid-1990, SUMOylation has been linked to biological

processes ranging from transcriptional regulation to DNA damage repair (Bettermann et al., 2011; Cremona et al., 2012; Cubeñas-Potts and Matunis, 2013; Müller et al., 2004; Palancade and Doye, 2008; Pasupala et al., 2012; Praefcke et al., 2011). Studies proposed that SUMO conjugation can modulate protein function, subcellular localization, and the formation of multi-protein complexes. An important aspect of SUMOylation is the reversible nature of this modification. Usually, SUMO targets undergo rapid cycles of SUMOylation and deSUMOylation, resulting in low levels of steady state SUMOylated proteins (Geiss-Friedlander and Melchior, 2007).

SUMOylation was initially discovered in budding yeast with the identification of the SUMO gene *SMT3* (Johnson and Gupta, 2001). Smt3 is a small 12 kDa protein that is conjugated to target proteins through an isopeptide bond between the lysine present in substrates and the C-terminal glycine of Smt3 (Geiss-Friedlander and Melchior, 2007; Müller et al., 2004). Despite the characterization of enzymes involved in the SUMOylation process, the effects of SUMOylation in a target protein are still not fully elucidated (David, 2010). To date, several high-throughput screenings have identified possible SUMO targets (Denison et al., 2005; Wohlschlegel et al., 2004). However, the low abundance of SUMOylated proteins in conjunction with inherent experimental difficulties create a challenging scenario in which to establish a global catalog of SUMOylated

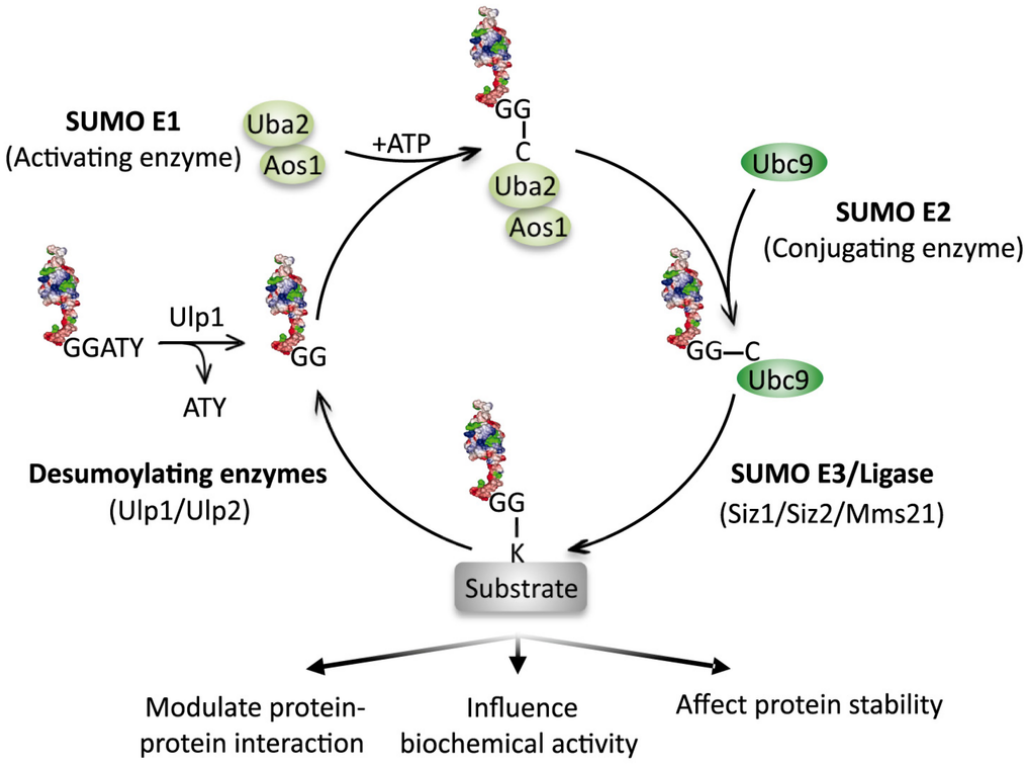

Figure 1-5. The SUMOylation cycle in S. cerevisiae.

The SUMOylation process is initiated by the C-terminal proteolytic activation of the immature Smt3 by Ulp1, thus exposing the C-terminal peptides - GG. After Smt3 maturation, the E1 heterodimer Aos1–Uba2 activates Smt3. Next, the activated Smt3 is transferred to the E2 enzyme Ubc9. Finally, the E3 ligases (Siz1, Siz2, Mms21, and Zip3) mediate the Smt3p ligation to the target protein. SUMOylation can be reversed by the action of the SUMO proteases Ulp1 and Ulp2. *Adapted from (Cremona et al., 2012)*

proteins (Makhnevych et al., 2009; Wilson and Heaton, 2008; Wohlschlegel et al., 2004).

1.10.1 SUMO proteins

SUMOylation is essential for most organisms and a well-conserved process throughout the eukaryotes. SUMO proteins are part of the ubiquitin-like proteins (Ubls) family (Hochstrasser, 2000; Hochstrasser, 2009). They share the characteristic globular β-grasp fold and the presence of a Gly-Gly motif at the C-terminus. The diglycine motif present at the C-terminus forms an immature form of SUMO (Bayer et al., 1998; Jadhav and Wooten, 2009). The cleavage of the diglycine motif is mediated by the SUMO-specific protease, and is required for the SUMO to conjugate with its target (David, 2010; Geiss-Friedlander and Melchior, 2007).

To date, SUMO proteins have been found in all eukaryotic cells. The mammalian cells express four variants (SUMO 1-4) while yeast expresses one (Smt3) (Miteva et al., 2010). The SUMO proteins contain less than 20% of amino acid identity, and they have a distinct distribution of surface charges (Yavuz and Sezerman, 2014). As a consequence, different SUMO proteins require different sets of enzymes and binding partners. Finally, a conserved stretch of ~20 amino acids is present at the N-terminus of all SUMO proteins. (David, 2010).

1.10.2 SUMO E1 enzymes:

The SUMO E1 enzyme has two subunits, SUMO-activating enzyme subunit 1 (Aos1) and SUMO-activating enzyme subunit 2 (Uba2) (Gong et al., 1999; Johnson et al., 1997). These enzymes activate the C-terminal domain of mature SUMO in a two-step ATP-dependent reaction. The first step involves the formation of a SUMO-adenylate conjugate, followed by a remodeling of the E1-active site and subsequent thioester bond between Uba2 and SUMO. The second step occurs when the thioester-charged E1 enzymes interact with Ubc9, finally transferring the SUMO peptide to the E2 enzyme (David, 2010; Okuma et al., 1999).

1.10.3 SUMO E2 enzymes

Ubc9 is the single E2 conjugating enzyme and not only delivers the activated SUMO to potential SUMOylation candidates, but is also directly involved in selecting the SUMO targets (Knipscheer et al., 2008). In order to be SUMOylated, SUMO targets must contain the peptides consensus motif yKxD/E, a sequence that can directly interact with Ubc9. The low-affinity binding observed between the Ubc9 and the consensus motif raised questions about how Ubc9 facilitates the targeting of specific proteins. To address this question, a study demonstrated that changes in Ubc9 expression altered the overall levels of SUMOylated proteins (Knipscheer et al., 2008). Furthermore, the target specificity of Ubc9 can be regulated by its interactions with other proteins, and by PTM such as

phosphorylation (David, 2010; Geiss-Friedlander and Melchior, 2007; Hwang et al., 2011; Müller et al., 2004).

1.10.4 SUMO E3 ligases

The SUMO E3 ligases mediates the transfer of the SUMO peptide from the SUMO E2 enzyme to a target protein (Hochstrasser, 2001). SUMO E3 ligase can be divided mainly into two groups of proteins, the larger group characterized by the presence of an SP-RING motif and a smaller group containing the vertebrate nucleoporin RanBP2 (Geiss-Friedlander and Melchior, 2007; Johnson and Gupta, 2001).

In budding yeast, proteins containing the SP-RING motif can be subdivided into two groups, the PIAS family, and the SP-RING ligases (Geiss-Friedlander and Melchior, 2007). Two proteins, Siz1 and Siz2, comprise the PIAS family. These proteins share a conserved N-terminus (~400 amino acids) in addition to the SP-RING motif. In addition to the PIAS family, the budding yeast also has two SP-RING ligases, Mms21 and Zip3 (Johnson and Gupta, 2001; Takahashi et al., 2001; Zhao and Blobel, 2005).

The SP-RING motif resembles the RING domain present in the ubiquitin E3 ligases. Several studies have provided a mechanism by which E3 ligases facilitate the SUMO transfer from the E2 enzyme to the target protein (Gareau and Lima, 2010). Generally, it is accepted that the SP-RING ligases bridge the interaction between the target protein and Ubc9,

and bind the SUMO non-covalently via the SUMO-interacting motif (SIM) and SUMO binding motif (SBM) present in the target protein (Song et al., 2004). Thus, it is assumed that E3 ligases create a platform responsible for positioning the thioester-charged formed between the SUMO-Ubc9 and the target protein in an orientation favoring the SUMO transfer (Gareau and Lima, 2010).

SUMOylation usually occurs through the addition of a single SUMO peptide to an individual Lys acceptor. However, the addition of a polySUMO chain has been well documented in budding yeast. To date, the biological relevance of polySUMO chains is still not fully understood, but studies performed in yeast strains unable to form polySUMO chains showed a deficiency in the completion of meiosis (Mullen et al., 2011).

1.10.5 SUMO Proteases:

SUMO proteases have two functions: maturation of the SUMO protein by cleaving the diglycine motif present at the C-terminus, and removal of SUMO from targeted proteins (Hickey et al., 2012). Despite the critical role of SUMO maturation, there is no conclusive evidence demonstrating this is the rate-limiting step for SUMOylation. Conversely, deSUMOylation rates are essential to determine the steady state levels of SUMOylated proteins (Hay, 2007; Mukhopadhyay and Dasso, 2007; Sharma et al., 2013; Wang and Dasso, 2009).

To date, only a small number of cysteine proteases have been identified as SUMO isopeptidases. In budding yeast, the SUMO isopeptidase family encompasses two proteins, Ulp1 and Ulp2 (Wang and Dasso, 2009). Importantly, the N-terminal domain of these proteins plays a role in determining target specificity and intracellular localization. While Ulp2 is mainly present dispersed across the nucleoplasm, Ulp1 is anchored to the nuclear envelope through its interaction with NPCs (Geiss-Friedlander and Melchior, 2007). Ulp1p localization at NPCs has been conserved during evolution. In budding yeast, Ulp1 association with NPCs requires the interaction between its N-terminal domain with two nuclear transport factors, Kap121 (residues 1-150) and Kap60-95 (residues 150-340). The interaction between Kaps and Ulp1 does not require the Ran-GTP gradient, suggesting that Ulp1 might establish a permanent interaction with Kaps (Palancade and Doye, 2008). Moreover, the Ulp1 association with NPC also requires the nuclear basket nucleoporins Nup60, Mlp1, and Mlp2. This observation is further supported by the exclusion of Ulp1 from regions abutting the nucleolus, similar to what has been observed for Mlps proteins. Furthermore, a recent study showed that the deletion of the *ESC1* gene affects the assembly of the nuclear basket, and consequently relocalizes Ulp1 to a few perinuclear foci containing Nup60 and Mlps (Lewis et al., 2007).

The fact that overexpression of Ulp1 or its binding partner Kap121 leads to an even distribution across the NE, including the regions devoid

of NPCs, raises the possibility of an additional mechanism for tethering Ulp1 at the nuclear envelope. Finally, Ulp1 levels and localization are affected in cells carrying mutations in the Nup84 complex (Nagai et al., 2008; Palancade et al., 2007a). Based on the observation that Nup84 mutations do not alter the distribution of Nup60 and Mlps, the mislocalization of Ulp1 cannot be attributed to the disruption of the nuclear basket.

1.10.6 SUMOylation cycle

In summary, the SUMOylation cycle starts with the maturation of the SUMO peptide by Ulp1. After the maturation step, the E1 activation enzymes (Aos1/Uba2) activate SUMO. Following the peptide activation, an E2 conjugating enzyme (Ubc9) conjugates the SMT3 to the target protein. Finally, E3 ligase enzymes (Siz1, Siz2, Mms21 and Zip3) catalyze the isopeptide bond between the SUMO peptide and the acceptor lysine in the target protein. SUMOylation can be reversed by the action of deSUMOylation enzymes Ulp1p and Ulp2p (David, 2010; Wilkinson and Henley, 2010).

1.11 Dissertation focus

The current literature has a vast amount of work linking chromatin regulation/organization with Esc1p, NPCs, and SUMOylation. However,

despite all these observations we still do not completely understand the relationship between these proteins and chromatin regulation. Previously, we described how Nup170 regulates chromatin tethering and gene silencing. This dissertation focuses on identifying new Nup170 interactors, and understanding how this protein interaction network is altered in order to modulate chromatin localization. Initially, we found that Sir4 and Nup170 present a similar enrichment profile across the budding yeast genome. Through biochemical analysis, we identified a protein interaction network formed between Nup170, Esc1p, and Sir4p. Moreover, the deletion of any single gene present in this network disturbs the distribution of the remaining proteins, further indicating a functional link between these proteins. We also showed that Sir4p interacts with nups from the inner and outer rings, leading us to propose the existence of a distinct population of NPCs, hereby named Sir4-associate Nup or Snup. Importantly, we also observed that the SUMO E3 ligase Siz2p interacted with Sir4 and the Snup proteins. Finally, we showed that SUMOylation mediated by Siz2p is required to increase the Sir4p affinity for chromatin, indicating that Siz2 presence in the Snup complex might have an important role in chromatin biology.

2. Experimental Procedures

2.1 Yeast strains and media

The yeast strains were grown at 30°C in YPD (1% yeast extract, 2% bactopeptone and 2% glucose) with constant agitation to a mid-log phase (OD_{600} 0.3-1.0). Selection for yeast strains transformed with plasmid harboring prototrophic markers were performed by using synthetic drop out complete medium (SC) lacking the necessary nutrient and 2% glucose. Yeast transformations by autonomously replicating plasmid or PCR derived liner DNA were performed using the lithium acetate/polyethylene glycol method (Gietz and Woods, 2002). Briefly, overnight cell cultures (15 mL) were grown to early-logarithmic growth phase (OD600 ≤ 0.5), harvested by centrifugation (Eppendorf 5810R, A-4-62 rotor at 6000 x g for 2 min), washed once with 2 mL ddH2O, and then washed with 1 mL transformation buffer (10 mM Tris-HCl pH 7.5, 1 mM EDTA, 100 mM LiOAc). Cells were re-suspended with 50 µL of transformation buffer, and 300 µL of PEG solution (0.8 g/mL polyethylene glycol 3350 in transformation buffer). Following, 10 µL of 3 mg/mL heat-denatured salmon sperm DNA, and 5 µg of the PCR-amplified transformation cassette were added and mixed vigorously. The cells were then incubated at 30°C for 1 h, and heat shocked at 42°C for 15 min in a water bath. The cells present in the solution were harvested by centrifugation (Beckman Coulter microfuge 18, 6000 x g for 30 s) and the resulting cell pellets were diluted in 1 mL and incubated at 30° C for 3 h prior to plating on appropriate marker selection plates.

Genomic manipulation, such as gene fusion and deletion, were performed using the PCR-based, one-step method for gene modification (Longtine et al., 1998). DNA cassettes used for genomic integration were PCR-amplified using the Expand High Fidelity PCR system (Roche Applied Science, Indianapolis, IN, USA). The PCR templates were preferably isolated from chromosomal DNA, or less preferably, from plasmid DNA. For genomic integrations of carboxy-terminal protein A, $V5_3$, 13xMYC, eGFP, RFP-T, ~60 bp oligonucleotide primers were designed with 40 bp 5'-overhangs that anneal to regions immediately upstream and downstream of the stop codon of the gene of interest. All the positive colonies were primarily confirmed by PCR, and when possible, western blotting or microscopy.

To overcome possible genomic stability, "fresh" haploid of *nup170Δ* strains were isolated by tetrad dissection of a heterozygous NUP170/*nup170Δ* diploid strain prior to experimentation. When unable to perform tetrad dissections, the *nup170Δ* strains were constructed by integrative transformation. Tetrads were genotyped by platting assay and PCR analysis. Positive transformants were grown overnight and frozen stocks for use in future experiments.

Table 2-1. Yeast Strains

Strain	Relevant Genotype	Source
BY 4741	*MATa his3Δ1 leu2Δ0 ura3Δ0 met15Δ0*	Brachmann et al., 1998
BY	*MATα his3Δ1 leu2Δ0 ura3Δ0 lys3Δ0*	Brachmann

4742		et al., 1998
DVY 1713	*MATa his3Δ1 leu2Δ0 ura3Δ0 met15Δ0 nup170Δ::natR*	This Study
CPY 3726	*MATa his3Δ1 leu2Δ0 ura3Δ0 met15Δ0 GFP-Siz2::HIS5 Nup170-RFP::natR*	This Study
CPY 3757	*MATa his3Δ1 leu2Δ0 ura3Δ0 met15Δ0 Esc1-pA::URA Nup170-13xMYC::hphR mlp1Δ::natR mlp2Δ::kanR*	This Study
DL 164	*MATa his3Δ1 leu2Δ0 ura3Δ0 met15Δ0 Mlp1-eGFP::HIS5*	This Study
DL 165	*MATa his3Δ1 leu2Δ0 ura3Δ0 met15Δ0 Mlp2-eGFP::HIS5*	This Study
DL 284	*MATa his3Δ1 leu2Δ0 ura3Δ0 met15Δ0 Sir4-pA::HIS5 Nup170-13xMYC::kanR bar1Δ::natR*	This Study
DL 286	*MATa his3Δ1 leu2Δ0 ura3Δ0 met15Δ0 Esc1-pA::HIS5 Nup170-13xMYC::kanR bar1Δ::natR*	This Study
DL 290	*MATa his3Δ1 leu2Δ0 ura3Δ0 met15Δ0 Mps3-pA::HIS5 Nup170-13xMYC::kanR bar1Δ::natR*	This Study
DL 294	*MATa his3Δ1 leu2Δ0 ura3Δ0 met15Δ0 siz1Δ::natR*	This Study
DL 296	*MATa his3Δ1 leu2Δ0 ura3Δ0 met15Δ0 siz2Δ::natR*	This Study
DL 304	*MATa his3Δ1 leu2Δ0 ura3Δ0 met15Δ0 Sir4-pA::HIS5 Nup170-13xMYC::kanR bar1Δ::natR siz2Δ::hphR*	This Study
DL 313	*MATa his3Δ1 leu2Δ0 ura3Δ0 met15Δ0 Esc1-pA::HIS5 Sir4-13xMYC::KanR bar1Δ::natR nup170Δ::HphR*	This Study
DL 331	*MATa his3Δ1 leu2Δ0 ura3Δ0 met15Δ0 Sir4-pA::HIS5 Nup170-13xMYC::HphR bar1Δ::natR esc1Δ::KanR*	This Study
DL 345	*MATa his3Δ1 leu2Δ0 ura3Δ0 met15Δ0 Esc1-pA::HIS5 Nup170-13xMYC::HphR bar1Δ::natR sir4Δ::KanR*	This Study
DL 352	*MATa his3Δ1 leu2Δ0 ura3Δ0 met15Δ0 Esc1-pA::URA Nup170-13xMYC::hphR bar1Δ::natR siz2Δ::kanR*	This Study
DL 371	*MATa his3Δ1 leu2Δ0 ura3Δ0 met15Δ0 Esc1-eGFP::HIS5 p[Nop1-RFP::URA]*	This Study
DL 372	*MATa his3Δ1 leu2Δ0 ura3Δ0 met15Δ0 Esc1-eGFP::HIS5 nup170Δ::KanR p[Nop1-RFP::URA]*	This Study
DL 375	*MATa his3Δ1 leu2Δ0 ura3Δ0 met15Δ0 Esc1-eGFP::HIS5 siz2Δ::KanR p[Nop1-RFP::URA]*	This Study
DL 376	*MATa his3Δ1 leu2Δ0 ura3Δ0 met15Δ0 Esc1-eGFP::HIS5 sir4Δ::KanR p[Nop1-RFP::URA]*	This Study

DL 382	*MATa his3Δ1 leu2Δ0 ura3Δ0 met15Δ0 Mlp1-eGFP::HIS5 nup170Δ::hphR*	This Study
DL 383	*MATa his3Δ1 leu2Δ0 ura3Δ0 met15Δ0 Mlp2-eGFP::HIS5 nup170Δ::hphR*	This Study
DL 389	*MATa his3Δ1 leu2Δ0 ura3Δ0 met15Δ0 Nup84-eGFP::HIS5 nup133Δ::KanR*	This Study
DL 397	*MATa his3Δ1 leu2Δ0 ura3Δ0 met15Δ0 Nup159-eGFP::HIS5 nup133Δ::KanR*	This Study
DL 404	*MATa his3Δ1 leu2Δ0 ura3Δ0 met15Δ0 Pom34-eGFP::His5*	This Study
DL 405	*MATa his3Δ1 leu2Δ0 ura3Δ0 met15Δ0 Nup53-eGFP::His5*	This Study
DL 408	*MATa his3Δ1 leu2Δ0 ura3Δ0 met15Δ0 Nup170-eGFP::His5*	This Study
DL 410	*MATa his3Δ1 leu2Δ0 ura3Δ0 met15Δ0 Nup53-eGFP::HIS5 nup133Δ::KanR*	This Study
DL 411	*MATa his3Δ1 leu2Δ0 ura3Δ0 met15Δ0 Nup157-eGFP::HIS5 nup133Δ::KanR*	This Study
DL 412	*MATa his3Δ1 leu2Δ0 ura3Δ0 met15Δ0 Nup188-eGFP::HIS5 nup133Δ::KanR*	This Study
DL 426	*MATa his3Δ1 leu2Δ0 ura3Δ0 met15Δ0 Nup170-eGFP::HIS5 nup133Δ::KanR*	This Study
DL 429	*MATa his3Δ1 leu2Δ0 ura3Δ0 met15Δ0 Sir4-eGFP::His5 Nup170-TagRFP-T::natR*	This Study
DL 444	*MATa his3Δ1 leu2Δ0 ura3Δ0 met15Δ0 Nup157-eGFP::HIS5 Nup170-TagRFP-T::natR*	This Study
DL 445	*MATa his3Δ1 leu2Δ0 ura3Δ0 met15Δ0 Nup188-eGFP::HIS5 Nup170-TagRFP-T::natR*	This Study
DL 462	*MATα his3Δ1 leu2Δ0 ura3Δ0 met15Δ0 Sir4-eGFP::NatR Sec63-TagRFP-T::His5*	This Study
DL 463	*MATα his3Δ1 leu2Δ0 ura3Δ0 met15Δ0 Sir4-eGFP::NatR Sec63-TagRFP-T::His5 esc1Δ::KanR*	This Study
DL 465	*MATα his3Δ1 leu2Δ0 ura3Δ0 met15Δ0 Sir4-eGFP::NatR Sec63-TagRFP-T::His5 siz2Δ::KanR*	This Study
DL 467	*MATα his3Δ1 leu2Δ0 ura3Δ0 met15Δ0 Sir4-eGFP::NatR Sec63-TagRFP-T::His5 nup170Δ::KanR*	This Study
DL 474	*MATa his3Δ1 leu2Δ0 ura3Δ0 met15Δ0 Nup53-eGFP::HIS5 esc1Δ::KanR*	This Study
DL 477	*MATa his3Δ1 leu2Δ0 ura3Δ0 met15Δ0 Nup53-eGFP::HIS5 siz2Δ::KanR*	This Study
DL 479	*MATa his3Δ1 leu2Δ0 ura3Δ0 met15Δ0 Nup53-eGFP::HIS5 siz2Δ::KanR*	This Study
DL	*MATa his3Δ1 leu2Δ0 ura3Δ0 met15Δ0 Nup60-*	This Study

488	*Tap::HIS5 Nup170-3xHA::kanR*	
DL 490	*MATa his3Δ1 leu2Δ0 ura3Δ0 met15Δ0 Nup53-Tap::HIS5 Nup170-3xHA::kanR*	This Study
DL 494	*MATa his3Δ1 leu2Δ0 ura3Δ0 met15Δ0 Nup53-eGFP::HIS5 Nup170-TagRFP-T::natR*	This Study
DL 495	*MATa his3Δ1 leu2Δ0 ura3Δ0 met15Δ0 Sir4-eGFP::HIS5 Nup53-TagRFP-T::natR*	This Study
DL 506	*MATa his3Δ1 leu2Δ0 ura3Δ0 met15Δ0 Sir4-pA::HIS5 Nup170-13xMYC::hphR bar1Δ::natR Nup188-V5$_3$::Kan*	This Study
DL 508	*MATa his3Δ1 leu2Δ0 ura3Δ0 met15Δ0 Sir4-pA::HIS5 Nup170-13xMYC::hphR bar1Δ::natR Nup192-V5$_3$::Kan*	This Study
DL 509	*MATa his3Δ1 leu2Δ0 ura3Δ0 met15Δ0 Sir4-pA::HIS5 Nup170-13xMYC::hphR bar1Δ::natR Nup157-V5$_3$::Kan*	This Study
DL 515	*MATa his3Δ1 leu2Δ0 ura3Δ0 met15Δ0 Sir4-eGFP::His5 Nup157-TagRFP-T::natR*	This Study
DL 518	*MATa his3Δ1 leu2Δ0 ura3Δ0 met15Δ0 Nup84-eGFP::HphR*	This Study
DL 522	*MATa his3Δ1 leu2Δ0 ura3Δ0 met15Δ0 Nup60-eGFP::HIS5 Nup170-TagRFP-T::natR*	This Study
DL 525	*MATa his3Δ1 leu2Δ0 ura3Δ0 met15Δ0 Nup157-eGFP::His5 Nup53-TagRFP-T::natR*	This Study
DL 526	*MATa his3Δ1 leu2Δ0 ura3Δ0 met15Δ0 Nup170-eGFP::His5 Nup53-TagRFP-T::natR*	This Study
DL 527	*MATa his3Δ1 leu2Δ0 ura3Δ0 met15Δ0 Nup60-eGFP::His5 Nup53-TagRFP-T::natR*	This Study
DL 529	*MATa his3Δ1 leu2Δ0 ura3Δ0 met15Δ0 Nup188-eGFP::His5 Nup53-TagRFP-T::natR*	This Study
DL 532	*MATa his3Δ1 leu2Δ0 ura3Δ0 met15Δ0 Nup170-eGFP::His5 sir4Δ::KanR*	This Study
DL 534	*MATa his3Δ1 leu2Δ0 ura3Δ0 met15Δ0 Nup53-eGFP::His5 sir4Δ::KanR*	This Study
DL 535	*MATa his3Δ1 leu2Δ0 ura3Δ0 met15Δ0 Pom34-eGFP::His5 sir4Δ::KanR*	This Study
DL 536	*MATa his3Δ1 leu2Δ0 ura3Δ0 met15Δ0 Nup84-eGFP::His5 sir4Δ::KanR*	This Study
DL 537	*MATa his3Δ1 leu2Δ0 ura3Δ0 met15Δ0 Siz2-PrA::His5 Nup157-V5$_3$::KanR*	This Study
DL 538	*MATa his3Δ1 leu2Δ0 ura3Δ0 met15Δ0 Sir4-PrA::His5 Esc1-V5$_3$::KanR*	This Study

2.2 Plasmid

The following plasmids were provided by others and used in this dissertation: pRS313, CEN/HIS3 (Sikorski and Hieter, 1989). pRS315, CEN/LEU2 (Sikorski and Hieter, 1989). The following plasmids were a gift of Dr. Susan Gasser, Friedrich Miescher Institute, Basel, Switzerland: The plasmid pSR13 was used for tagging telomeres with ~256xLacO::LEU2, and the plasmid pAFS78, carrying GFP-LacI::His3, was used to target and localize telomeres containing the 256xLacO array (Rohner et al., 2008).

Genomic integrations of carboxy-terminal gene fusions were carried out by amplifying PCR cassette from plasmids pGFP/HIS5 (EGFPF64L,S65T-HIS5) (Lee et al., 2013), pRFP-T/HIS5 (RFP-T::HIS5) (Lee et al., 2013) were kind gifts from Dr. Richard Rachubinski, University of Alberta, AB, Canada. The pBXA plasmid (protein-A/HIS5) (Aitchison et al., 1995), pFA6a-13Myc-kanMX6 (13xMYC-KanR) (Longtine et al., 1998). The following plasmids were generated for this work in which the inserts were PCR-amplified from genomic DNA using the Expand High Fidelity PCR system (Roche Applied Science, Indianapolis, IN, USA). The plasmid pTM1198 was made by modifying the plasmid pFA6-GFP(S65T)-kanMX6 (Longtine et al., 1998), wherein the coding sequence for GFP(S65T), bounded by the Pac1 and Asc1 restriction enzyme sites, was replaced by the coding sequence for $V5_3$, using the same restriction enzyme sites. pSIZ2pr-GFP was made by modifying the plasmid pFA6-HisMX6-PGAL1-GFP (Longtine et al., 1998), wherein the GAL1 promoter sequence,

bounded by the Bgl-II and Pac1 restriction enzyme sites, was replaced by the SIZ2 promoter sequence, using the same restriction enzyme sites.

Table 2-2. Plasmids

Plasmid	Background	Source/Reference
pSR13	~256xLacO::LEU2	(Rohner et al., 2008) (Provided by Dr. Susan Gasser, Friedrich Miescher Institute, Switzerland)
pAFS78	GFP-LacI::HIS3	(Rohner et al., 2008) (Provided by Dr. Susan Gasser, Friedrich Miescher Institute, Switzerland)
pGFP	eGFP-S65T,F64L-HIS5	(Lee et al., 2013) (Provided by Dr.Richard Rachubinski, University of Alberta, Edmonton, AB)
pTagRFP-T	TagRFP-S158T-HIS5	Lee et al., 2013 (Provided by Dr. Richard Rachubinski, University of Alberta, Edmonton, AB)
pBXA	Protein A-His5	(Aitchison et al., 1995)
p13xMYC	pFA6a-13xMyc-kanMX6	(Longtine et al., 1998)
pNop1-RFP	pRS316-Nop1-RFP-URA	(Sydorskyy et al., 2005)
pTM1198	pFA6a-3xV5-kanMX6	This Study
pSIZ2pr-GFP	pFA6a-His3MX6-SIZ2pr-GFP	This Study

2.3 Antibodies and buffers:

Table 2-3. Antibodies

Antibody	Dilution	Type	Source/References
α-Nup53	1:5000	Rabbit polyclonal	Lusk et al., 2002
α-Gle1	1:500	Rabbit polyclonal	Suntharalingam et al., 2004 (Provided by Dr. Ben Montpetit, UC Davis, Davis, CA)
α-Mlp1	1:5	Mouse monoclonal	Strambio-de-Castillia et al., 1999 (Provided by Dr. Michael P. Rout, Rockefeller University, New York, NY)
α-Pom152	1:5	Mouse monoclonal	Marelli et al., 2001
α-Sir4	1:2500	Rabbit polyclonal	Rudner et al., 2005 (Provided by Dr. Adam Rudner, University of Ottawa, Ontario, ON)
α-PrA	1:10000	Rabbit polyclonal	Sigma (Cat No: P3775)
α-Myc (9E10)	1:5000	Mouse monoclonal	Roche (Cat No: 11667149001)
α-V5 (ab27671)	1:5000	Mouse monoclonal	Abcam (Cat No: ab27671)

Table 2-4. Solutions:

Buffer	Composition
FACS buffer	50 mM Tris-HCl, pH8.0
Pre-lysis IP wash buffer	20 mM HEPES-KOH, pH 7.4, 110 mM KOAc, 2 mM MgCl2
IP wash buffer	20 mM HEPES-KOH, pH 7.4, 110 mM KOAc, 2 mM MgCl2, 0.1% Tween-20, 1:5000 dilution antifoam B
IP buffer	20 mM HEPES-KOH, pH 7.4, 110 mM KOAc, 2mM $MgCl_2$, Tween-20, antifoam-B emulsion (1:5000), protease inhibitor pellets (complete EDTA-free)
K-Pi buffer	100 mM potassium phosphate, pH 6.5
PBS	137 mM NaCl, 2.7 mM KCl, 4.3 mM Na2HPO4, 1.4 mM KH2PO4, pH 7.4
PBS-T	137 mM NaCl, 2.7 mM KCl, 4.3 mM Na2HPO4, 1.4 mM KH2PO4, pH 7.4, 1% Tween-20
SDS-PAGE sample buffer	0.5 M Tris-base, 100 mM DTT, 15% glycerol, 6.5% SDS, 0.25% bromophenol blue
TE	10 mM Tris-HCl, 1 mM EDTA, pH7.5
Transformation buffer	10 mM Tris-HCl, pH 7.5, 1 mM EDTA, 100 mM LiOAc
Yeast breaking buffer	2% Triton X-100, 1% SDS, 100 mM NaCl, 10mM Tris-HCl pH 8.0, 1mM EDTA pH 8.0.
Milk blocking buffer	5% skim milk powder, 0.1% Tween-20, 20mM Tris-HCl pH 7.5, 150 mM NaCl
BSA blocking buffer	2.5% skim milk powder, 0.1% Tween-20, 20mM Tris-HCl pH 7.5, 150 mM NaCl
Amido black	40% methanol, 10% acetic acid, 0.1% amido black

2.4 Affinity purification

2.4.1 Affinity purification of protein-A fusion proteins

The Protein-A tagged proteins were purified from the cell lysate by using magnetic beads coupled with IgG. Epoxy activated Dynabeads (Invitrogen) were conjugated with Rabbit IgG (Sigma-Aldrich) as previously described (7). Yeast strains producing the protein fusion of interest (Nup53-TAP, Nup60-TAP, Esc1-PrA, Mps3-PrA, Sir4-PrA, Siz1-PrA, and Siz2-PrA) were grown in 2 L cultures of YPD to an OD600 of 0.8-1.0 and then harvested. Cells were washed twice with 500 mL of water and once with 250 mL of washing buffer (20mM HEPES buffer pH 7.4, 110mM potassium acetate, 2mM magnesium chloride). After the washing step, the cells were pelleted and transferred to a syringe. Cells were flash frozen by passage into liquid nitrogen to form frozen yeast "noodles". Frozen yeasts were ground using a planetary ball mill (PM100; Reitch), yielding 1.0- 2.0 grams of lysed cell powder. The cell powder was suspended in lysis buffer at a proportion of 1 g of cell lysate to 2 mL of lysis buffer (20mM HEPES buffer pH 7.4, 110mM potassium acetate, 2mM magnesium chloride, 0.1% Tween-20, antifoam-B emulsion [1:5000] and protease inhibitor pellets [complete EDTA-free; Roche]). The cell solution was incubated on ice for 30 minutes, with agitation every five minutes, for complete protein solubilization. After incubation, the lysate was cleared by centrifugation (1500 x g for 10 min at 4ºC). The cleared lysates were

incubated with IgG-conjugated magnetic beads in a proportion of 3 mg of beads to 2 ml of lysate. Cleared lysate and beads were incubated for 1 hour at 4ºC with rotation. After incubation, beads were pelleted using a magnet and washed with lysis buffer. Proteins bound to the beads were eluted using incremental concentrations of MgCl2 (0.05, 0.5 and 2M). A final elution using 0.5M of acetic acid was used to release the Protein-A from the beads. Eluates were subjected to TCA precipitation and lyophilized in a CentriVap Centrifugal Vacuum (Labconco).

2.4.2 IgG-conjugated magnetic beads

The IgG conjugation to magnetic beads was performed as described (Alber et al., 2007a). First, 8 mg rabbit lyophilized IgG (Sigma-Aldrich, St. Louis, MO, USA) was dissolved in 800 µL Na-phosphate buffer (0.1 M NaPO4 pH 7.4) and then cleared by centrifugation (Eppendorf 5810R, F45-30-11 rotor at 20800 x g for 10 min at 4°C). Second, 2 mL Na-phosphate buffer and 1.33 mL of 3 M ammonium sulfate pH 7.5 were added to the cleared IgG. This IgG solution was filtered through a 0.22 µm low-protein binding PVDF filter syringe by (Millipore, Billerica, MA, USA). Third, the filtered IgG solution was added to 60 mg of pre-washed Epoxy M-270 Dynabeads (Invitrogen, Carlsbad, CA, USA). Fourth, the IgG conjugation to the magnetic beads was incubated for 20 hours at 30°C with rotation. Finally, IgG-conjugated beads were washed in the following order: once with 1 mL 100 mM glycine pH 2.5, once with 1 mL 10 mM Tris

pH 8.8, once with 1 mL 100 mM triethylamine pH 6.0, four times with 1 mL PBS for 5 min, once with 1 mL PBS + 0.5% triton X-100 for 5 min, once with 1 mL PBS + 0.5% triton X-100 for 15 min, followed by three consecutive washes with 1 mL PBS for 5 min. Washed beads were then resuspended in 2 mL PBS + 0.02% sodium azide and stored at 4°C.

2.5 Western blotting

2.5.1 Preparation of yeast whole cell lysate:

The whole cell lysates were acquired from overnight cultures at an OD_{600} of 1.0. The cells from 1 mL of culture were pelleted by centrifugation, and then washed with ddH_2O. Cells pellets were resuspended in SDS-PAGE sample buffer, sonicated and boiled in a heating block at 94ºC for approximately 10 minutes. Following denaturation, samples were clarified by centrifugation and loaded onto SDS-PAGE gels for analysis.

2.5.2 SDS-PAGE and western blotting analysis:

Proteins were separated using SDS-PAGE and transferred to nitrocellulose membranes. Membrane containing proteins were blocked using PBS containing 0.1% Tween-20 and 5% milk powder. The Protein-A or TAP was detected using 1:10000 dilution of rabbit polyclonal IgG (anti-PrA), Sir4p was identified using the rabbit polyclonal anti-Sir4 in a 1:2500

dilution (a generous gift from Dr. Adam Rudner, University of Ottawa, ON, Canada), Nup53p and Nup60p were detected by the rabbit polyclonal Nup53 and Nup60 antibodies in a concentration of 1:5000 (15), the SUMOylated proteins were detected by rabbit polyclonal SMT3 antibody in a concentration of 1:10000. Gle1p was detected using the rabbit polyclonal Gle1 antibody in a concentration of 1:500 (generous gift from Dr. B. Montpetit, University of Alberta, AB, Canada), Mlp1p and Pom152 were detected by rabbit polyclonal Mlp1 and Pom152 antibodies in a concentration of 1:5 (gift from Dr. Michael P. Rout, Rockefeller University, NY, USA). The V5 tagged proteins were identified using the mouse monoclonal anti-V5 antibody (ab27671; Abcam) and the Myc-tagged proteins were detected using the mouse monoclonal anti-Myc antibody in a 1:5000 dilution (9E10; Roche).

2.5.3 Protein quantification:

The amount of interacting protein purified to selected PrA fusions in WT and deletion mutants were compared. The PrA fusions were affinity-purified from WT and mutant strains in parallel and under identical conditions. Fractions were analyzed simultaneously by western blotting as described above. Images of scanned membranes were analyzed using the ImageQuant software (GE) to determine total pixel intensities (TPI) of the interacting species present in the Mg^{2+} elution fractions - 50 mM, 0.5 M and 2 M. The pixels from the three samples were added, and then the

background pixels were subtracted, thus yielded a total pixel intensity for the interaction protein (TPIIP). Western blot analysis was also used to determine the total pixel intensities of the bound PrA fusion (TPIPrA). The amount of the interacting protein eluted relative to the amount of PrA bound to beads, was then determined by calculating the TPIIP/TPIPrA ratio. These values were then scaled such that the relative amount of interacting protein that co-purified with the PrA fusion (TPIIP/TPIPrA ratio) derived from WT cell was set at 1.0. TPIIP/TPIPrA ratio from the deletion mutant cell extract was expressed as a ratio relative to WT.

2.6 Cell cycle arrest and release

For affinity purification experiments, cells carrying a deletion in the *BAR1* gene were grown overnight in 6 L of YPD at 30ºC to an OD_{600}: 0.4-0.5. To arrest cells in G1-phase, cultures were incubated for 3 hours with the yeast pheromone α-factor in a final concentration of 10ng/mL. The cell morphology was used to evaluate the arrest efficiency. After <95% of cells were synchronized in G1-phase, they were released from the cell cycle arrest by washing the cultures with ice cold water, and resuspended in fresh YPD containing 10µg/mL of Pronase E (Heichman and Roberts, 1996). The release efficiency was immediately measured by the budding index, and later evaluated by flow cytometry and Clb2p levels. The samples were harvested every 30 minutes and store at -80ºC for affinity purification.

For assessing the levels of Siz2 post translational modification during the cell cycle progression, strains carrying Siz2-$V5_3$ and respective Siz2- $V5_3$ mutation were grown overnight in 20 mL of YPD to an OD_{600}: 0.4-0.5. Prior to G1-arrest, cells were harvested by centrifugation, and resuspended in YPD containing α-factor in a final concentration of 1µg/mL. Cultures containing α-factor were incubated at 30ºC for 2 hours, and arrest efficiency was initially assessed by budding index and posteriorly by Clb2 levels. Cell cycle release was performed by washing cultures with ice cold water, and then incubated in fresh YPD. Samples were harvested every 10 minutes for the total time of 120 minutes. The levels of Siz2 post translational modification was measured by SDS-PAGE and Western Blot.

2.7 FACS analysis

Cells were washed once with 50mM of Tris-HCl (pH 8.0), fixed with 70% ethanol and stored at 4ºC overnight. Prior analysis by flow cytometry, samples were washed twice 50mM of Tris-HCl (pH 8.0) and incubated for 2 hours at 37ºC with 200µg of heat-inactivated RNAseA. After incubation, cells were pelleted and resuspended in 1mg/ml of Pepsin and incubated for 1 hour at 37ºC. Following, cells were washed with 50mM of Tris-HCl (pH 8.0) and the genetic material was stained using Propidium Iodide (180mM Tris Base, 190mM NaCl, 150mM MgCl2, 1µg/ml Propidium Iodide). The DNA content in the samples was evaluated using the BD FACSDiva and visualized usingt BD FACSDiva Software.

2.8 Fluorescence Microscopy

All images were acquired using the epifluorescence microscope Axio Observer.Z1 microscope (Carl Zeiss Inc.), equipped with an UPlanS-Apochromat 100x/1.40 NA oil objective lens (Carl Zeiss Inc.) and an AxioCam MRm digital camera with a charge-coupled device (Carl Zeiss Inc.). All cells used for live cell imaging were grown in YPD liquid culture to an OD600 ~0.5. Cells were harvested, washed once with SC medium then pelleted and suspended in a small volume of SC medium to ~10^6 cells/µL. Prior to imaging, 1.5 µL of cell suspension was spotted onto a microscope slide coated with a 2% agarose pad. AxioVision software and rendered using Image J software (National Institute of Health) for display.

2.9 Image analysis

2.9.1 Subnuclear localization of telomere 14-L

Yeast cells containing the ~256xLacO array repeats inserted into the ~19 kb from Tel14-L, and its interactor partner Lac-I fused with GFP to fluorescent locate the tagged telomere were grown in YPD medium supplemented with adenine (40µg/mL). Before imaging, cells were washed twice with SC medium, and immobilized on 2% agarose pads. Telomere position inside the nucleus was determined relative to the NE marker Sec63-eGFP (Tel14-L) (Van de Vosse et al., 2013). The images were

acquired as 12-18 consecutive 0.2 µm stacks in the Z-axis. Only the telomere present in the stack containing the brightest foci was counted. The telomere sub-nuclear localization was determined by dividing the telomere distance from the NE (TD) by the nuclear radius (r). The TD/r ratio (R) was used to group telomeres into three concentric zones of equal area. Zone 1 represents foci with ratios ≤ 0.184 x R, zone 2 foci with ratios > 0.184 x R and < 0.422 x R, and zone 3 represents foci with ratios ≥ 0.422 x R.

2.9.2 Sir4-GFP tethering to the NE

The *SIR4* gene was C-terminally fused with eGFP, thus rendering the expression of Sir4-eGFP. Next, we deleted the *nup170Δ, esc1Δ, siz2Δ* genes in the Sir4-eGFP strain, and evaluated the effects of each deletion on the Sir4 perinuclear localization were defined by their co-localization with the NE/ER marker Sec63-RFP-T. Cells producing the Sir4-eGFP Sec63-RFP-T fusions were acquired as 12-18 consecutive 0.2 µm stacks in the Z-axis. Images were deconvolved using the nearest neighbour function of the AxioVision software deconvolution module (Carl Zeiss Inc.), and rendered using ImageJ (National Institute of Health). Distinct Sir4-eGFP foci were counted, and grouped as either: colocalizing, where complete or partial signal overlap was observed between Sir4-eGFP and Sec63-RFP-T, or not colocalizing, where no signal overlap was observed between Sir4-eGFP and Sec63-RFP-T. Percent co-localization was then

expressed as the number of colocalizing Sir4-eGFP foci divided by the total number of Sir4-eGFP foci, and these values plotted on a bar graph and error bars shown indicate Standard Deviation (SD).

2.9.3 Esc1-eGFP exclusion from nucleolar region

Esc1 localization surrounding the nuclear envelope was assessed by C-terminally tagging the *Esc1* gene with GFP, and Nop1-RFP expressed from plasmid. The reference strain containing Esc1-eGFP and Nop1-RFP were transformed with PCR cassettes containing different gene deletion (*nup170Δ, sir4Δ, siz2Δ, nup53Δ*). Images of reference and mutant cells carrying the Esc1-eGFP Nop1-RFP fusions were acquired as 12-18 consecutive 0.2 µm stacks in the Z-axis. Images were deconvolved using the nearest neighbour function of the AxioVision software deconvolution module (Carl Zeiss Inc.), and rendered using ImageJ (National Institute of Health). Only those cells in which the Esc1-GFP and Nop1-RFP signals were clearly visible in the focal plane of the acquired image were counted. Those cells in which the Esc1-GFP signal has excluded from regions of the NE abutting the nucleolus and those cells that showed a clear localization at the NE adjacent to the nucleolus were counted. The percentage of the total cells showing exclusion was plotted.

2.9.4 GFP-Siz2 imaging and colocalization

Siz2 localization was assessed by N-terminally tagging the *SIZ2* gene. Images of assycronous cells were acquired as 12-18 consecutive 0.2 µm stacks in the Z-axis. Acquired images were filtered using the Unsharp Mask function (Radius (Sigma): 3.0 pixels; Mask Weight: 0.8) of the Image J software (National Institute of Health) to differentiate signals at the nucleus edge from the more uniform nucleoplasmic signal.

2.9.5 Double-tagged colocalization quantification using MatLab

Images of eGFP/Tag-RFP-T fusions used for comparison of Sir4-eGFP to Nup-Tag-RFP-T and Nup-eGFP to Nup-Tag-RFP-T colocalizations were acquired as 12-18 consecutive 0.2 µm stacks in the Z-axis. Images were deconvolved using the nearest neighbour function of the AxioVision software deconvolution module (Carl Zeiss Inc.). Images were then rendered in ImageJ (National Institute of Health) using a custom macro (Capitanio, 2016) to separate specific channels prior to importing processed images into MATLAB 2015a (MathWorks). The following procedures were used to quantify the colocalization of eGFP and Tag-RFP-T signals.

Our approach to determine colocalization is based in a series of unbiased steps, in which the designed software ARO (Wu and Rifkin, 2015) identifies candidate spots in both channels - separately - and

determine colocalization using the spot coordinates obtained for each individual channel (RFP/GFP). In the ARO software, the initial step is applying a mask filter to exclude background, next image segmentation is created and centroids are defined by 3D Gaussian fit. Using machine learning this software does not rely on parameters arbitrary defined by user, instead it uses local intensity maxima to classify spots by using a supervised random forest classifier. After spot identification the ARO software allows a user supervised training in order to improve the reliability and robustness of the foci detection. During this step the software allows users to classify whether a focus is true or false, and using the most relevant parameters identified during this step the software once again applies the random forest classifier to further improve its ability to correctly identify foci. It is important to note that all the initial spot detection for each channel (RFP/GFP) is automatically created by the software, and that the possible biases inserted by the users are overcome by the use of random forest classier.

The number of overlapping eGFP/Tag-RFP-T foci (i.e. distance between of maximum intensity pixel within two separate foci less than 300nm or 5 pixels) was expressed as a percentage of the total number of eGFP or Tag-RFP-T foci identified (as indicated in the figure). All colocalization experiments were carried out using three biological replicates. Averages of these replicates were graphed and error bars for SD are shown.

2.10 High-throughput analysis

The Sir4 ChIP-Seq data were obtained from Ellahi et al., 2015, deposited in the NCBI Sequence Read Archive under accession number SRP034921. Analysis was performed using Galaxy (https://usegalaxy.org/). Duplicated reads were removed using Trimmomatic (Bolger et al., 2014). Reads were mapped to sacCer1 genome using Bowtie2 (Langmead and Salzberg, 2012). Data normalization and per-base-read counts were determined using deeptools2 (Ramírez et al., 2016). We determined enrichment using deeptools2 by dividing the IP reads by the input reads for every 5 bp. The Nup170 ChIP-chip data were obtained from Van de Vosse et al., 2013, deposited in NCBI Genome Expression Omnibus under accession number GSE36794. The plotted Nup170 values represent the fold enrichment determined by comparing the IP and input samples for bound probes with a p value ≤ 0.05. Data were compared and visualized using the Integrative Genomics Viewer application.

3. Sir4-Nup complexes, distinct from nuclear pore complexes, tether telomeres to the nuclear envelope

A version of this chapter has been under review and was co-authored in conjunction with Lapetina, L.D., Ptak, C., Roesner,K., and R.W. Wozniak. (2016). Sir4-Nup complexes, distinct from nuclear pore complexes, tether telomeres to the nuclear envelope. Journal of Cell Biology, in revision.

3.1 Overview

Interactions occurring at the nuclear envelope/chromatin interface influence both NE structure and the organization and functional state of chromatin. The study of yeast telomere association with the NE has yielded important mechanistic insights into the significance of NE/chromatin interactions. In this study, we have examined the relationship between various telomere-tethering pathways. We show that four proteins, each separately shown to function in gene silencing and NE-tethering of subtelomeric chromatin, including the silencing factor Sir4, NE-associated Esc1, the SUMO ligase Siz2, and the nuclear pore complex (NPC) protein Nup170, physically and functionally interact with one another as well as several additional NPC components (Nups). These Nups include known binding partners of Nup170 that constitute the inner ring subcomplex of the NPC core scaffold. Importantly, we show that this complex lacks Nups present in other NPC subcomplexes, and represents a structure distinct from NPCs. We propose that this Sir4-associated Nup complex functions in subtelomeric chromatin organization and NE-tethering.

3.2 Results

3.2.1 Nup170 interacts with proteins functioning in telomere localization to the NE

The nucleoporin Nup170 binds subtelomeric chromatin (regions within 20 kb of chromosome ends) and is required for normal subtelomeric gene silencing and telomere tethering to the NE (Van de Vosse et al., 2013). Closer inspection of Nup170 binding sites within subtelomeric chromatin reveals that this Nup is enriched at distinct sites within these regions. Strikingly, a comparison of the Nup170 chromatin binding profile with a recently published ChIP-seq data set for the SIR complex components reveals that most of these binding sites overlap (Fig. 3.1). These data are consistent with the previously reported physical interaction between Sir4 and Nup170 and the proposal that Sir4 mediates the binding of Nup170 to subtelomeric chromatin (Van de Vosse et al., 2013).

Apart from Nup170, Sir4 also interacts with other proteins at the NE, including two membrane-associated proteins, Esc1 and Mps3, implicated in anchoring telomeres to the NE (Andrulis et al., 2002; Taddei et al., 2004; Bupp et al., 2007; Schober et al., 2009). On the basis of these observations, we investigated the physical interactions between Nup170, Esc1, Mps3, and Sir4. To do this, the endogenous genes encoding Sir4, Esc1, or Mps3 were modified to produce a C-terminally tagged protein A (PrA) fusion. The fusion proteins were affinity-purified from cell extracts

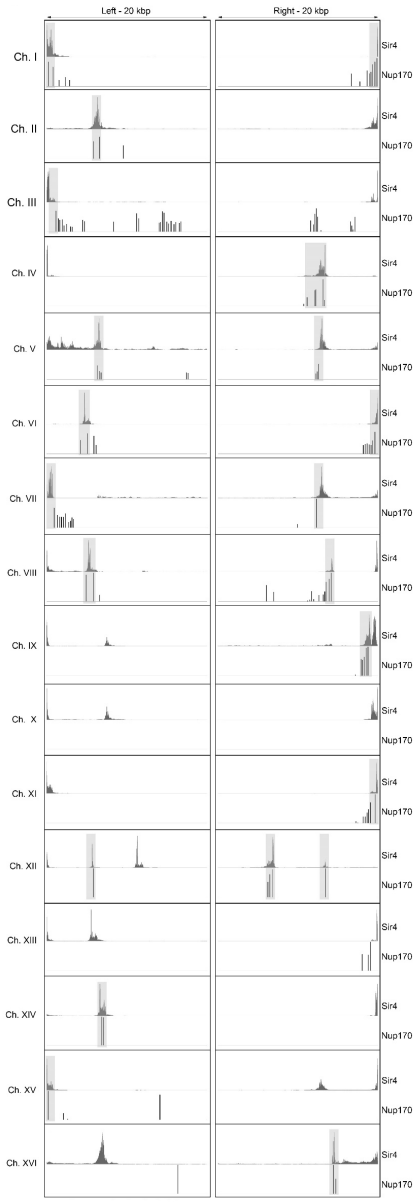

Figure 3-1. Nup170 and Sir4 enrich at similar regions within subtelomeric chromatin.

Previously reported Sir4 ChIP-Seq (Ellahi et al.,2015; Top track) and Nup170 ChIP-chip (Van de vosse et al., 2013; Bottom track) data are compared within the first (left) and last (right) 20 kbp of each of the 32 yeast telomeres. Peak heights correspond to fold enrichment as defined in these studies. Data is represented in sacCer1 genome with a resolution of 5 bp (Sir4) and 56 bp (Nup170). Note, six telomeric regions (IX-L, X-L, X-R, XV-R, XIV-L, and XVI-L) had too few probes to accurately represent Nup170 enrichment. Sir4 and Nup170 enrichment in similar telomeric and subtelomeric regions are highlighted in light grey.

and probed for interacting partners. Consistent with previous reports suggesting Esc1 and Mps3 interact with Sir4, we detected Sir4 bound to Esc1-PrA and Mps3-PrA (Fig. 3.2 A and B). However, Nup170 was only detected in association with Esc1-PrA, but not Mps3-PrA. Purification of Sir4-PrA also revealed associated Nup170 and Esc1 (Fig. 3.2 C). The binding of Sir4-PrA (Fig. 3.2 C) to Esc1 appeared less robust than binding between Esc1-PrA and Sir4 (Fig. 3.2 A), perhaps due to the combination of C-terminal tags used in the former. These data and previous observations are consistent with the existence of a complex containing Sir4, Esc1, and Nup170.

To further assess the physical association between Nup170, Esc1, and Sir4, we examined the effect of losing one of these three proteins on the association of the two remaining proteins. To test this, Esc1-PrA or Sir4-PrA was affinity-purified from cellular extracts of a strain containing a *sir4Δ*, *nup170Δ*, or *esc1Δ* null mutation (Fig. 3.3). Collectively, comparison of co-affinity purifications from WT cell extracts with those from mutant cell extracts revealed that the absence of any one member of this trio of proteins led to specific and reproducible changes in the association of the two remaining proteins. We observed that the amount of Nup170 bound to Esc1-PrA was reduced in the absence of Sir4 (Fig. 3.3 A). By contrast, purified Esc1-PrA showed increased amounts of associated Sir4 in the absence of Nup170 (Fig. 3.3 B). We also examined the effect of the *esc1Δ* mutant on the association of Sir4-PrA with Nup170.

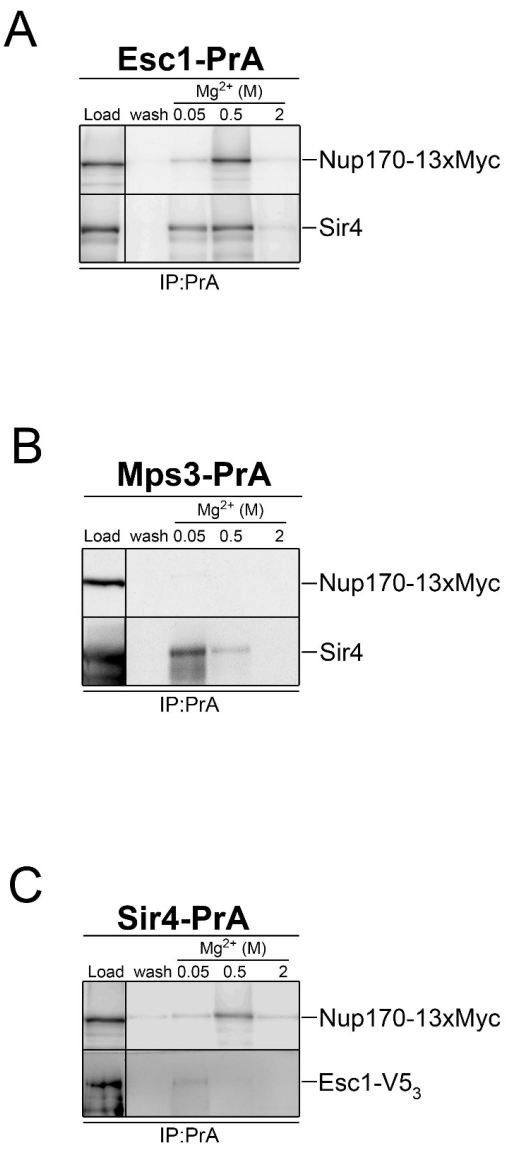

Figure 3-2. Nup170 physically interacts with proteins involved in telomere regulation.

Extracts from cells producing Nup170-13xMyc and Esc1-PrA (Panel A) or Mps3-PrA (Panel B), as well as extracts from cells producing Sir4-PrA, Nup170-13xMyc, and Esc1-V5$_3$ (Panel C), were subjected to co-affinity purification. Extracts (load) were mixed with IgG beads to bind the PrA fusion. Beads were then washed (wash) and proteins bound to the PrA fusion were eluted with buffer containing increasing $MgCl_2$ (Mg^{2+}) concentrations of 0.05 M, 0.5 M, and 2 M. Samples from each step were analyzed by western blotting using antibodies directed against the Myc and V5 peptides and Sir4.

In this case, we observed a reproducible decrease in the levels of Nup170 recovered in association with Sir4-PrA (Fig. 3.3 C). Of note, changes in the affinity purification profiles in the mutants were observed as alterations in the amount of the interacting partner bound to the PrA-fusion rather than a change in the relative proportion of purified protein that eluted at each Mg^{2+} concentration, (Fig. 3.3 A, B, and C). These results are consistent with the idea that the loss of one member of this group of proteins is less likely to affect the strength of the interactions between the remaining two proteins, but rather influence the accessibility of these proteins to one another. Together, these experiments show that Nup170, Esc1, and Sir4 exhibit multiple interactions that are interdependent.

3.2.2. The subcellular localization of Sir4, Esc1, and Nup170 are interdependent.

Co-purification results led us to conclude that Nup170, Esc1, and Sir4 interact. To expand upon this idea, we examined the interdependence of the subcellular distribution of these proteins. To test this, the endogenous gene coding for each protein was modified to produce Esc1-GFP, Sir4-GFP, or Nup170-GFP in WT cells and mutant cells lacking one of the other interacting partners (*nup170Δ*, *sir4Δ*, or *esc1Δ*). The subcellular distribution of each GFP fusion was then determined using fluorescence microscopy (Fig. 3.4). In WT cells, Esc1-GFP exhibited a punctate distribution along the NE, but was excluded from regions

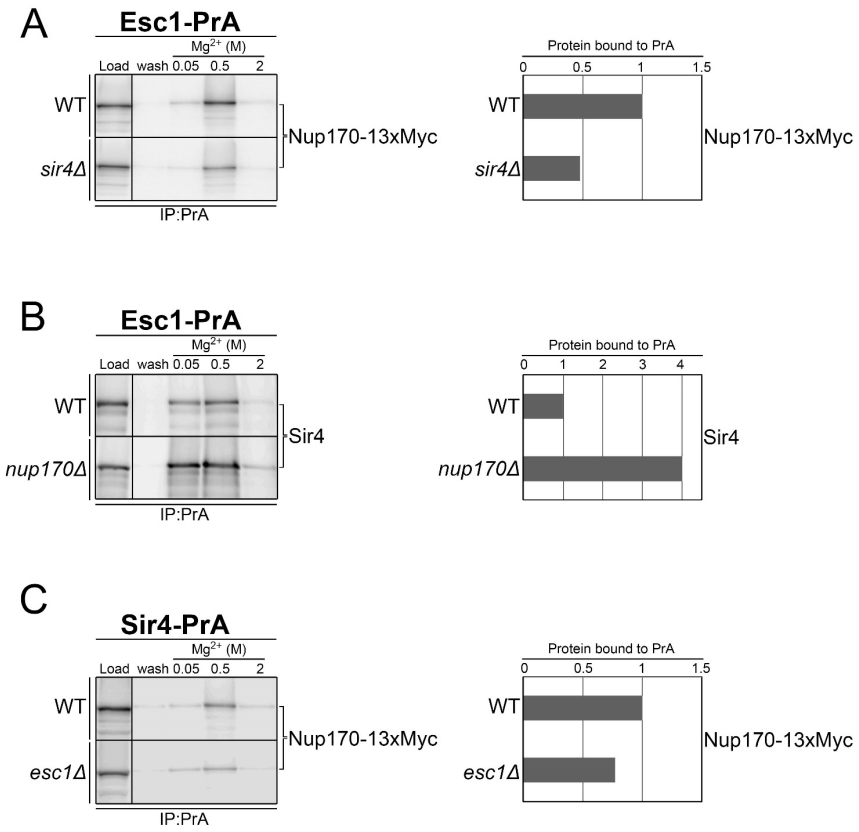

Figure 3-3. Interactions between Nup170, Esc1, and Sir4 are affected in deletion mutants.

Protein A fusions were affinity purified from cell extracts derived from WT and deletion mutant strains producing Esc1-PrA and Nup170-13xMyc (WT and *sir4Δ*, Panel A), Esc1-PrA (WT and *nup170Δ*, Panel B), or Sir4-PrA and Nup170-13xMyc (WT and *esc1Δ*, Panel C). Analysis of the indicated fractions by western blotting (left) to detect the specified proteins was performed as described in Fig. 2. Signal derived from western blots of the indicated proteins were quantified as described in the Materials and methods section and results are shown to the right of the western blots. To compare relative levels of the indicated proteins (Nup170-13xMyc or Sir4) bound to the PrA fusion between WT and mutant strains, the signal arising from Nup170-13xMyc or Sir4 in the elution fractions were summed and normalized to the amount of PrA fusion bound to the beads. The ratio of the bound protein to PrA fusion in the WT strain was assigned a value of 1. Decreased or increased ratios of co-purifying protein relative to the bound PrA fusion are indicated as less than or greater than 1, respectively. These values were plotted on a bar graph (right). Note, 1) the cellular levels of Nup170-13xMyc and Sir4 (see load fractions), and the PrA fusions were similar in the WT and mutant cells, and 2).

adjacent to the nucleolus (detected with the nucleolar marker Nop1-RFP; Fig. 3.4 A), similar to previous reports (Andrulis et al., 2002). This exclusion was clearly visible in ~70% of WT cells. However, Esc1-GFP nucleolar exclusion dropped to ~30% in *nup170Δ* cells and to ~40% in *sir4Δ* cells. Thus, both Nup170 and Sir4 contribute to the exclusion of Esc1 from regions of the NE that interact with the nucleolus (Fig. 3.4 A). Exclusion of Esc1-GFP from NE regions adjacent to the nucleolus is also dependent on the NPC nuclear basket-associated proteins Mlp1 and Mlp2 (Lewis et al., 2007; Niepel et al., 2013). Therefore, we tested whether the loss of Nup170 indirectly affected the distribution of Esc1-GFP by altering Mlp localization. This was not the case as localization of the Mlps were not affected by the loss of Nup170 (Fig. 3.5), suggesting that Nup170 affects Esc1-GFP localization without disrupting the integrity of the NPC nuclear basket.

Sir4-GFP is associated with subtelomeric chromatin and it is also concentrated at the NE, generally in 4-8 foci (Gotta et al., 1996; Luo et al., 2002). We examined the localization of Sir4-GFP in growing cultures of WT, *esc1Δ*, and *nup170Δ* cells. In contrast to WT cells, *esc1Δ* and *nup170Δ* mutants showed a decrease in the number of Sir4-GFP foci associated with the NE. The defect in the *esc1Δ* mutant was restricted to G1-phase (Fig. 3.4 B, WT vs. *esc1Δ*). Similarly, *nup170Δ* cells also showed a reduction in the peripheral localization of Sir4-GFP during G1- and S-phase (Fig. 3.4 B) (Van de Vosse et al., 2013).

Figure 3-4. Interdependence of Nup170, Esc1, and Sir4 on their respective subcellular distribution.

Panel A) WT, *nup170Δ*, and *sir4Δ* cells producing Esc1-eGFP and the nucleolar marker Nop1-RFP were examined by epifluorescence microscopy. Images of Esc1-eGFP, Nop1-RFP, and a merged image are shown on the left. The number of cells in which the Esc1-eGFP signal was excluded from regions along the NE adjacent to the nucleolar Nop1-RFP signal was determined and expressed as a percentage of the total number of cells examined. Shown on the right is a scatter plot of data obtained from 3 biological replicates. Data points for WT (closed square), *nup170Δ* (triangle) and *sir4Δ* (open square) were derived from 100 total cells counted per experiment. ***p ≤ 0.001. Panel B) WT, *nup170Δ*, and *sir4Δ* cells producing Sir4-eGFP and the NE/ER marker Sec63-RFP-T were examined by epifluorescence microscopy. Images of Sir4-eGFP, Sec63-RFP-T, and a merged image are shown on the left. Using bud size to differentiate between G1- and S-phase cells, the percentage of total Sir4-eGFP foci that co-localize with the NE/ER marker Sec63-RFP-T in these two groups of cells was determined. The bar graphs plot is shown on the right. Bars represent the mean from three biological replicates. Error bars indicate SD. ***p ≤ 0.001. Panel C) Subcellular distribution of various Nup-eGFP fusions in WT, *esc1Δ*, and *sir4Δ* cells were examined and images were obtained using an epifluorescence microscope. Arrows indicates the position of Nup170-eGFP clusters in *esc1Δ* cells. Bars, 2 μm.

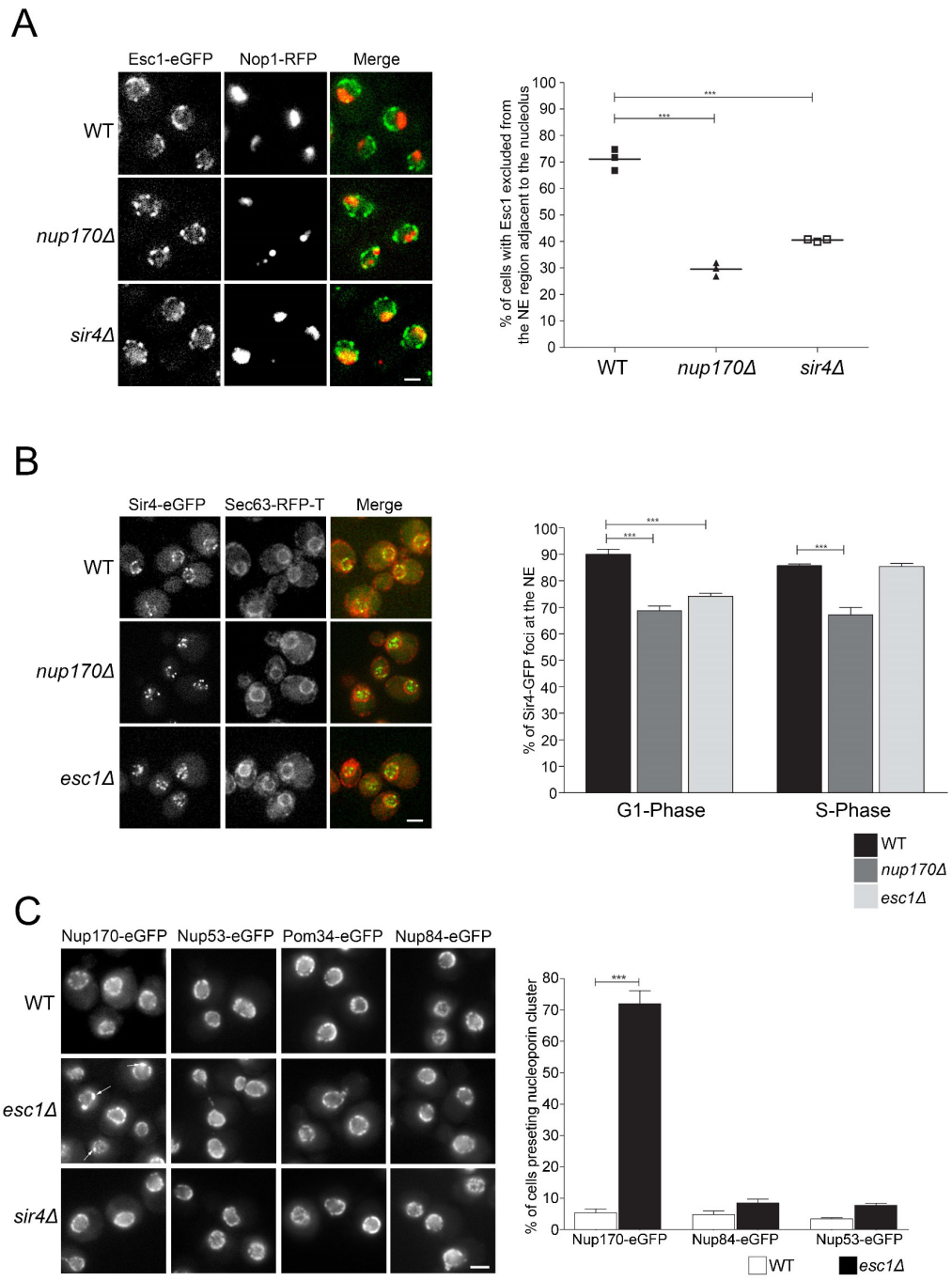

Figure 3.4. *Interdependence of Nup170, Esc1, and Sir4 on their respective subcellular distribution.*

Finally, we also examined the consequences of *esc1Δ* and *sir4Δ* mutations on the localization of Nup170-GFP. In *sir4Δ* cells, the localization Nup170-GFP and other representative Nup-GFP fusions appear unchanged when compared to WT cells (Fig. 3.4 C). In each case, cells exhibit relatively uniform punctate NE distribution of the GFP-fusions consistent with their association with NPCs. By contrast, in *esc1Δ* cells, Nup170-GFP clustered into bright foci along the NE. This clustering pattern was not detected with various other Nup-GFP fusions examined, including the Nup170 binding partner Nup53-GFP (Fig. 3.4 C). These results imply a specific role for Esc1 in mediating localization of Nup170 that is not detected with the other NPC-associated proteins examined including Nup53, Pom34, and Nup84. Cumulatively, the analysis of the subcellular localization of Nup170-GFP, together with that of Esc1-GFP and Sir4-GFP, further support the conclusion that Nup170, Esc1, and Sir4 physically interact at the nuclear periphery.

3.2.3 The SUMO E3 ligase Siz2 interacts with Nup170 and Sir4

The physical interactions we detect between Nup170, Esc1, and Sir4 are consistent with each protein's involvement in the maintenance of subtelomeric chromatin structure and NE tethering. Recent studies have reported that the SUMO ligase, Siz2, is required for Sir4 SUMOylation and

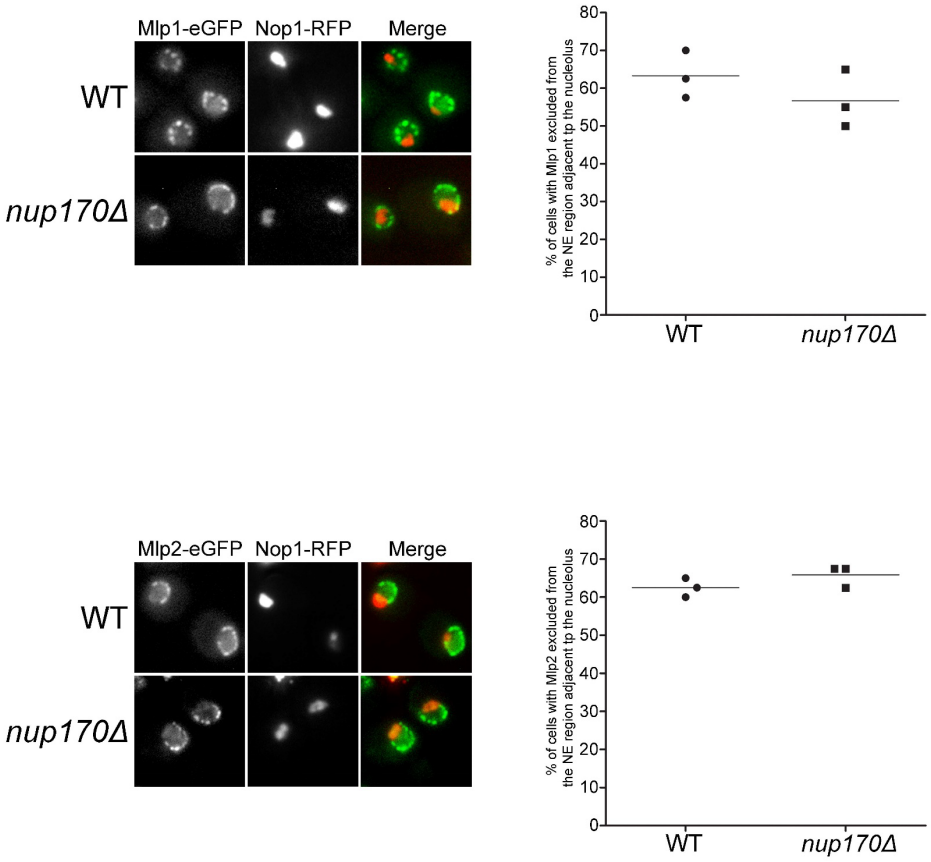

Figure 3-5. Distribution of Mlp1 and Mlp2 in nup170Δ mutants.

Mlp localization is not altered upon loss of Nup170. Subcellular distribution of Mlp1-eGFP and Mlp2-eGFP was assessed in WT and *nup170Δ* cells by epifluorescence microscopy.

the association of subtelomeric chromatin with the NE (Ferreira et al., 2011).

Thus, we examined whether Siz2 is physically associated with Nup170, Esc1, and Sir4. Analysis of proteins associated with Siz2-PrA purified from cell extracts revealed an interaction with both Sir4 and Nup170, but not the Nup170-interacting partner Nup53 (Fig. 3.6 A). Consistent with these results, we observed that GFP-Siz2, while visible throughout the nucleoplasm as previously reported (Huh et al., 2003), was also detected at the NE (Fig. 3.6 B).

Siz2 was also detected bound to Esc1-PrA (Fig. 3.6 C). Moreover, like Sir4 and Nup170, Siz2 was also required for proper NE localization of Esc1. In a strain lacking Siz2, Esc1 was not efficiently excluded from regions of the NE adjacent to the nucleolus (Fig. 3.6 D). These results implied that the loss of Siz2 may alter the association of Nup170, Sir4, and Esc1 with one another. We tested this by examining the interactions of these proteins in strains lacking Siz2. Comparison of Esc1-PrA or Sir4-PrA affinity purifications from WT to those from *siz2Δ* cell extracts revealed a reproducible reduction in the amount of Nup170 bound to Esc1 but little or no change in the binding profiles of Nup170 with Sir4, or Sir4 with Esc1 (Fig. 3.6 E). Furthermore, the loss of Siz2 did not appear to influence the subcellular distribution of Nup170-GFP or Sir4-GFP (Fig. 3.7 A and B).

Figure 3-6. The SUMO E3 ligase Siz2 interacts with both Nup170 and Sir4.

Panel A) Co-affinity purification was performed and analyzed by western blotting as described in Fig.2 using a cell extract from a strain producing Siz2-PrA and Nup170-13xMyc. Panel B) WT cells producing GFP(S65T)-Siz2 and Nup170-RFP-T were examined by epifluorescence microscopy. Images of GFP(S65T)-Siz2, Nup170-RFP-T, and a merged image are shown. Arrows point to representative GFP(S65T)-Siz2 foci that co-localize with Nup170-RFP-T at the NE. GFP(S65T)-Siz2 images were filtered, using the unsharp mask function in ImageJ, to highlight foci at the nuclear periphery. Panel C) Co-affinity purification was performed and analyzed by western blotting as described in Fig. 2 from a strain producing Esc1-PrA, Nup170-13xMyc, and Siz2-$V5_3$. Panel D) Subcellular distribution of Esc1-eGFP relative to the nucleolar marker Nop1-RFP was assessed in WT and *siz2Δ* cells as described for Fig. 4 A. ***$p \leq 0.001$. Panel E) Co-affinity purification was performed and analyzed by western blotting as described in Fig. 2, using cell extracts from WT and *siz2Δ* deletion mutant strains producing Sir4-PrA and Nup170-13xMyc (Sir4-pA) or Esc1-PrA and Nup170-13xMyc (Esc1-pA). To the right of the western blots, the indicated proteins were quantified as described in Fig. 3.3.

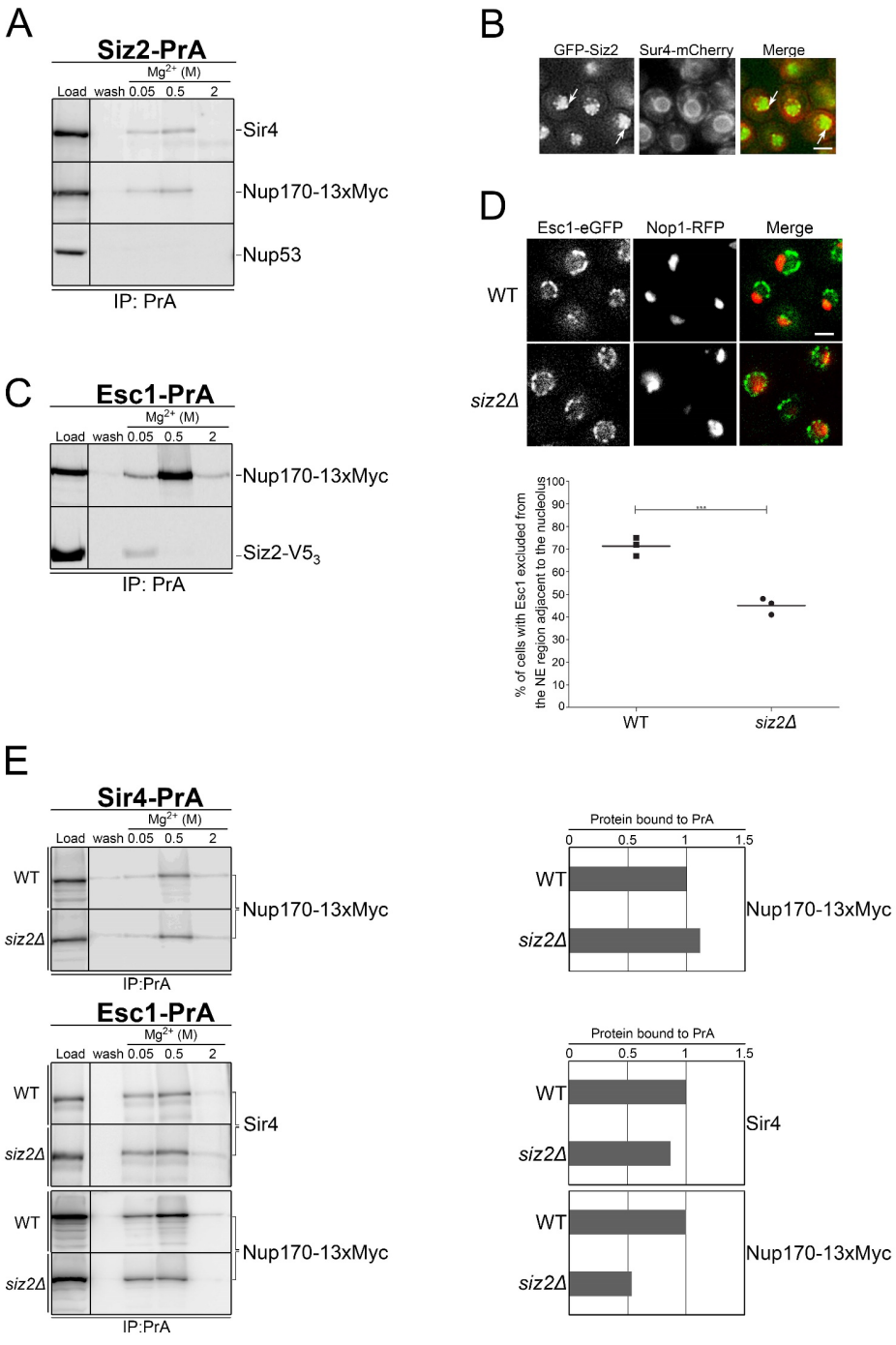

Figure 3.6. *The SUMO E3 ligase Siz2 interacts with both Nup170 and Sir4.*

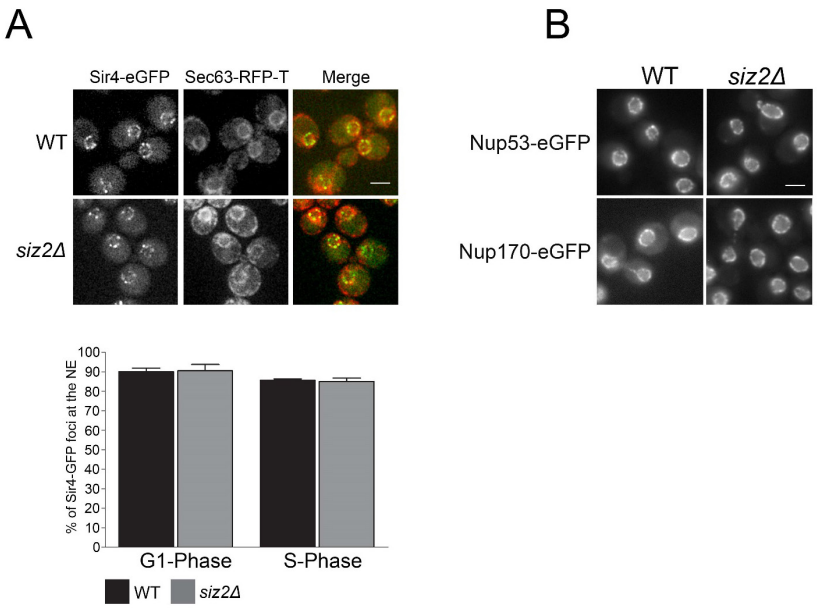

Figure 3-7. Subcellular distribution of nuclear envelope associated proteins in mutant strains.

Panel A) Subcellular distribution of Sir4-eGFP and the NE/ER marker Sec63-RFP-T was assessed in asynchronously growing WT and *siz2Δ* cells by epifluorescence microscopy. Using bud size to define G1- and S-phase cells, the percentage of total Sir4-eGFP foci that co-localize with the NE/ER marker Sec63-RFP-T in these cells was determined. A bar graph plots the percentage of total Sir4-eGFP foci that co-localize with the NE/ER marker Sec63-RFP-T. Error bars (SD) reflect the mean from three biological replicates. Panel B) Subcellular distribution of Nup53-eGFP and Nup170-eGFP was assessed in WT and *siz2Δ* cells by epifluorescence microscopy. Bar, 2 µm.

Together these results support the conclusion that Siz2 is part of a network of interacting proteins that includes Nup170, Sir4, and Esc1.

3.2.4 Esc1 is bound to two separate Nup170-containing complexes

The physical association of Sir4, Esc1, Siz2, and Nup170 suggests that these proteins exist within a protein complex(es) at the NE. As Nup170 is a structural component of NPCs, its association with members of this group of proteins led us to examine whether this complex is associated with NPCs. Previous fluorescence microscopy analysis has shown that Esc1 and Sir4 foci at the NE exhibit both overlapping and non-overlapping signals with Nups (Andrulis et al., 2002; Taddei et al., 2004; Niepel et al., 2013). To better understand the physical relationships between these proteins and NPCs, we focused on further defining their interactions with a broader spectrum of Nups.

Esc1 has been reported to exhibit partial colocalization with FG-Nups using fluorescence microscopy analysis (Taddei et al., 2004a). Moreover, two Nups, Nsp1 and Nup192, as well as the NPC-associated proteins Mlp1 and Mlp2, were detected bound to affinity-purified Esc1-PrA (Niepel et al., 2013). Since Nup170 directly interacts with Nup192 (Alber et al., 2007a; Alber et al., 2007b; Amlacher et al., 2011), we further analyzed the interactions of Esc1 with Nup170 and Nup192 interacting Nups. As shown in Fig. 3.8 A, Nup53, a direct binding partner of Nup170 (Lusk et

al., 2002; Makio et al., 2009; Onischenko et al., 2009) and Nup60, a binding partner of Nup192 (Alber et al., 2007a; Alber et al., 2007b), were also detected bound to Esc1. Consistent with the association of Esc1 with an NPC subcomplex containing Nup170, the binding of Esc1-PrA to Nup53 and Nup60 was reduced in a strain lacking Nup170 when compared to a WT counterpart (Fig. 3.8 A).

Similar to what we observed in the absence of Nup170 (Fig. 3.4 A), the distribution of Esc1-GFP within the NE is altered in a strain lacking Mlp1 and Mlp2 (Niepel et al., 2013), leading Niepel and colleagues to suggest that these proteins, directly or indirectly, mediate Esc1 association with NPCs. We tested this idea by affinity-purifying Esc1-PrA from cells lacking Mlp1 and Mlp2. As shown in Fig. 3.8 B, loss of the Mlp proteins reduced the amount of Nup53 and Nup60 that co-purify with Esc1-PrA. These results are consistent with the conclusion that the Mlp proteins are required for the association of Esc1 with NPCs.

The loss of the Mlps, however, did not have a similar effect on the interactions of Esc1-PrA with Nup170 and Sir4. For example, the amount of Sir4 that co-purified with Esc1-PrA was similar whether derived from *mlp1Δmlp2Δ* or WT cells (Fig. 3.8 B). For Nup170, while the total amount of Nup170 bound to Esc1-PrA was reduced in the *mlp1Δmlp2Δ* mutant, consistent with the loss of Esc1 at NPCs, a significant proportion of Nup170 remained bound to Esc1. These observations are consistent with

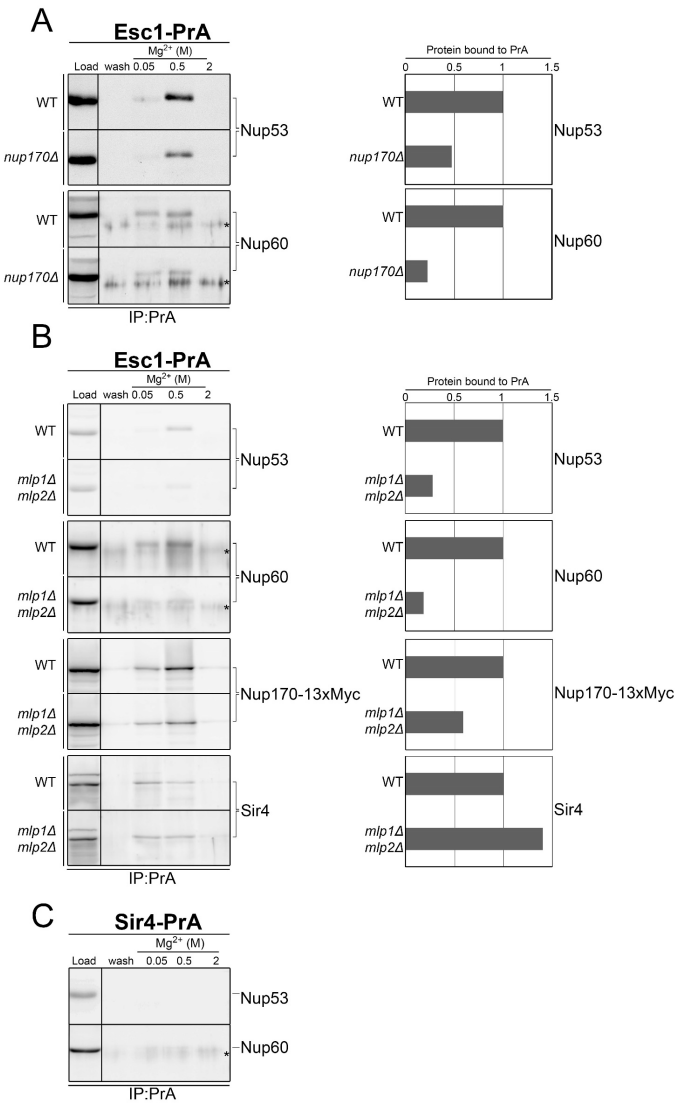

Figure 3-8. Esc1 and Sir4 binding to Nups.

Co-affinity purifications were performed and analyzed by western blotting as described in Fig. 2 using cell extracts from strains producing Esc1-PrA and Nup170-13xMyc in WT, *nup170Δ* (panel A), and *mlp1Δ mlp2Δ* (panel B) strains. To the right of the western blots, the indicated proteins were quantified as described in Fig. 3. Asterisks shown in anti-Nup60 blots denote the position of a background band present in the wash and elution fractions. Note, biological replicates of the affinity purification experiments shown in these panels are presented in Fig. 3-13. Panel C shows the results of western blotting analysis of samples from affinity purification experiments performed using extracts from cells expressing Sir4-PrA and Nup170-13xMyc performed as described in Fig. 3.2 and probed with antibodies directed against Nup53 and Nup60.

the presence of an Esc1/Nup170-containing complex that is resistant to the loss of the Mlp proteins and likely occurring outside of NPCs.

3.2.5 Sir4 associates with Nups linked to the inner ring of the NPC core.

Our observation that an Esc1/Nup170 complex may exist away from NPCs was of particular interest as the purification of Sir4 and the analysis of associated proteins were also consistent with Sir4 interacting with Nup170 and Esc1 outside of NPCs. As was previously shown (Van de Vosse et al., 2013) and is shown here in Fig. 3.2 C and Fig. 3.6 E, Sir4-PrA avidly binds Nup170, but a direct interacting partner of Nup170 within the NPC, Nup53, was not detected suggesting that this complex was distinct from fully assembled NPCs (Fig. 3.8 C). Moreover, affinity purification of Nup53-PrA or Nup60-PrA revealed little or no detectable Sir4 while exhibiting strong binding to Nup170 (Fig. 3.9 A and B). Notably, since Nup60 interacts with Nup192 (Fig. 3.10 A) (Alber et al., 2007a; Alber et al., 2007b), the presence of Nup170 and Nup53 in complex with Nup60-PrA suggests that bridged molecular interactions within NPCs are maintained under the conditions used here for complex isolation, as are the interactions between Nup170 and Nup53.

These results have led us to conclude that Sir4 interacts with a population of Nup170 that is not associated with Nup53 or Nup60, and thus, is distinct from intact NPCs. As discussed above, our analysis of

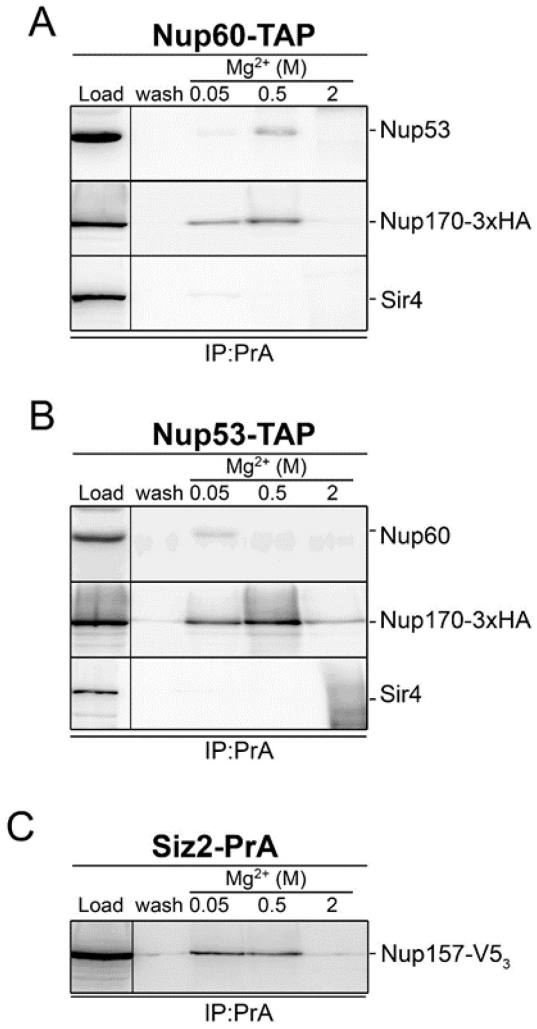

Figure 3-9. Analysis of Nup53-PrA, Nup60-PrA, and Siz2-PrA associated proteins.

Co-affinity purifications of protein A fusions were performed as described in Fig. 2 using extracts from cells producing Nup60-TAP and Nup170-13xMyc (panel A), Nup53-TAP and Nup170-13xMyc (panel B), and Siz2-PrA and Nup157-V5$_3$. Samples were analyzed by western blotting to detect the proteins indicated on the right.

Sir4-PrA associated proteins also detected Siz2. Importantly, purified Siz2-PrA was similarly bound to Sir4 and Nup170, but not Nup53 (Fig. 3.6 A). Since both Sir4 and Siz2 are also detected bound to Esc1, we envisage that these three proteins interact, directly or indirectly, with Nup170 in a complex(es) distinct from NPCs.

We next examined whether Nup170 alone or additional Nups were associated with the complex of proteins containing Sir4, Siz2, and Esc1. For this analysis, we focused on defining the spectrum of Nups associated with affinity purified Sir4-PrA. Targeted Nups included those found within various sub-structural regions of the NPC, including members of the inner ring Nup170 subcomplex (Nup170, Nup192, Nup157, Nup188), the outer ring (Nup84, Nup145C, Nup133) the FG-Nups Nup53 and Nup59, the linker Nup Nic96, a pore membrane protein (Pom152), nuclear basket proteins (Mlp1, Nup60), and a cytoplasmic filament Nup (Gle1) (Hoelz et al., 2011; Rout et al., 2000). As shown in Fig. 3.10 B, Sir4-PrA specifically co-purified with components of the core scaffold (Nup170 subcomplex, Nup84 subcomplex and Nic96), and to a lesser extent with the pore membrane component Pom152 (Fig. 3.10 A) (Makio et al., 2009). These data are consistent with previous reports showing Nup157 is associated with Sir4 (Van de Vosse et al., 2013) and our observed interaction of Siz2-PrA with Nup157 (Fig. 3.9 C). By contrast, Gle1, Nup53, Mlp1, and Nup60 showed little or no association with Sir4. These results suggested that a

Figure 3-10. Sir4 associates with Nups of the NPC inner ring complexes.

Panel A) Shown is a schematic diagram for the physical interaction network between Nups present in the Nup170-containing inner ring complexes of the NPC (blue) and neighboring Nups (shown as nodes) (see Alber et al. 2007a). Solid edges represent established physical interactions between Nups of inner ring complexes (light blue), the pore membrane Pom152 (light green), and FG-Nups Nup53 and Nup60 (cyan). The dashed edges between Nup60 and Mlp1 and Mlp2 (yellow) represents the requirement of Nup60 for the NPC association of the Mlp proteins. Panel B) Co-affinity purifications were performed and analyzed by western blotting as described in Fig. 2 using cell extracts from Sir4-PrA producing strains also containing Nup170-13xMyc, Nup192-$V5_3$, Nup157-$V5_3$, or Nup188-$V5_3$. Western blots for Pom152, Mlp1, Nup60, Nup53 and Gle1 were carried out using samples from the Sir4-PrA/Nup170-13xMyc producing strain and antibodies directed against the indicated proteins. Asterisks shown in anti-Nup60 blots denote the position of a background band present in the wash and elution fractions. Panel C) Shown are deconvoluted epifluorescence microscopy images depicting the localization of Sir4-eGFP and either Nup53-RFP-T, Nup157-RFP-T, or Nup170-RFP-T (top). Co-localization of the indicated pairs of fluorescent proteins was quantified as the percentage of total Sir4-GFP foci ($n > 4500$) that overlap with the respective Nup-eGFP foci. Bars represent the mean of three biological replicates for each co-localization experiment. Error bars indicate SD. $^{**}p \leq 0.01$; $^{***}p \leq 0.001$. Bar, 1 µm.

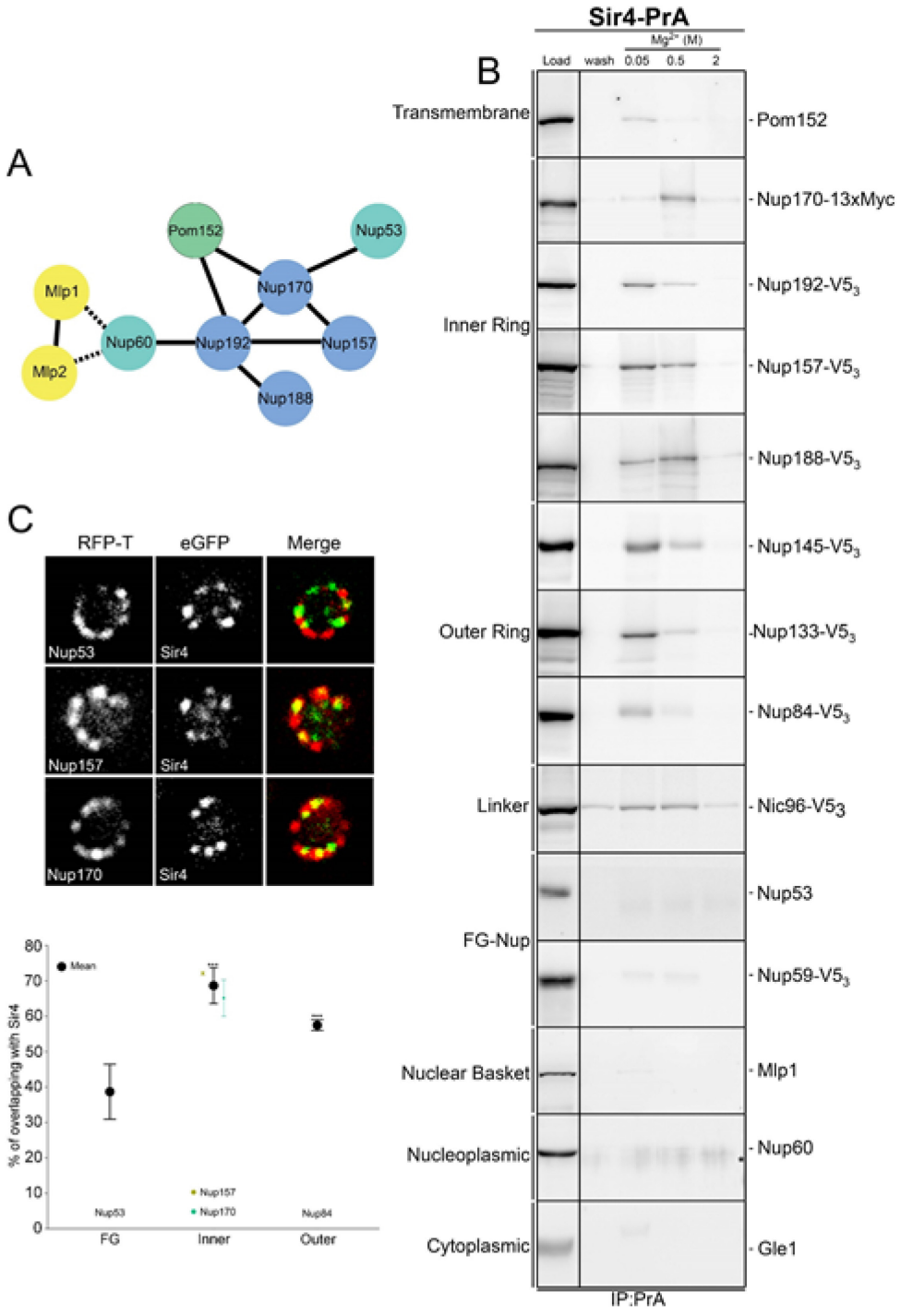

Figure 3.10. *Sir4 associates with Nups of the NPC inner ring complexes.*

Sir4-associated Nup (Snup) complex exists separate from fully intact NPCs.

We predicted that Nups associated with the Snup complex, such as Nup170 and Nup157, would exhibit a greater degree of colocalization with Sir4 than those absent from the Snup complex (e.g. Nup53). To test this, Sir4-GFP foci positioned at the nuclear periphery were compared to those of various RFP-tagged Nups (Fig. 3.10 C). Examining different dual tagged strains, we observed that NE-associated foci arising from Nup170-RFP or Nup157-RFP showed multiple foci that co-localized with Sir4-GFP. Quantification of the frequency of overlap in optical sections revealed that ~65% and ~70% of Sir4-GFP foci colocalize with Nup170-RFP and Nup157-RFP, respectively. By contrast, Nup53-RFP showed a significantly lower co-localization with Sir4-GFP (~40%). Thus, Sir4p exhibits preferential co-localization with those Nups detected in the Snup complex.

3.2.6 The Snup complex localizes to regions of the NE separate from NPCs

The presence of a Snup complex separate from NPCs also led to a second prediction, namely, that Nups present in Snup complexes and NPCs (e.g. Nup170 and Nup157) would exhibit a higher level of colocalization when compared to one another than when compared to Nups present only in NPCs, such as Nup53 and Nup60. To test this

prediction, we examined the co-localization of Nup170-RFP (in Snups and NPCs) with several GFP-tagged Nups. As shown in Fig. 3.11 A, optical sections of cells producing Nup170-RFP and Nup53-GFP or Nup60-GFP (present in NPCs but not the Snup complex) revealed overlapping or adjacent foci, as well as distinct regions of non-overlapping Nup170-RFP. By contrast, images of Nup170-RFP and Nup157-GFP revealed more similar patterns. We quantified the percentage of Nup-GFP signal that overlapped with Nup170-RFP at the nuclear periphery (see materials and methods). We found that Nup53-GFP and Nup60-GFP showed significantly lower co-localization with Nup170-RFP (~50%) than that observed between Nup170-RFP and Nup157-GFP or Nup188-GFP (~70%; Fig. 3.11 A). These data are consistent with the presence of Nup170 within two NE-associated complexes, those that contain Nup53 and Nup60 (NPCs) or those that lack Nup53 and Nup60 (Snup complex). Moreover, the higher degree of colocalization of Nup170 with Nup157 or Nup188 is consistent with the presence of these Nups in both Snup complexes and NPCs.

The presence of members of the Nup170 complex in structures separate from NPCs also prompted us to examine the localization of several Nups in a *nup133Δ* mutant strain were NPCs cluster, generally within a single region of the NE. Using fluorescence microscopy, we find that all Nup-GFP fusions tested localized to NPC clusters in *nup133Δ* mutant cells (Fig. 3.11 B). However, several Nups associated with the

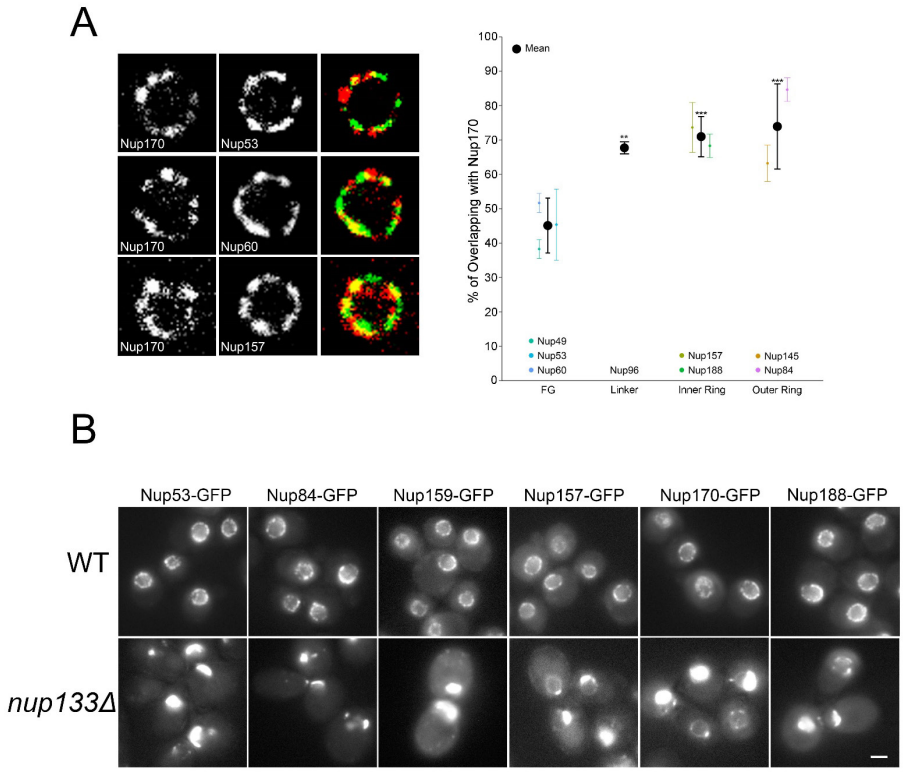

Figure 3-11. Co-localization of Nups present in the Snup complex and/or NPCs.

Panel A) Shown are deconvoluted epifluorescene microscopy images depicting the co-localization of Nup170-RFP-T with Nup53-eGFP, Nup60-eGFP, and Nup157-eGFP. Co-localization was quantified (right) as the percentage of total Nup170-RFP-T foci (n > 16000) that overlap with the respective Nup-eGFP foci. Bars represent the mean of three biological replicates for each co-localization experiment. Error bars indicate SD. *p ≤ 0.05; **p ≤ 0.01. Bar, 1 µm. Panel B) Subcellular distribution of various Nup-eGFP fusions in WT and *nup133Δ* cells was assessed by epifluorescence microscopy. Bar, 2 µm.

Snup complex, including Nup170-GFP, Nup157-GFP, and Nup188-GFP, were also visible at the NE in regions distinct from the NPC clusters. This pattern was not observed for Nup53-GFP, Nup84-GFP, or Nup159-GFP. These data are consistent with the conclusion that Nup170-GFP, Nup157-GFP, and Nup188-GFP are present both within and outside of NPCs.

3.3 Discussion

The study of telomere and subtelomeric chromatin tethering to the NE has provided insights into the interactions of chromatin and the NE membrane, and the significance of this association in determining chromatin structure and regulating gene expression. Numerous studies have identified multiple proteins that contribute to telomere tethering (Kupiec, 2014). However, in many instances the functional and physical relationships between these factors is ill-defined. In this study, we identified a network of interactions between a subset of proteins previously shown to contribute to telomere anchoring to the NE and gene silencing, including the chromatin-associated proteins Sir4, the SUMO ligase Siz2 and the nuclear NE membrane components Esc1 and Nup170. Importantly, we show that, while Esc1 is associated with NPCs and Nup170, a constitutive component of this structure, the Esc1-Nup170 association with Sir4 and Siz2 occurs outside of fully assembled NPCs. Instead, Sir4 and Siz2 are bound to a complex consisting of Esc1, Nup170, and a subset of Nups, including Nup170-interacting partners that

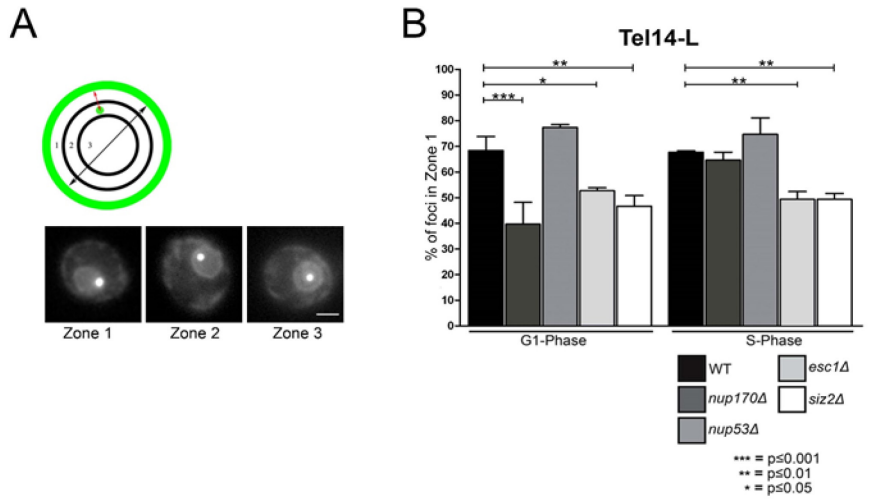

Figure 3-12. Telomere tethering to the NE is altered by proteins present in the Snup complex.

Panel A) Telomere positioning was evaluated by introducing an array of LacO repeats near Tel14-L. The LacO array interacts with the LacI-GFP revealing its nuclear localization. The telomere localization was assessed by measuring the distance between GFP loci to the NE marker Sec63-GFP. Telomeres were classified into three regions of equal volume. A schematic depicting these nuclear zones is shown (Zone 1 = p<0.184, Zone 2 = 0.184<p<0.422, and Zone 3 = p>0.422; p = LacI-GFP focus distance from the NE divided by the nuclear radius). Examples of cells producing Sec63-GFP and the localization of GFP-labeled Tel14-L in each zone are shown. Bar, 5 μm. Panel B) The localization of Tel14-L in WT cells and *nup170Δ, nup53Δ, esc1Δ*, and *siz2Δ* mutants was examined. The subnuclear position of 50 foci was determined for cells in G1 and S phase as defined by cell morphology. The bar graph represents the average percentage of telomeres in zone 1 determined from three independent experiments. *p ≤ 0.05; **p ≤ 0.01; ***p ≤ 0.001. Mean and SD are presented.

contribute to the core scaffold of the NPC, which we term the Snup complex. On the basis of functional analysis, the Snup complex is proposed to contribute to subtelomeric chromatin structure and gene silencing.

The presence of Sir4, Esc1, Nup170, and Siz2 within a physical complex is consistent with accumulating data pointing to their shared functional properties. Foremost amongst these are their roles in the physical association of telomeres with the NE (Palladino et al., 1993; Andrulis et al., 2002; Ferreira et al., 2011; Van de Vosse et al., 2013). The association of telomeres with the NE is dependent on partially redundant pathways that use several NE-associated proteins including Mps3, Esc1, and Nup170 as tethering factors (Andrulis et al., 2002; Bupp et al., 2007; Van de Vosse et al., 2013). These proteins interact with telomeric and subtelomeric chromatin-associated proteins such as Sir4, yKu70/80, and Est1. Siz2 is also required for NE-association of telomeres, potentially functioning in this role through its SUMOylation of chromatin-associated Sir4 and yKu70 (see below) (Ferreira et al., 2011). Why these multiple tethering pathways exist is unclear, but a discriminating property of them is their role in telomere anchoring during different stages of the cell cycle, with most studies focusing on their telomere tethering capabilities during G1- and S-phase. For example, Mps3, through its interactions with Sir4 and Est1, contributes to anchoring telomeres to the NE during S-phase (Schober et al., 2009). By contrast, Nup170 is required for telomere

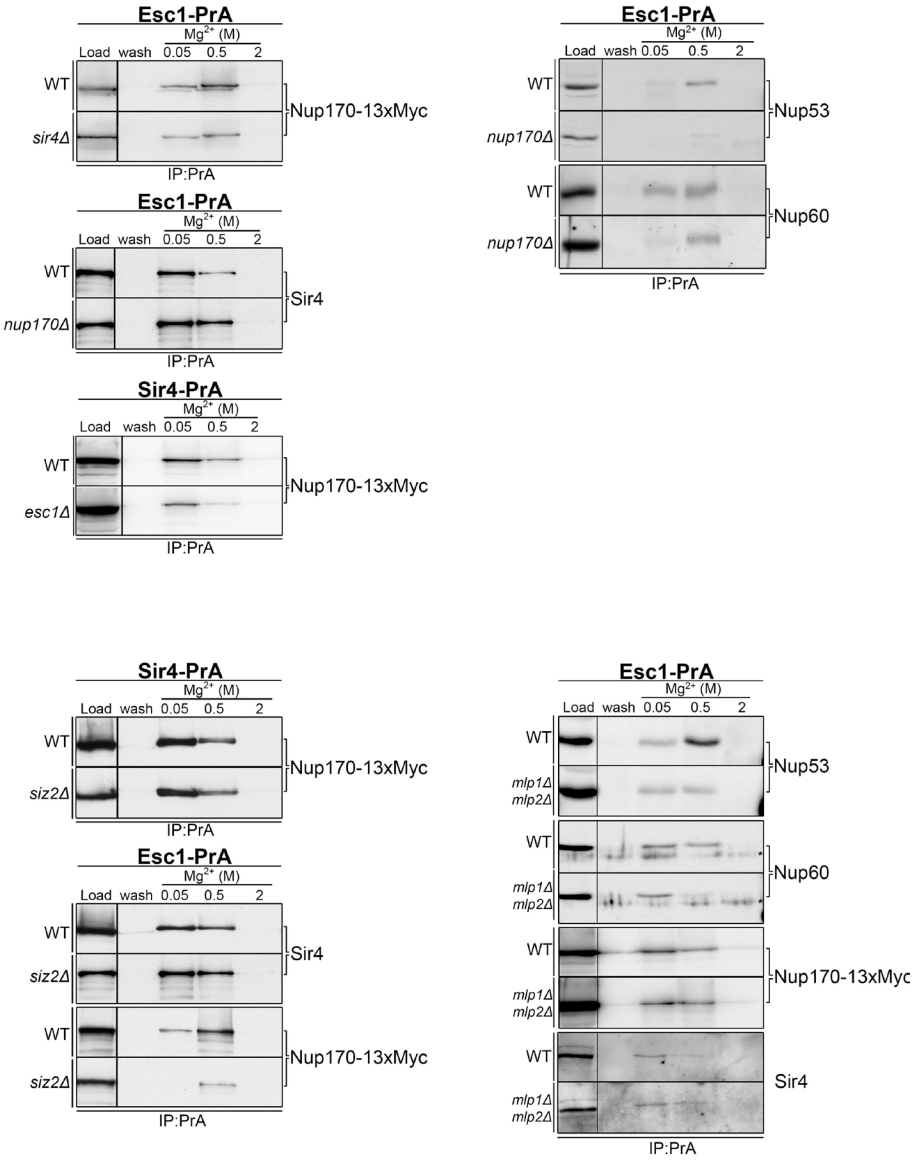

Figure 3-13: Biological replicates of co-affinity purification experiments

Additional examples of the co-affinity purification experiments comparing WT and mutant cells are presented here. The experimental results shown represent biological replicates of those presented in Fig. 3.3 (panel A), Fig. 3.6 E (panel B), Fig. 3.8 A (panel C), and Fig. 3.8 B (panel D). The experiments and analysis was performed as described in the main figures. Note, asterisks shown in anti-Nup60 blots denote the position of a background band present in the wash and elution fractions.

tethering in G1-phase (Van de Vosse et al., 2013). Similarly, Esc1 also plays a role in G1-phase telomere tethering (Taddei et al., 2010a). These functional distinctions between Nup170 and Mps3 place these proteins in distinct tethering pathways, which is consistent with our data showing that Nup170 and Esc1 are present in a complex that is physically distinct from Mps3 (Fig. 3.2).

Our data further places Esc1 and Nup170 in a complex with Sir4 (Fig. 3.2). These data are consistent with previous publications separately reporting Sir4/Esc1 (Andrulis et al., 2002) and Sir4/Nup170 interactions (Van de Vosse et al., 2013). In the latter case, the proposed interaction between Nup170 and Sir4 was supported by ChIP-Chip analysis that revealed the association of Nup170 with subtelomeric chromatin, and the dependence of this binding on Sir4. As shown in Fig. 3.1, the binding of Nup170 to subtelomeric chromatin was not uniform but rather occurred within discrete regions, and a similar discontinuous pattern of Sir4 enrichment on subtelomeric chromatin was also observed (Ellahi et al., 2015). Remarkably, comparison of these two binding profiles shows extensive overlap (Fig. 3.1). These data, together with our observations that these proteins co-affinity purify (Fig. 3.2) and are detected in overlapping foci at the NE (Fig. 3.10), provide strong support for the existence of a chromatin-associated complex consisting of Nup170 and Sir4.

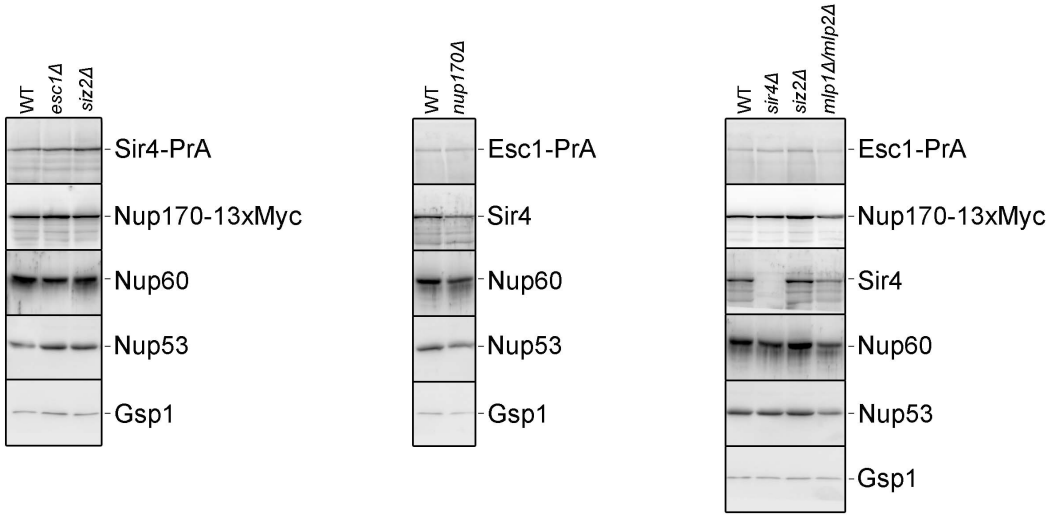

Figure 3-14: Deletion mutations do not alter protein levels.

The different deletion mutant strains, producing either Sir4-PrA/Nup170-13xMyc or Esc1-PrA/Nup170-13xMyc protein fusions, were grown overnight in liquid culture at 30°C. An aliquot of each culture was collected for western blot analysis. Protein levels were assessed using anti-PrA, anti-Myc, anti-Sir4, anti-Nup60, anti-Nup53, and anti-Gsp1 (used as a loading control) antibodies.

The chromatin associated Sir4/Nup170 complex is also predicted to contain Esc1. In addition to their co-purification (Fig. 3.2), various observations support the existence of a Sir4/Nup170/Esc1 complex. First, normal protein-protein interactions between these three proteins is dependent on all three members and loss of any one member alters the interaction of the remaining two (Fig. 3.3). Second, the normal NE distribution of these three proteins is interdependent upon one another. For example, the loss of Esc1 or Nup170 leads to a decrease in the NE association of Sir4 (Fig. 3.4 B), while the loss of Nup170 or Sir4 alters the NE distribution of Esc1 (Fig. 3.4 A). Third, the functional consequences of the loss of any one of these three proteins are also shared, including defects in the silencing of genes positioned in subtelomeric chromatin regions and a decrease in the NE association of telomeres (Fig. 3.12) (Palladino et al., 1993; Andrulis et al., 2002; Van de Vosse et al., 2013). These phenotypes are presumed to arise, at least in part, due to a failure of Sir4 to correctly load onto subtelomeric chromatin (Andrulis et al., 2002; Van de Vosse et al., 2013). These multiple observations lead us to conclude that the Snup complex plays a role in the structure and NE tethering of subtelomeric chromatin.

Both Sir4 binding partners Nup170 and Esc1 are associated with NPCs. Nup170 is a well-established component of the inner ring scaffold of the NPC. Esc1 has been detected bound to NPC-associated proteins, including Nup192 and Mlp2, and fluorescence microscopy revealed partial

colocalization of Esc1 with NPCs (Lewis et al., 2007; Niepel et al., 2013). In this study by Niepel and coworkers, they also showed that cells lacking the Mlp proteins exhibited an altered distribution of Esc1, suggesting that Mlp proteins may link Esc1 to NPCs. Here we have further shown that several Nups, including Nup53, Nup60, and Nup170, are associated with affinity-purified Esc1 (Fig. 3.8 B). In addition, we observed that the loss of the Mlps reduces binding of Esc1 to Nup53 and Nup60, providing more direct evidence for the role of the Mlp proteins in linking Esc1 to NPCs (Fig. 3.8 B).

Unlike the interaction of Esc1 with Nup53 and Nup60, deletion of the Mlp genes only partially decreased Esc1 binding to Nup170, and had no affect on the association of Esc1 with Sir4 (Fig. 3.8 B). A reasonable interpretation of this result is that, in addition to a Mlp-dependent association of Esc1 with NPCs, a Nup170/Esc1/Sir-containing complex exists outside of NPCs and it is unaffected by the loss of Mlp proteins. Several observations are consistent with this hypothesis. First, affinity purification of Sir4 reveals an associated complex of Nups that is distinct from NPCs. Bound to Sir4 are a subset of Nups that include, in addition to Nup170, several inner ring complex Nups (Nup192, Nup157, Nup188) outer ring complex (Nup133, Nup84, Nup145C), linker Nup Nic96, and Pom152, but lacking other Nups such as Nup53, Nup59, Nup60, and Mlp1 (Fig. 3.8 C and 3.10 B). This observation is striking as Nup60 and Nup53 are direct binding partners of Nup192 and Nup170 within the NPC and the

purification of Nups, even indirectly bound to Nup170, reveals associated Nup53 (e.g. see Nup60-pA, Fig. 3.9). Thus, purification of Sir4 with bound inner ring complex Nups, including Nup170 and Nup192, but devoid of other NPCs neighbors, suggests the Sir4-associated Nups are distinct from NPCs.

We interpret our affinity purification data to reflect the existence of two Nup complexes associated with the NE, the Snup complex and NPCs. A prediction of this fractionation data is that if we compare the localization of two groups of Nups, one restricted to NPCs and the other present in both the Snup complex and NPCs, we would observe a higher degree of colocalization between two Nups from one group than we would observe if we compare two Nups, one from each group. Our examination of the localization of various pairs of GFP- and RFP-tagged Nups revealed this trend (Fig. 3.11 A). Nup170 and Nup157 (present in both NPCs and Snup complexes) showed significantly higher levels of colocalization (~70%) than that observed between Nup53 and Nup170 (~50%). To our knowledge, such a comparison of Nup localization has not been previously explored in detail. These results indicate a previously unanticipated compositional heterogeneity in Nup-containing foci at the NE, an observation consistent with our affinity purification data and the presence of distinct Nup complexes.

Our localization data also revealed a higher degree of fluorescence colocalization between Sir4 and those Nups detected bound to Sir4 in our

affinity purifications experiments, including Nup170 and Nup188 (Fig. 3.10 C). This is in contrast to Nup53, which is absent from the Snup complex. The existence of Snup complexes with distinct composition and localization from NPCs may provide insight into the reasons for conflicting reports on the association of telomeres with NPCs. On the basis of our data, Nups not associated with the Snup complex and are predicted to exhibit only random levels of colocalization with telomere-associated Sir4. These results shed light on initial reports that Mlp proteins interact with telomeres (Galy et al., 2000), which where refuted in a later study (Hediger et al., 2002). Consistent with the latter study, we do not detect Mlps in association with the Snup complex (Fig. 3.10 B). Another negative result used to argue against the association of NPCs and telomeres was a lack of telomere and Sir4 clustering in *nup133Δ* mutant cells (Hediger et al., 2002), where structurally abnormal NPCs cluster together in a region of the NE (Doye et al., 1994). As shown in Fig. 3.11 B, several Nups that are components of the Snup complex, including Nup170 and Nup157, exhibit an incomplete clustering phenotype and are visible widely disturbed along the NE outside of clusters. Moreover, we have observed that Nup170 binding to Sir4 is maintained in a *nup133Δ* mutant (data not shown). These data raise the possibility that the Snup complex does not cluster in the *nup133Δ* mutant, and they are consistent with the conclusion that the Snup complex is distinct from NPCs.

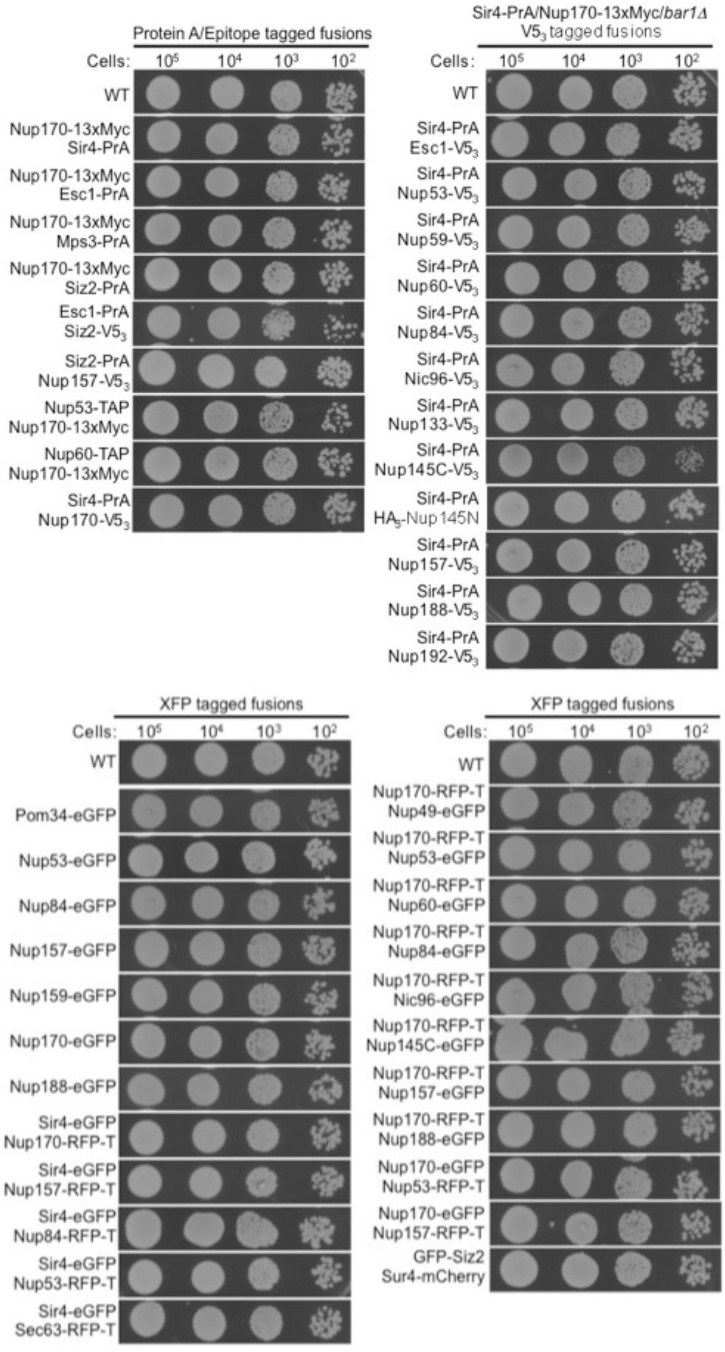

Figure 3-15: Tagging of genes did not alter the growth rates of the strains used in this study.

Cultures of the indicated strains were grown overnight at room temperature. Each culture was then diluted appropriately to provide spots on YPD plates containing 10^2-10^5cells. Plates were incubated for 2 days at 30°C then imaged.

The existence of the Snup complex raises many questions about its functional relationship to NPCs. Our initial characterization of the Snup complex described here (Fig. 3.10 B) reveals that its Nup components are largely contributed by members of the Nup170-containing inner ring complex and Nup84-containing outer ring proteins, while lacking nucleoporins from the substructures including Nup60 and Mlp1 (nuclear basket), Nup53 and Nup59 (FG-Nup), and Gle1 (cytoplasmically positioned Nup). Any contribution of other Nups to the Snup complex will await cataloging the remaining members of ~30 yeast Nups. Considering the compositional difference between the Snup complex and NPCs, including the lack of proteins functioning in mRNA export, we envisage that the Snup complex is unlikely to function in nuclear transport. However, like their NPC counterparts, the properties of Nup170 and other Nups present in the Snup complex, including Nup192, Nup188, and the integral membrane protein Pom152 (Aitchison and Rout, 2012), would suggest these Nups are capable of interacting with the NE membrane outside of the context of NPCs. Considering functional data linking Nup170 to subtelomeric chromatin structure (Van de Vosse et al., 2013), a plausible function for the Snup complex Nups is as a membrane-associated platform on which Sir4 and other factors are sequestered and rendered competent to interact with specific regions of subtelomeric chromatin.

The identification of the Snup complex also raises the question of their physical relationship to NPCs; for example, are they formed separately and represent distinct functional units, or are they temporally related to NPCs, perhaps representing an intermediate in NPC assembly capable of performing specific tasks prior to their maturation into NPCs? In the latter scenario, maturation of the Snup complex into a mature NPC would be predicted to suppress the chromatin binding activity of Nup170. Of note, a recent study conducted by Breuer and Ohkura reported on results that support the idea that some Nups may mask or regulate the function of other Nups (Breuer and Ohkura, 2015). They showed in Drosophila cells that an ortholog of yeast Nup170, Nup155, could mediate chromatin interactions with the NE. Importantly, this function of Nup155 could be repressed by other Nups, namely Nup62 and Nup93. We speculate that a similar masking event in yeast could regulate the accessibility of Nup170; in the absence of the masking event a Nup170-containing Nup complex could bind Sir4 and contribute to the formation of the Snup complex, while the binding of masking Nups (with Nup53 representing a candidate) to the Nup170 complex could facilitate the maturation of the structure into an NPC.

Other observations also suggest that the Snup complex may transition between assembled and disassembled states during the cell cycle. This concept has its origins in observations that telomeres exhibit dynamic behavior during the cell cycle, being released from the NE for

variable lengths of time during G1- and S-phase, as well as late in S-phase when telomeres replicate (Taddei and Gasser, 2012; Kupiec, 2014). Importantly, Nups are not detected away from the NE, thus any release of telomeres from the NE is predicted to break this linkage. The association of telomeres with the NE has been postulated to be controlled by the posttranslational modification of telomere-associated proteins by SUMO. Supporting this idea, the association of telomeres with the NE is dependent on the Siz2 SUMO ligase. In addition, several studies have reported that Siz2 functions in the SUMOylation of Sir4, yKu80, and Esc1 (Ferreira et al., 2011; Pasupala et al., 2012). Our results showing that Siz2 interacts with the Snup complex (Fig. 3.6 A and C) suggests Siz2-mediated SUMOylation may promote telomere association with the Snup complex, while removing this modification could contribute to the release of telomeres from the NE during the cell cycle. In support of this conclusion, we observed specific changes in protein-protein interactions between Nup170 and other members of the Snup complex in cells lacking Siz2. While the loss of Siz2 did not affect the binding of Sir4 to Nup170, nor did it alter the NE association of Sir4 (Fig. 3.6 E and 3.7 A), both the binding of Nup170 with Esc1 as well as the NE distribution Esc1 were altered (Fig. 3.6 D, E). These specific molecular changes in the interactions of components of the Snup complex support both the observation that Siz2 is associated with the Snup complex and the concept that it contributes to the structural integrity of the Snup complex.

Moreover, they reinforce the conclusions of previous studies establishing the importance of SUMO modification in the tethering of subtelomeric chromatin to the NE (Ferreira et al., 2011) as well as provide greater insight into role of Siz2 in this process.

4. The function of post-translational modification in Siz2 regulation

*This work was performed in collaboration with Dr. Christopher Ptak.

4.1 Overview

The recent development of high-throughput screening has allowed for a deeper understanding of chromatin structure and organization. This continuous effort has generated a multitude of data revealing chromatin-protein interaction networks, improving our understanding of chromatin formation and gene expression. In eukaryotic cells chromatin is found as either euchromatin or heterochromatin, and the formation of these distinct chromatin structures is dictated by the presence of different protein groups. The molecular and cellular changes observed during cell cycle progression, DNA repair, and the regulation of gene expression impose a dynamic landscape to which cells must quickly adapt. Cellular compartmentalization increases the efficiency of biological processes by sequestering and concentrating proteins at specific regions within a cell. However, intricate subcellular environments such as the nucleus require proteins to establish transient interactions in response to cellular changes, such as progression through the cell cycle. Post-translational modification (PTM) represents one strategy used by cells to quickly alter protein interactions in such a dynamic environment. Many post-translational modifications have been identified in eukaryotic cells, and more recently SUMOylation has been implicated in chromatin organization (Cubeñas-Potts and Matunis, 2013; Lukas et al., 2011; Rossetto et al., 2012). SUMOylation occurs in a coordinated manner, with Smt3 being activated by E1 SUMO activating enzymes, conjugated to its target by the E2

SUMO conjugating enzyme, and finally ligated to the target protein by the E3 SUMO ligase enzymes. In budding yeast, the Siz1 and Siz2 are part of the SUMO E3 ligase family, and have been implicated with SUMOylation of nuclear proteins (Chung and Zhao, 2015; Ferreira et al., 2011; Hannan et al., 2015; Takahashi et al., 2003).

In the previous chapter, we identified Siz2 as a regulator of the interaction between Nup170 and Esc1. Moreover, the observed interactions between Siz2 and a specific group of nucleoporins suggest the existence of distinct NPC sub-complexes with possible roles in telomeric chromatin organization. The important role of SUMOylation in regulating protein interactions and chromatin tethering to the NE led us to further characterize Siz2 and its role in these processes. In this chapter, we investigated the localization of Siz2 during different stages of the cell cycle, the role of Siz2 in telomere tethering, and Siz2 association with proteins associated with chromatin regulation. We also examined how PTM altered Siz2's ability to interact with the protein partners Nup170 and Esc1. Consistent with the observed interaction between Siz2 and Nups, strains carrying GFP-Siz2 contain foci that often overlap with the NE, and at times with Nup170. We observed a robust enrichment of Siz2 to the NE in during M-phase. The perinuclear localization observed during M-phase coincides with the appearance of post translationally modified species of Siz2. Finally, we identified this post-translational modification as Siz2 phosphorylation at serine residues 522/527 and characterized the effects

of this phosphorylation in the Siz2 recruitment to the NE, in the interaction of Nup170 with Siz2 and Esc1, and in the telomere association with the nuclear envelope.

4.2 Results

4.2.1 The Siz2 distribution during the cell cycle

Siz2 is an exclusively nuclear protein, with even distribution throughout the nucleoplasm (Johnson and Gupta, 2001). To date, the nuclear localization of Siz2 has been associated with several biological processes, such as DNA repair and telomere localization (Chung and Zhao, 2015; Ferreira et al., 2011). Generally, GFP-Siz2 is dispersed across the nucleoplasm. However, upon careful examination, we noticed the presence of bright foci overlapping with the NE / endoplasmic reticulum marker Sur4-mCherry (Fig. 4.1 - Arrows). We also observed a GFP-Siz2 exclusion from large nuclear regions (Fig. 4.1 - Asterisk). As cells progressed through the cell cycle, we observed a robust recruitment of GFP-Siz2 to the nuclear periphery. The NE accumulation of GFP-Siz2 was detected during early anaphase and persisted until telophase as determined by nuclear morphology (Fig. 4.1). To our knowledge, cell cycle specific peripheral recruitment has not been previously described for Siz2. It is important to note that we have no indication that Siz2 is differently expressed during cell cycle progression (Spellman et al., 1998), but the

strong intra nuclear depletion observed during the M-phase could be the result of GFP-Siz2 degradation.

To investigate Siz2 distribution during different stages of the cell cycle, we used α-factor to synchronize cells producing Siz2 C-terminally tagged with three repeats of the V5 peptide (Siz2V5$_3$). These G1 phase cells were then released from arrest and samples harvested at different time points. Samples of total cell lysate were analyzed by western blot using a monoclonal antibody against V5$_3$. We observed three different species of Siz2 based on molecular mass, suggesting that Siz2 undergoes PTM. While potential PTM species of greater molecular mass than the primary species of Siz2 were seen throughout the cell cycle (Fig. 4.2 – asterisk), we observed a Siz2 species that was only detected during the M-phase (Fig. 4.2 – dot), as indicated by the presence of the mitotic specific protein Clb2. Finally, using Gsp1 as a loading control, we did not observe a significant alteration in Siz2 protein levels. Thus, we conclude that Siz2 is not subject to cell cycle-dependent degradation. Importantly this apparent PTM of Siz2 coincides with the recruitment of Siz2 to the NE, suggesting that this PTM may play a role in NE association of Siz2 in M-phase. Thus, we expanded our Siz2 investigation to characterize if these PTMs play a role in the Siz2 function.

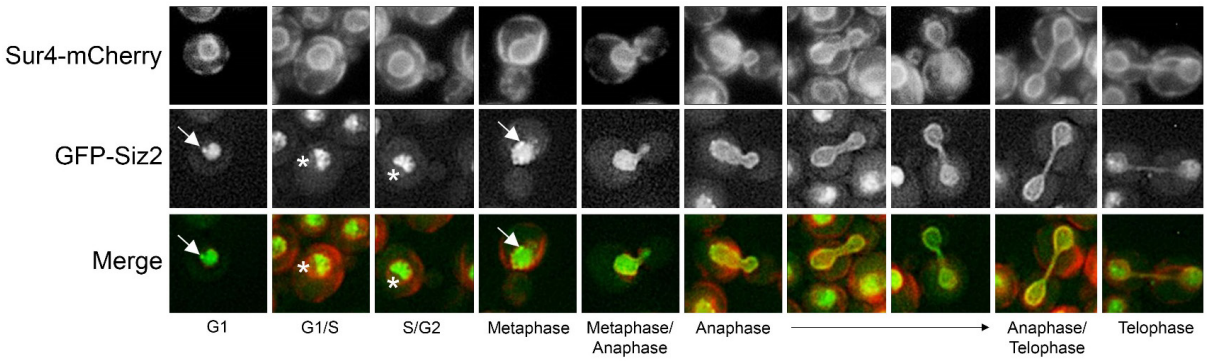

Figure 4-1. GFP-Siz2 relocates to the nuclear periphery during M-phase

A strain producing GFP-Siz2 and Sur4-mCherry were imaged by epifluorescence microscopy. Cells in different stages of the cell cycle, as identified by morphology, are shown. The GFP-Siz2 is recruited to the NE, here delineated by Sur4-mCherry, during M-Phase. Arrows represent regions containing bright GFP-Siz2 foci. Asterisks show nuclear regions from which Siz2 is excluded. *Images obtained and analyzed by Christopher Ptak.

4.2.2 Identifying post-translational modifications in Siz2.

Siz2 contains several distinct structural features. The N- terminal region of Siz2 possesses the SAP domain (SAF-A/B, Acinus and PIAS) that binds to DNA, as well as the PINIT and the SP-RING (Siz/PIAS-RING) domains required for SUMOylation. The C-terminal region of Siz2 does not contain any obvious structural motifs, but it has several potential PTM sites, including phosphorylation motifs at serine 522, 527 and 674 and SUMOylation motifs at lysine 438 and 446 (Fig. 4.3 A) (Holt et al., 2009; Takahashi et al., 2003).

Based on the molecular mass shift observed in our arrest/release experiments, we hypothesized that Siz2 likely contained several PTMs, some of which were visible throughout the cell cycle and others that occurred during mitosis. The mass difference between the predominant Siz2 species and slowest migrating species of Siz2 (132kD; see Fig. 4.2 – Asterisks) was consist with a SUMO modification. To test this, we transformed the Siz2-$V5_3$ strains with a GFP tagged version of Smt3 (GFP-Smt3), and asynchronous cells were analyzed by western blot using the $V5_3$ specific monoclonal antibody. By using a GFP-Smt3 construct, SUMOylated forms of Siz2-$V5_3$ are predicted to be of a greater mass. Indeed, we observed that in the GFP-Smt3 containing strain the 132kD Siz2-$V5_3$ species was replaced by a slower migrating Siz2-$V5_3$ species (Fig. 4.3 B). Based on consensus SUMOylation site sequences and the amino acid sequence of Siz2, we identified lysine 438 and 446 of Siz2 as

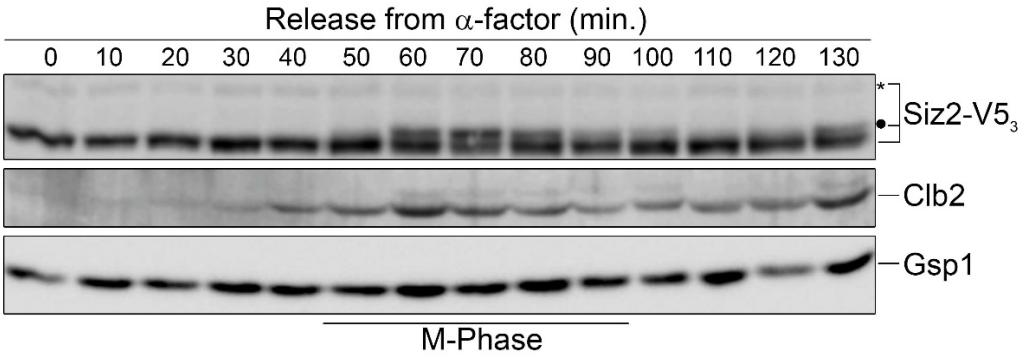

Figure 4-2. Siz2 is modified by different post translational modifications.

To arrest cells in G1-phase, cultures were incubated with α-factor. The cell morphology was used to evaluate the arrest efficiency. After synchronization in G1-phase, cells were released from arrest by washing with water and re-suspending cells in fresh YPD containing Pronase E. Progression through the cell cycle and into mitosis was monitored by harvesting samples at 10 minutes intervals after release. Western blotting was performed to detected M-phase specific production of Clb2 and Siz2-$V5_3$ using a monoclonal antibody against the $V5_3$. Asterisk denotes the position of the slower migrating species of Siz2 present throughout the cell cycle. Dot shows the cell-cycle specific species of Siz2. *Initial observation made by Christopher Ptak. Data shown here were obtained by Diego Lapetina.

potential SUMOylation sites. To test this, site-directed mutagenesis was used to mutated these lysine residues to arginine residues. We observed that strains carrying the Siz2$^{(K438/446R)}$ point mutation did not contain the the 132kD species of Siz2 (Fig. 4.3 C). These observations suggested that Siz2 is SUMOylated.

We further investigated the PTM responsible for cell cycle-specific mass shift of Siz2 during M-phase. Large scale studies aiming to identify the phosphoproteome in yeast describe three detected phosphorylated amino acid residues in Siz2 (Albuquerque et al., 2008; Holt et al., 2009). To identify whether the molecular mass shift observed during M-phase is related to phosphorylation, we treated the cells lysates obtained from mitotic cultures with alkaline phosphatase. Western blot showed that phosphatase treatment eliminated the slower migrating, cell cycle-specific Siz2 species (Fig. 4.3 D). This observation support previous observations reporting Siz2 phosphorylation, and they suggest that the relocalization of Siz2 to the NE coincides with its phosphorylation.

4.2.3 Post-translational modification function in Siz2 recruitment to the nuclear periphery.

Studies examining the phosphoproteome of yeast have identified three potential phosphorylation sites in Siz2 (Albuquerque et al., 2008; Holt et al., 2009). Moreover, Holt and colleagues (Holt et al., 2009)

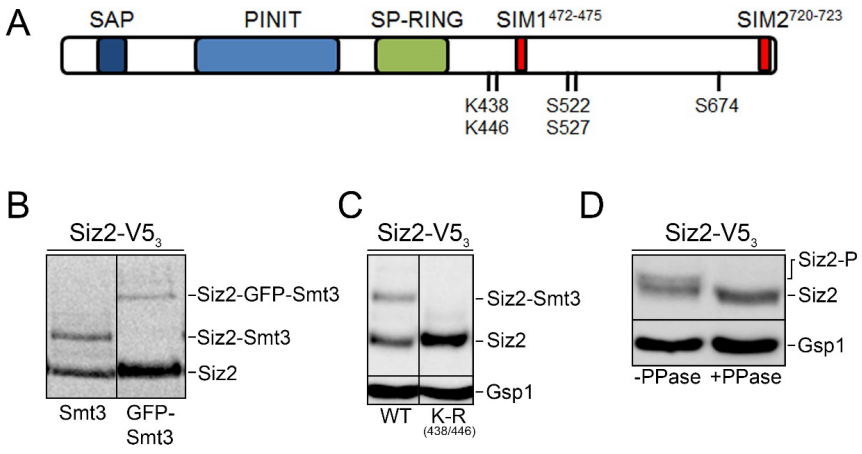

Figure 4-3. Siz2 is subjected to different post translational modification.

A) Schematic diagram depicting the different domains contained in the Siz2, and potential sites of PTM. B) Lysates from cells producing Siz2-V5$_3$ and either WT SUMO or a GFP-SUMO fusion (GFP-Smt3) were examined by western blotting using an anti-V5 antibodies. Siz2 SUMOylation was assessed by comparing the molecular mass shift in cells containing the GFP-Smt3 to that of WT cells. C) Site-directed mutagenesis was used to switch the lysine 438/446 to arginine. The siz2$^{(K438/446R)}$-V5$_3$ mutant did not contain the SUMOylated form of Siz2. D) Siz2 phosphorylation was confirmed by adding phosphatase to the whole cell lysate, running samples in SDS-Page gels and blotting membrane against Siz2-V5$_3$. *Initial observation and experiments performed by Christopher Ptak.

identified the serine residues 522, 527 and 674 of Siz2 as phosphorylation substrates for Cdk1, a master regulator of phosphorylation in mitotic cells. The potential role of Cdk1 in Siz2 phosphorylation supports our data demonstrating that Siz2 is phosphorylated during the M-phase.

Considering this information, we used site-directed mutagenesis to assess whether these site are modified by phosphorylation. We constructed strains in which the serine residues 522 and 527 (Cdk1/MAPK consensus sites), or 674 (PKA consensus) were mutated to alanine in Siz2-$V5_3$. These mutants Siz2$^{(S522/527)}$-$V5_3$ and Siz2$^{(S674A)}$-$V5_3$ were used to assess the Siz2 phosphorylation. We synchronized cultures using α-factor and collected samples at different time points after release cells from α-factor arrest. Cell lysate obtained from the synchronized cultures were examined by western blotting to evaluate Siz2 levels and phosphorylation.

Cells producing the Siz2-$V5_3$ fusion contained the three different species discussed above, the 132KD species representing the SUMOylated Siz2-$V5_3$, the the M-phase specific phosphorylated Siz2-$V5_3$ species, and the lesser molecular mass and most abundant Siz2-$V5_3$ species presumed to represent the unmodified protein (Fig. 4.4 – top row). Cells carrying the SUMOylation deficient *siz2$^{(K438/446R)}$-V5$_3$* allele did not show the 132kD SUMOylated species of Siz2. Moreover, M-phase specific phosphorylation was not altered in the SUMOylation mutants, supporting the previous observation that SUMO conjugation did not change Siz2 phosphorylation (Fig. 4.4 – second row). We also observed that the

SUMOylated species of Siz2 was still visible throughout the cell cycle in the phosphomutant strains containing the Siz2$^{(S522/527A)}$-V5$_3$ and the Siz2$^{(S674A)}$-V5$_3$ fusions. Based on the Clb2 levels, and the lack of detectable bands corresponding to the phosphorylated species of Siz2 in the samples derived from the M-phase (samples collected from 60 to 90mins), we concluded that serine residues 522/527 are the motifs for the mitotic phosphorylation (Fig. 4.4 – third row). Finally, we noted that the Siz2$^{(S674A)}$-V5$_3$ fusion did not alter the protein profile of Siz2 when compared to that the WT cells, leading us to conclude that serine 674 is not required for SUMOylation or phosphorylation (Fig. 4.4 – fourth row).

To investigate whether Siz2 targeting to the NE during M-phase is dependent of phosphorylation, we assessed the localization of the Siz2-V5$_3$ point mutants tagged at the N-terminus with GFP. As previously described, we observed that Siz2 is sequestered to the NE during the M-phase in WT cells (Fig. 4.1). Similar results were observed with the Siz2$^{(S674A)}$-V5$_3$ mutant. By contrast, cells carrying the GFP-Siz2$^{(S522/527A)}$ fusion did not accumulate Siz2 to the NE during the M-phase (Fig. 4.5). We also examined whether blocking SUMOylation of Siz2 would alter the nuclear distribution Siz2. GFP-Siz2$^{(K438/446R)}$ point mutant showed that Siz2 sequestering to the nuclear periphery was not affected in the SUMO mutant (Fig. 4.5). In conclusion, these results suggest that M-phase specific recruitment of Siz2 to the NE is dependent on the phosphorylation. Furthermore, we identified the serine residues 522/527

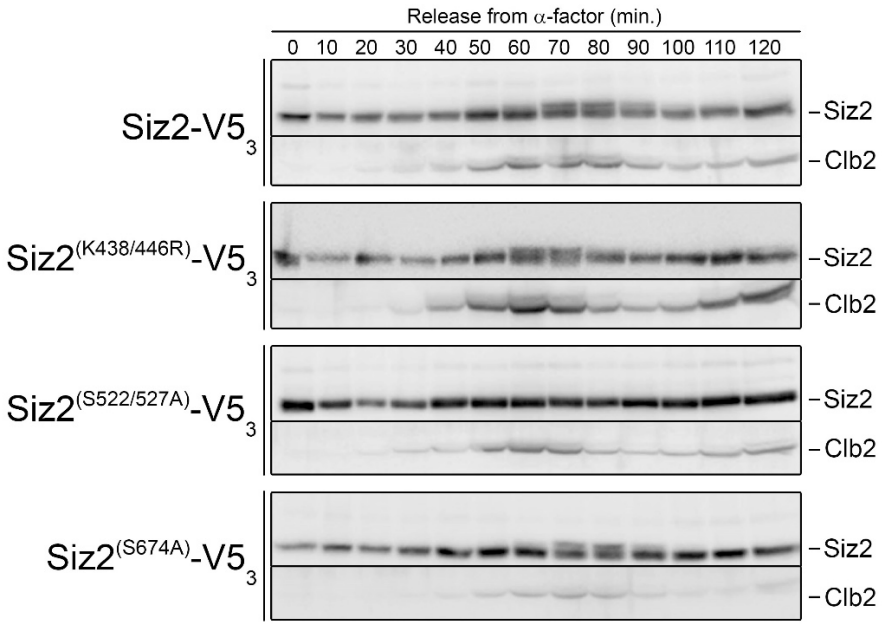

Figure 4-4. The serine residues 522/527 are required for Siz2 phosphorylation during M-phase.

We assessed the phosphorylation of the Siz2$^{(K438/446R)}$, Siz2$^{(S522/527A)}$, and Siz2$^{(S674A)}$. Cells were synchronized in G1-phase by incubating cultures with α-factor. After synchronization in G1-phase, cells were released from arrest by washing with water and re-suspending cells in fresh YPD. Samples were collected in 10 minutes intervals. The cell lysate from cultures expressing Siz2$^{(K438/446R)}$-V5$_3$, Siz2$^{(S522/527A)}$- V5$_3$, and Siz2$^{(S674A)}$-V5$_3$ were blotted using a monoclonal antibody against the V5$_3$. The cell cycle progression was evaluated monitoring the levels of Clb2. *Initial observation made by Christopher Ptak. Data shown here were obtained by Diego Lapetina.

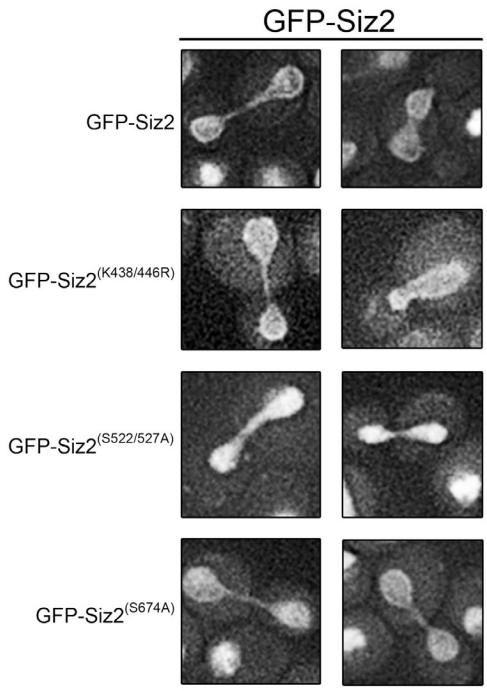

Figure 4-5. GFP-Siz2 recruitment to the nuclear periphery requires the phosphorylation of serine residues 522/527.

We created three strains containing different GFP-Siz2 point mutations by employing site-directed mutagenesis. We assessed the localization of GFP-Siz2, GFP-Siz2$^{(K438/446R)}$, GFP-Siz2$^{(S522/527A)}$, and GFP-Siz2$^{(S674A)}$ by imaging cells under epifluorescence microscope. The presented images contain cells in M-phase. *Image acquisition and treatment performed by Christopher Ptak

as the Siz2 phosphorylation motifs.

4.2.4 Effects of post-translational modification on Siz2 functions

The identification of amino-acid residues required for the post-translational modifications of Siz2 has the potential to improve our knowledge of Siz2 function. Unlike gene deletion, the use of point mutants allows the precise assessment of the role of a distinct region/domain of a protein. Given the role of Siz2 in SUMOylation, we investigated if the Siz2 point mutations altered the global SUMOylation patterns by comparison to the WT cells. To assess global SUMOylation patterns, we analyzed cell lysates by western blotting using antibodies directed against SUMO. This analysis reveals a characteristic and reproducible pattern of SUMO-modified proteins in cell extracts. We observed differences in the global SUMOylation profile in the Siz2$^{(S522/527A)}$ point mutant when compared to WT cells, including the absence of two SUMOylated bands (Fig. 4.4 – asterisks). By contrast, the Siz2$^{(K438/446R)}$ and Siz2$^{(S674A)}$ mutants showed SUMOylation profiles similar to the WT. It is important to note that the SUMOylation profile was altered only in the point mutant showing a defect in relocating Siz2 to the nuclear envelope, GFP-Siz2$^{(S522/527A)}$ (Fig. 4.5). Based on this observation we conclude that phosphorylation is required for

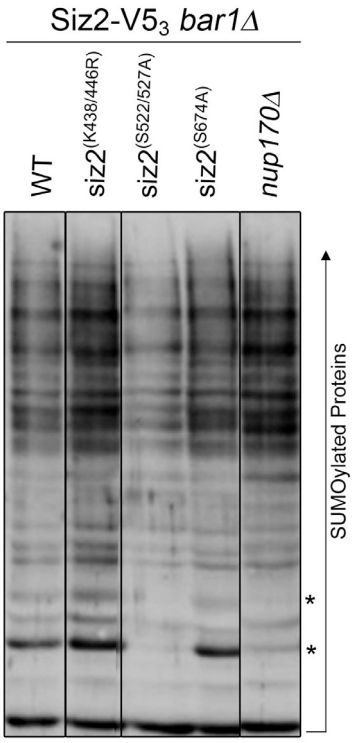

Figure 4-4. The effects of Siz2 point mutations on the global SUMOylation profile.

Cultures containing cells expressing *SIZ2$^{(K438/446R)}$-V5$_3$*, *SIZ2$^{(S522/527A)}$-V5$_3$*, and *SIZ2$^{(S674A)}$-V5$_3$*, and *nup170Δ* were grown overnight in YPD at 30ºC and harvested. The cells were washed and incubate with sample buffer. The cell lysate was analysed by SDS-PAGE followed by western blotting. The global SUMOylation profile of these mutants were assessed by using the SUMO antibody. *Initial observation and experiment performed by Christopher Ptak.

relocating Siz2 to the nuclear periphery, and presumably for facilitating the SUMOylation of a subset of proteins.

4.2.5 Nup170 is required for the NE association of Siz2 during M-phase.

Because we described an interaction between Siz2 and Nup170 in the previous chapter (Fig. 3.6), we speculated that M-phase specific association of Siz2 with the NE could be mediated through its interaction with Nup170. We predicted that Siz2 recruitment to the NE would be altered in the *nup170Δ* mutant. Consistent with our prediction, the *nup170Δ* mutant failed to recruit GFP-Siz2 to the nuclear periphery (Fig. 4.7 A). This effect appeared specific for the loss of Nup170 as the perinuclear localization of Siz2 was not affected by the deletion of other Nup genes including *nup157Δ*, *nup53Δ*, and *nup60Δ* (Fig. 4.7 A). Furthermore, the loss of Sir4 and Esc1, two proteins we detected in association with Siz2 (Fig. 3.6) were not required for the correct sequestering of Siz2 during the cell cycle (Fig. 4.7 A).

Our observation that the deletion of *NUP170* changed Siz2 distribution during the cell cycle coupled with the observation that GFP-Siz2 enrichment to the NE is dependent on the Siz2 phosphorylation, led us to examine whether Nup170 was required for Siz2 phosphorylation. We used Siz2-$V5_3$ to monitor phosphorylation levels in the *nup170Δ* mutants. *NUP170* deletion did not alter the overall protein levels of Siz2. However,

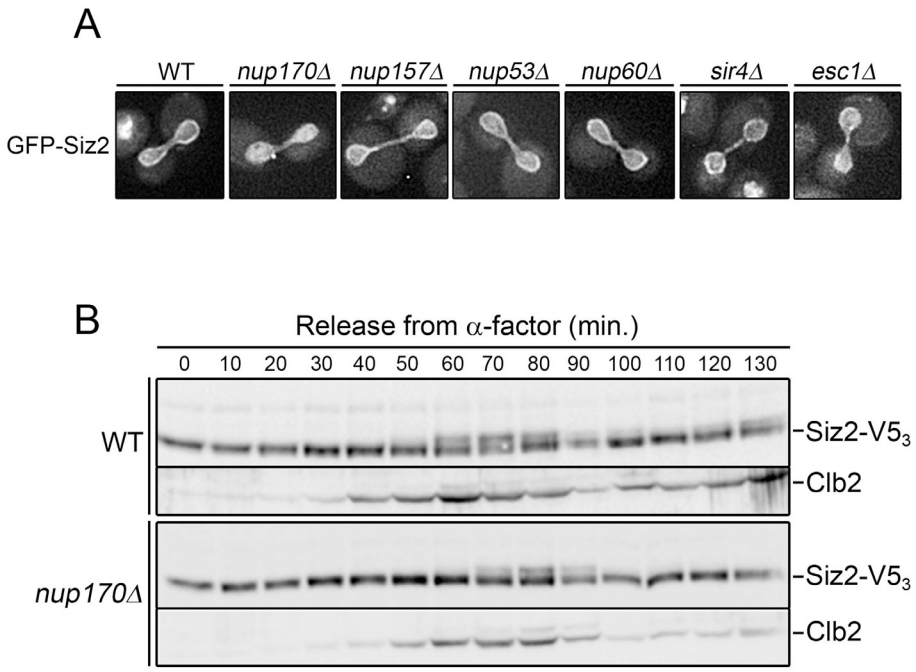

Figure 4-5. Siz2 phosphorylation and recruitment to the nuclear periphery requires Nup170.

A) The cells carrying the GFP-Siz2 were transformed with cassettes containing deletion of different Nups and proteins involved with telomere anchoring. The GFP-Siz2 localization in these mutants was evaluated by imaging cells by epifluorescence microscope. B) Cultures containing WT cells or *nup170Δ* were grown overnight in YPD at 30ºC and harvested. The cells were washed and incubate with sample buffer. The cell lysates were blotted using a monoclonal antibody against the $V5_3$. The cell cycle progression was evaluated monitoring the levels of Clb2. *Initial observation and experiment performed by Christopher Ptak.

loss of Nup170 did cause a subtle and reproducible reduction of the species corresponding to Siz2 phosphorylation (Fig. 4.7 B). These results suggest that Siz2 relocation to the NE is dependent on phosphorylation, and that Nup170 plays a role in this process.

The requirement for Nup170 in the NE association of Siz2, together with our observation that point mutants in Siz2 alter both its NE binding and it function in SUMOylation, lead us to examine the effects of the loss of Nup170 on global SUMOylation. As shown in Fig 4.6, the cells lacking Nup170 showed changes in the SUMOylation profile. While the *nup170Δ* mutant did not drastically reduce the global SUMOylation, it lacked two prominent SUMOylated protein species also absent in the Siz2$^{(S522/527A)}$ cell lysate (Fig. 4.6 – asterisks).

4.2.6 The effects of Siz2 point mutation on telomere localization

It has been previously described that Siz2 is responsible for SUMOylating several telomeric proteins, such as Sir4, yKU70, yKU80, Rap1, and Esc1 (Ferreira et al., 2011; Pasupala et al., 2012; Wohlschlegel et al., 2004). Furthermore, we showed in the previous chapter that Siz2 interacts with proteins involved in telomere anchoring, it is required for the normal distribution of Esc1 across the NE, and it is necessary for telomere localization at the NE during G1 and S-phases. Given our recent observations, we aimed to characterize the role of Siz2 PTMs in telomere

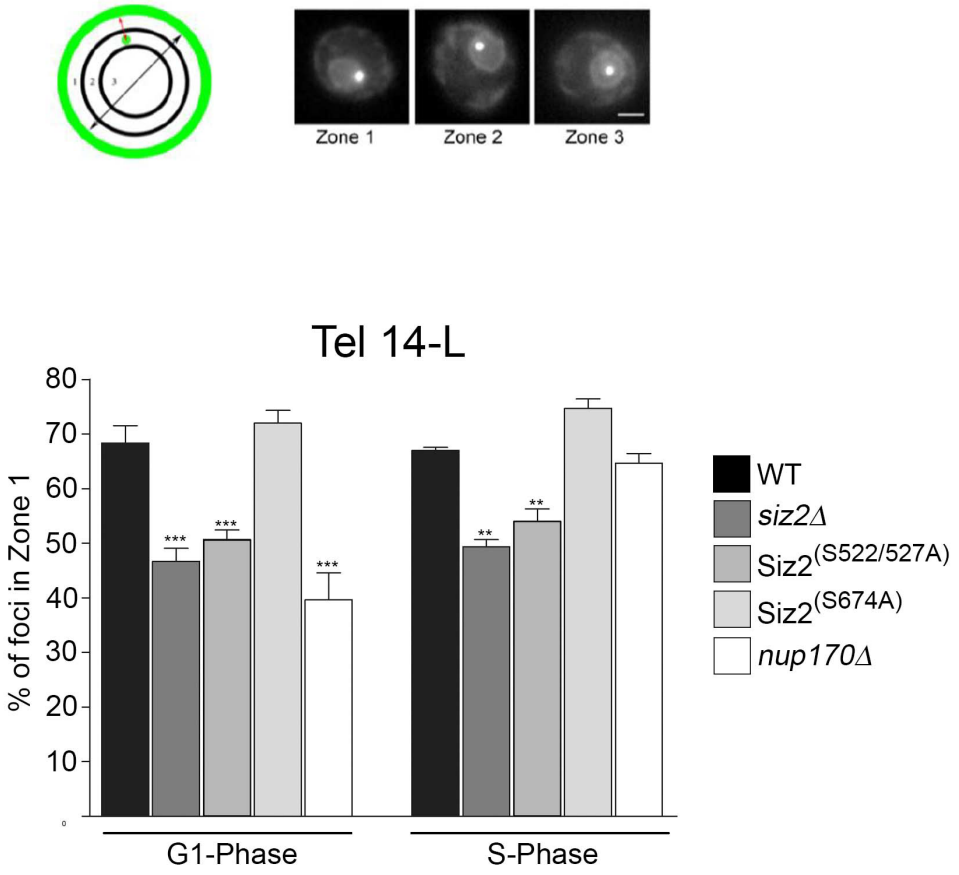

Figure 4-6 The effects of Siz2 phosphorylation on telomere positioning.

A) Telomere positioning was evaluated by introducing an array of LacO repeats near Tel14-L. The LacO array interacts with the LacI-GFP revealing its nuclear localization. The telomere localization was assessed by measuring the distance between GFP loci to the NE marker Sec63-GFP. Telomeres were classified into three regions of equal volume. A schematic depicting these nuclear zones is shown (Zone 1 = $p<0.184$, Zone 2 = $0.184<p<0.422$, and Zone 3 = $p>0.422$; p = LacI-GFP focus distance from the NE divided by the nuclear radius). Examples of cells producing Sec63-GFP and the localization of GFP-labeled Tel14-L in each zone are shown. Bar, 5 µm. B) The localization of Tel14-L in WT cells and *siz2Δ, SIZ2*$^{(S522/527A)}$*, SIZ2*$^{(S674A)}$*, nup170Δ* mutants was examined. The subnuclear position of 50 foci was determined for cells in G1 and S phase as defined by cell morphology. The bar graph represents the average percentage of telomeres in zone 1 determined from three independent experiments. *$p \leq 0.05$; **$p \leq 0.01$; ***$p \leq 0.001$. Mean and SD are presented. *Initial observation and experiments performed by Diego Lapetina.

anchoring. Since the Siz2$^{(K438/446R)}$ was recruited to the NE and did not affect the global SUMOylation profile, we limited our investigation to the phosphomutants.

The localization of Tel14-L has been widely used as a representation of telomere anchoring. As shown Fig. 4.8, during G1 and S-phase of the cell cycle Tel14-L was anchored to the NE in approximately 70% of the WT cells. In the *siz2Δ* mutant Tel14-L was anchored to the NE in 48% and 50% of the G1 and S-phase cells, respectively (Fig. 4.8 – dark gray bar). Similar to the *siz2Δ* mutant, we observed that the Siz2$^{(S522/527A)}$ phospho-mutant exhibited reduced Tel-14L anchoring (51% and 55% of G1 and S-phase cells, respectively) to the NE (Fig. 4.8 – gray bar). By contrast, the Siz2$^{(S674A)}$ phospho-mutant did not affect the localization of Tel14-L (Fig. 4.8 – light gray bar). These observations support the concept that phosphorylation of serine residues 522/527 also plays an important role in Siz2 function. We previously observed that Nup170 and Siz2 share a similar defect in telomere anchoring during the G1-phase (Fig. 4.8 – white bar).

4.2.7 The effects of Siz2$^{(S522/527A)}$ mutation on protein interaction.

Given the similarities observed between *nup170Δ* and Siz2$^{(S522/527A)}$ mutants in telomere localization and in the global SUMOylation profile, we

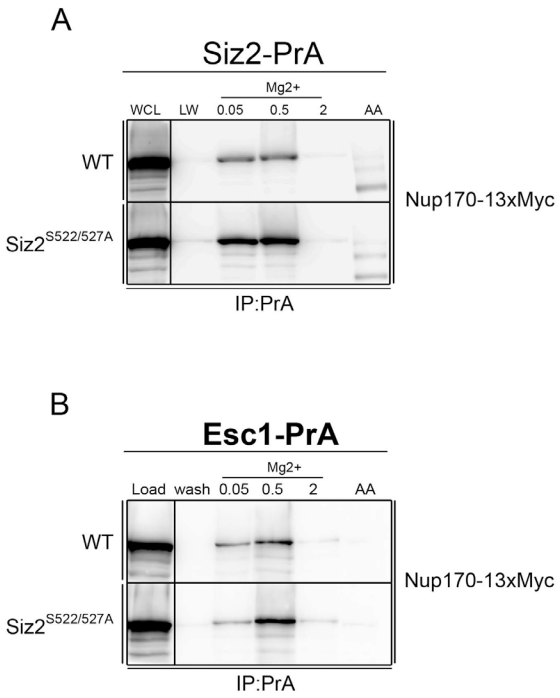

Figure 4-7 The lack of phosphorylation of serine residues 522/527 increases the Nup170p affinity for Siz2p.

Extracts from WT or Siz2$^{(S522/527)}$ cells producing Nup170-13xMyc and Siz2-PrA (Panel A) or Esc1-PrA (Panel B) were subjected to co-affinity purification. Extracts (load) were mixed with IgG beads to bind the PrA fusion. Beads were then washed (wash) and proteins bound to the PrA fusion were eluted with buffer containing increasing $MgCl_2$ (Mg^{2+}) concentrations of 0.05 M, 0.5 M, and 2 M. Samples from each step were analyzed by western blotting using antibodies directed against the Myc. *Initial observation and experiments performed by Diego Lapetina.

decided to investigate how the Siz2 phosphomutant altered the interactions of proteins involved in telomere tethering to the NE. In the previous chapter, we showed that interaction between proteins involved in telomere tethering was dependent on Siz2. In this chapter, we showed that siz2$^{(S522/527A)}$ mutant affected telomere tethering and Siz2 recruitment to the nuclear periphery during the M-phase (Fig. 4.4 and 4.8). These observations suggest that perinuclear localization of Siz2 is necessary for accurate telomere anchoring to the NE. Based on the observation that Siz2 recruitment to the NE was reduced in the Siz2$^{(S522/527A)}$ phosphomutant (Fig. 4.7 and 4.4), we predicted that Siz2 interactions with proteins present at the NE would be affected in the Siz2$^{(S522/527A)}$ mutant. However, our pull-down data showed a significant and reproducible increase in the Siz2$^{(S522/527A)}$-PrA interaction with Nup170 (Fig. 4.9 A). Intriguingly, while the Nup170-Esc1 interaction was significantly reduced in the *siz2Δ* mutant, the Siz2$^{(S522/527A)}$ mutant showed a visible increase in the interaction between these two proteins (Fig. 4.9 B). These observations suggested that phosphorylation of Siz2 modulates the interactions of Siz2 with several protein partners.

4.2.8 Phosphorylation enhances the interaction between Siz2 and Nup170p.

Since the Siz2 NE relocation is regulated through the cell cycle, we performed affinity purification in actively growing synchronized cultures. Using α-factor, we synchronized cells in G1-phase and collected samples

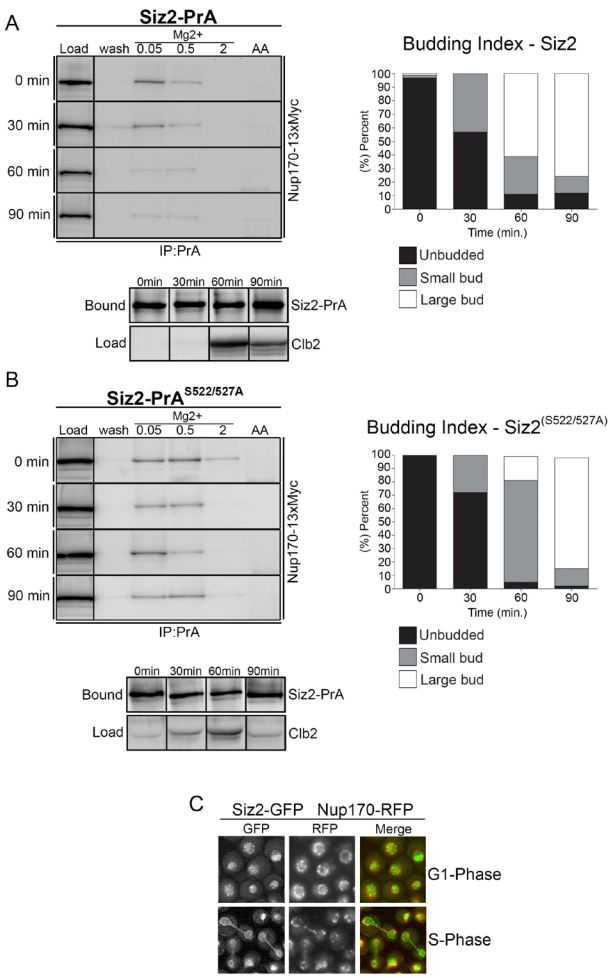

Figure 4-8 The dynamic interaction of SUMO E3 ligase Siz2p with Nup170p is regulated during cell cycle progression.

(A-B) Cells carrying Siz2-PrA-Nup170-13xMyc or Siz2$^{(S522/527A)}$-PrA-Nup170-13xMyc fusions were arrested with 10ng/mL of α-factor for three hours, and release as described in figure 4.2. Cell lysate were incubated with beads (Load). After conjugation beads were washed (wash) and protein bound to the PrA fusion were eluted by stepwise elution with increasing concentrations of $MgCl^{2+}$. The final wash was performed using 0.5M of acetic acid (AA). Eluted proteins were analyzed by SDS-Page followed by western blotting. The budding index and Clb2p levels were used to track the efficiency of the cell cycle release. Bound fraction represents the amount of protein interacting with the beads. (C) GFP-Siz2 strain was tagged with Nup170-RFP-T, and images were acquired using epifluorescence microscope. Acquired images were digitally enhanced using Unsharpening Mask followed by Smoothing filter. *Initial observation and experiments performed by Diego Lapetina.

at different time points. The data obtained using WT cells presented enrichment in Siz2-Nup170 interaction during G1 and the early S-phase with decreased binding in later stages of the cell cycle, including during mitosis (Fig. 4.10 A). Conversely, the Siz2$^{S522/527A}$-PrA was stably associated with Nup170 throughout the cell cycle. These data potentially explain the observed enrichment of Nup170 in the pull-down experiments using the Siz2$^{S522/527A}$-PrA (Fig. 4.10 B). Finally, because our microscopy data argued that Siz2 relocated to the NE during the M-phase, while our biochemical data showed a Siz2-Nup170 interaction mainly in the G1-phase, we double tagged cells with GFP-Siz2 and Nup170-RFP and looked for possible protein overlap. Overall, we noticed a strong GFP-Siz2 intra-nuclear signal during G1 and S-phase, making it difficult to analyse the GFP-Siz2 perinuclear enrichment. However, a few cells showed bright GFP-Siz2 foci that often overlapped with the NE, and frequently overlapped with Nup170-RFP (Fig. 4.10 C).

4.3 Discussion

The initial observation that SUMO enzymes are enriched within the nucleus suggests that SUMOylation is mainly involved in nuclear processes (Takahashi et al., 2003). Studies have shown that SUMOylation can alter a protein's interactions, stability, localization, and activity. The conjugation of SUMO peptides into SUMO motifs can alter the protein's surface charges, and consequently modulate its interactions by masking

or revealing binding domains (Geiss-Friedlander and Melchior, 2007). The low level of steady state SUMOylated proteins imposes a major challenge in the process of cataloguing SUMO targets. However, recent studies have suggested that SUMOylation often target several proteins functioning in the same biological processes, thus providing a certain degree of redundancy (Tatham et al., 2009; Wohlschlegel et al., 2004). For example, several proteins involved in telomere tethering to the NE - SIR proteins, yKu heterodimer and Rap1 - are SUMOylated. Based on these findings, several studies have implied that SUMOylation functions as a “molecular glue” responsible for mediating the assembly of macromolecular complexes (Makhnevych et al., 2009; Wohlschlegel et al., 2004).

The SUMOylation of a given protein can be triggered by a diverse range of biological stimuli. For example, studies in budding yeast have shown a cell cycle dependent relocation of the SUMO E3 ligase Siz1 from the nucleus to the bud neck during the M-phase. The Siz1 recruitment to the bud neck is responsible for the SUMOylation of proteins forming the septin ring (Johnson and Gupta, 2001). Moreover, the Ulp1 evacuation from the nucleus during M-phase represents another example of how variation in SUMO enzyme availability can regulate the cellular global SUMOylation (Makhnevych et al., 2007). To date, the cell cycle specific relocalization observed for Siz1 has not been described for Siz2. In this study, we reported that GFP-Siz2 was recruited to the nuclear periphery during the M-phase (Fig. 4.1). The relocalization of Siz1 and Siz2 during

the M-phase, combined to the defects during the cell cycle progression observed in the *siz1Δsiz2Δ* mutant (Reindle et al., 2006), suggest that SUMO redistribution during mitosis might be required for proper progression through the cell cycle.

Studies have shown that Siz1's relocation from the nucleus to the septin ring during M-phase is mediated by Siz1 phosphorylation (Johnson and Gupta, 2001). Since we observed that GFP-Siz2 was sequestered to the NE during M-phase, we decided to investigate whether Siz2 relocation was also dependent on post-translational modification. Initially, we detected three different species of Siz2 (Fig. 4.2 and 4.3). The slower migrating species of Siz2 was predicted to have the molecular mass of 132 MDa, and it was constitutively produced during the cell cycle. Further investigation showed that this band represented the SUMOylated species of Siz2. Another post translationally modified species of Siz2 was produced exclusively during the M-phase, and it was sensitive to phosphatase treatment. This observation suggests that the Siz2 band exclusively observed during M-phase represents the phosphorylated species of Siz2. Finally, we observed lower molecular mass and most abundant band representing the non-modified species of Siz2 (Fig. 4.3). To further investigate the role that phosphorylation plays in the Siz2 function, we created different Siz2 phosphomutants. Based on a recent high-throughput study identifying potential phosphorylation motifs in budding yeast (Holt et al., 2009), we created the phosphomutants

Siz2$^{(S522/527A)}$ and Siz2$^{(S674A)}$. The use of these mutants allowed us to identify the serine residues 522/527 as the Siz2's phosphorylation motif (Fig. 4.5). Of note, we also observed that the serine residues 522/527 are required for the Siz2 recruitment to the NE, as the GFP-Siz2$^{(S522/527A)}$ was not sequestered to the NE during late anaphase/telophase (Fig 4.1 and 4.2).

During the last decade, several studies have linked the SUMOylation process to the NPCs. Supporting the importance of NPCs in the regulation of the SUMOylation process (Palancade and Doye, 2008), we described in the previous chapter an interaction between Siz2 and Nup170 (Fig. 3.6 A and C). In this chapter, we observed that strains carrying the deletion of the core nucleoporin, Nup170, presented lower level of Siz2 phosphorylation, and also failed to sequester the GFP-Siz2 to the NE during M-phase (Fig. 4.7).

The similarities observed between Siz2$^{(S522/527A)}$ and *nup170Δ* mutant in the reduction of Siz2 phosphorylation, as well as in the lack of GFP-Siz2 recruitment to the NE, lead us to expect that phosphorylation is responsible for relocating Siz2 to the NE, possibly by increasing the Siz2 affinity for Nup170 (Fig. 4.4, 4.5, and 4.7). Therefore, we have hypothesized that by blocking phosphorylation and decreasing the sequestering of Siz2 to the NE, we would notice a reduction in the Nup170 interaction with Siz2. Surprisingly, we observed an increase in the interaction between Siz2$^{(S522/527A)}$ and Nup170 relative to Siz2 (Fig. 4.9 A).

The unexpected observation that siz2$^{(S522/527A)}$ purified more Nup170 suggested that interaction between these two proteins is destabilized by phosphorylation. However, the use of asynchronous culture to perform pull-down experiments do not address the dynamic nature of a protein-protein interaction during cell cycle progression. Considering that Siz2 is transiently phosphorylated and associated with the NE during M-phase, we decide to use actively growing synchronous cultures to better define the Siz2 interaction with Nup170. Using this approach, we investigate how Nup170 interacted with Siz2 or Siz2$^{(S522/527A)}$ during the different stages of the cell cycle. We observed that in WT cells Siz2 robustly purified Nup170 during G1- and early S-phase, and also observed a decrease in the Siz2 interaction with Nup170 during mitosis (Fig. 4.10 A). In agreement with the concept that phosphorylation destabilizes the Siz2 interaction with Nup170, the Siz2$^{(S522/527A)}$ mutant was stably associated with Nup170 throughout the cell cycle (Fig. 4.10 B).

The surprising observation that phosphorylation decreases Siz2's affinity for Nup170, while facilitating its recruitment to the NE during the M-phase, suggested that Siz2 association with the NE during M-phase is not mediated by Nup170. In agreement, the Siz2's smooth distribution throughout the NE during mitosis did not resemble the typical distribution of NPCs (Fig. 4.1), thus supporting our observation that Siz2 interaction with Nup170 did not occur in the M-phase (Fig. 4.10 A). However, based on the pull-down experiments showing an interaction between Siz2 and

Nup170 during G1 and S-phase, and the initial detection of bright GFP-Siz2 foci formed during interphase (Fig. 4.1 arrows), we investigated whether we could observe an overlap between Siz2 foci and Nup170. The analysis of the strains producing the Nup170-RFP-T and GFP-Siz2 presented visible overlapping between these two proteins during interphase (Fig. 4.10 C). Unfortunately, we were not able to quantify the degree of overlap between these two proteins due the transient presence of the GFP-Siz2 foci during the interphase.

In the previous chapter, we described that the interaction between Nup170 and Esc1 was significantly reduced in the *siz2Δ* mutant (Fig. 3.6 D). Thus, we speculated whether the increase in the Siz2$^{(S522/527A)}$ interaction with Nup170 would affect the Nup170 interaction with Esc1. In agreement with this hypothesis, our data suggested that higher levels of the Siz2-Nup170 interaction enhanced the Nup170 interaction with Esc1 (Fig. 4.9 B). Given the described interaction between Nup170, Esc1 and Siz2 (Fig. 3.6), and the fact that these proteins are involved in telomere tethering (Fig. 3.12), we decided to investigate whether Siz2$^{(S522/527A)}$ mutant altered telomere tethering to the NE. Similarly, to the *siz2Δ* mutant, we observed that Siz2$^{(S522/527A)}$ mutant failed to recruit telomeres to the NE during G1 and S-phases (Fig. 4.8). This observation suggests that correct phosphorylation of Siz2 is required for the telomere anchoring during the G1 and S-phases.

In conclusion, we showed that Siz2 phosphorylation occurring during M-phase is required for the Siz2 sequestering to the NE. Moreover, we showed that Siz2$^{(S522/527A)}$ mutant stably interacted with Nup170 during the cell cycle progression, and consequently increased the interaction between Nup170 and Esc1. The defects observed in the Siz2$^{(S522/527A)}$ could explain the defects seem in telomere tethering to the NE during G1 and S-phase. Our data lead us to propose that after telomere replication during M-phase, the perinuclear Siz2 facilitated the telomere recruitment and tethering to the NE, as suggested by the observation that mutations reducing the Siz2 association with the NE (Siz2$^{(S522/527A)}$ and *nup170Δ*) decreased the telomere anchoring to the NE. Moving forward, we will focus on identifying the proteins required for Siz2 sequestration to NE during M-phase. Given the observation that Siz2 localization to the NE is required for telomere tethering, we speculate that Siz2 is SUMOylating a protein associated with the NE, thus mediating the telomere recruitment. Since Siz2$^{(S522/527A)}$ and *nup170Δ* mutants affected GFP-Siz2 sequestering to the NE (Fig. 4.4 and 4.7 A), and both failed to produce SUMOylated proteins with similar molecular mass (Fig. 4.6 - asterisk), it is plausible to expect that the identification of these missing SUMOylated proteins might provide valuable insights into how Siz2 is recruited to the nuclear periphery, and consequently explain how Siz2 phosphorylation regulates the telomere tethering to the NE.

5. Perspectives

5.1 Synopsis

Over the past 50 years, NPCs have been implicated in nucleocytoplasmic transport. However, further research showed that nucleoporins can mediate a diverse range of biological processes (Ibarra and Hetzer, 2015; Jahed et al., 2016; Kabachinski and Schwartz, 2015; Texari and Stutz, 2015). Based on early microscopy studies, it was proposed that regions surrounding the NPC were enriched for euchromatin, and actively transcribing genes (Ptak et al., 2014; Ptak and Wozniak, 2016). However, recent studies demonstrated that NPCs can also mediate gene silencing (Ibarra and Hetzer, 2015; Van de Vosse et al., 2013). In view of these new findings, it has been suggested that NPCs might work as a hub for chromatin regulation (Ibarra and Hetzer, 2015). Giving the abundant and widespread distribution of chromatin in the nucleus and the limited number of NPCs, it is intriguing to imagine possible mechanisms by which NPCs regulate the expression of genes.

The work presented in this dissertation suggests a mechanism to reconcile the divergent role of NPCs in gene regulation. By expanding the protein interaction network of Nup170, we found that proteins present in the core scaffold of the NPCs interact with Sir4 and Esc1, proteins involved in heterochromatin formation and tethering to the NE. Our pulldown experiments showed that Esc1 and Sir4 purified several components from the NPC. Remarkably, while Esc1 purified proteins present in different sub-complexes of the NPC, Sir4 preferentially purified

proteins from NPC core scaffold. The preferential association of Sir4 with the core scaffold proteins was further conformed by microscopy studies, in which we observed an enrichment for the colocalization between Sir4 and core scaffold nucleoporins. Another protein that preferentially purified nucleoporins from the NPC core scaffold is the SUMO E3 enzyme Siz2. Despite the well established link between the SUMO isopeptidase Ulp1 and the nuclear basket of the NPCs (Lewis et al., 2007; Texari and Stutz, 2015; Zhao et al., 2004); to date NPCs have not been connected to SUMO E3 ligase. Our observation that Siz2 physical interacts with proteins involved in telomere tethering to the NE - such as Sir4, Siz2 and Snup complex (Fig. 3.6 A and C) - agrees with previous observation proposing that Siz2 is responsible for SUMOylation of the telomeric proteins Esc1 and Sir4. (Ferreira et al., 2011; Pasupala et al., 2012). Here we expand the analysis of Siz2 in telomere regulation, and we show that the interaction Nup170 and Esc1 is modulated by Siz2 (Fig. 3.6 E). Furthermore, in the fourth chapter we showed that Siz2 is SUMOylated and phosphorylated (Fig. 4.3). We also identified that phosphorylation of lysine residues 522/527 is required for the correct interaction between Nup170 and Siz2, and for telomere tethering at the NE (Fig. 4.4, 4.5, and 4.6).

5.2 The Snup complex and specialized NPCs

In order to support the essential process of nucleocytoplasmic transport, the NPCs must be constantly assembled during cell cycle progression and cellular division (Maeshima et al., 2011). As explained in the chapter 1.6 the number of NPC doubles during the interphase, illustrating the dynamic nature of this process (Winey et al., 1997). Considering the large amount of proteins, and the steps involved in the assembly of a NPC, it is possible to imagine the existence of intermediate stages of assembled NPCs, or pre-pores. Structures resembling pre-pores has been observed in cells undergoing open mitosis (Fernandez-Martinez and Rout, 2009; Franz et al., 2007; Gillespie et al., 2007; Suntharalingam and Wente, 2003). In mammalian cells, the re-assembly of NPC after mitosis is triggered by the interaction of nucleoporins with chromatin. The initial interaction between ELYS/Mel28 and chromatin recruits additional Nups leading to the formation of pre-pores (D'Angelo and Hetzer, 2008; Hetzer and Wente, 2009; Suntharalingam and Wente, 2003). Despite the initial structural description of pre-pores, we do not know whether these complexes have biological functions. However, given the large amount of biological functions attributed to the NPCs, it is tempting to speculate that pre-pores could be responsible for mediating a few of those biological processes. Corroborating this hypothesis, a recent study performed in Drosophila cells showed that chromatin association with Nup155, one of the first proteins recruited to pre-pores, can modulate the addition of other

Nups, namely Nup62 and Nup93, into the pre-pores (Breuer and Ohkura, 2015).

In this dissertation, we describe a similar mechanism occurring in *Saccharomyces cerevisiae.* In agreement with our published data showing that the interaction between Nup170 and Sir4 is required for telomeric silencing (Van de Vosse et al., 2013), we showed that Nup170 and Sir4 are similarly enriched at sub-telomeric and telomeric chromatin (Fig. 3.1). This observation further supports the role for Nup170 in telomeric recruitment and silencing. However, we were intrigued by the observation that Nup170, a scaffold Nup supposedly buried in the NPC core, interacted with Sir4 and chromatin. As we expanded our analysis we observed that Sir4 in fact preferentially interacted with Nups from the core scaffold (Fig.3.10). Our data shown that Sir4 purified several core nucleoporins, such as components from Nu170 and Nup84 complex, while failing to purify more peripheral nucleoporins such as Nup53 and Nup60. This observation suggested the presence of sub-population of NPC, namely Snup Complex. The simplified structure observed in the Snup complex could potentially explain the interaction of the proteins present in the core scaffold with chromatin and Sir4. The full characterization of this sub-population of NPCs represent an exciting research opportunity. Moving forward it will be paramount to understand whether the Snup complex represent a stable subset of NPCs, or it is transient population of not fully assembled pores.

5.3 The role of the NPC in chromatin regulation

Studies showing that NPCs are associated with actively expressing genes suggested that NPC not only mediated nucleocytoplasmic transport, but it also facilitated gene expression (Ahmed and Brickner, 2007; Van de Vosse et al., 2011). The tethering of transcriptionally active genes with NPCs facilitates transcription and increases the efficiency of mRNA transport (García-Oliver et al., 2012; Rodríguez-Navarro and Hurt, 2011). Also, it is suggested that the positioning of active genes close to the NPCs optimises gene expression by facilitating the interaction between active genes and newly imported transcriptional factors (Pemberton et al., 1999). Detailed investigation showed that different sub-complexes of the NPC are required for optimal gene expression. In budding yeast, while the interaction between Rap1/Gcr1/Gcr2 with the Nup84 complex is sufficient to promote the expression of Gcr1-dependent genes (Menon et al., 2005), the recruitment of the transcriptionally active GAL genes to the NPC requires the nuclear basket protein Mlp1 and SAGA complex (Luthra et al., 2007). Surprisingly, the studies using the *GAL* and *INO* genes showed that tethering to the nuclear periphery was not altered after the repression of these genes (Light et al., 2010). Furthermore, a study has demonstrated that tethering of silenced genes to the NE also depends on the nuclear basket and Nup84 complex, suggesting that NPCs might play several functions in chromatin regulation. Finally, it has been suggested that the interaction between Nups and

genes is remodeled following gene repression, and that the newly repressed locus stops interacting with nuclear basket and it starts to interact with components from the Nup84 complex (Brickner et al., 2007; Light et al., 2010).

The Nup170 complex has also been linked to gene repression. The observation that Nup170p was enriched, and required for silencing of sub-telomeric and telomeric genes further connected the core scaffold of the NPC to gene silencing (Van de Vosse et al., 2013). The Nup170 mediated silencing of sub-telomeric and telomeric genes is dependent on the Nup170 interaction with Sir4, as *nup170Δ* mutant failed to correctly load Sir4 onto chromatin (Van de Vosse et al., 2013). Since the Nup170 interaction with Sir4 represented a novel mechanism by which NPCs mediate gene silencing, we attempted to further define the nucleoporins interacting with Sir4. In agreement with the observation that core scaffold, namely Nup170 and Nup84 complex, is involved with gene silencing, we found that Sir4 purified the majority of the Nups forming this structure (Fig. 3.10). Of note, the observation that Sir4 interacts with the core scaffold, but not the peripheral Nups, suggests the existence of distinct population of NPCs, which we named as Snup complex. Despite the current work describing the Snup complex, further studies will be required to better establish the function of such complex. However, given the Snup complex protein composition, we propose this complex assembly is involved in gene silencing.

5.4 The biological links between NPC and SUMOylation

The SUMOylation process has long been linked to the NPC and nucleocytoplasmitic transport. The initial observations that SUMOylation was involved in nucleocytoplasmic transport were made in vertebrates (Matunis et al., 1996). Studies demonstranted that SUMOylation of vertebrate RanGAP1, a Ran GTPase-activating protein enzyme, was required for promoting the interaction between RanGAP1 and Nup358-RanBP2, and possibly for maintaining the Ran gradient (Mahajan et al., 1997; Palancade and Doye, 2008). SUMOylation was also linked to nucleocytoplasmic transport in budding yeast. The deletion of *UBA2* or mutation afecting the *ULP1* interaction with the NPC decreased the import of proteins containing cNLS, possibly by accumulating the cNLS adaptor protein Kap60 in the nucleus (Stade et al., 2002). The increased interrest in SUMOylation led several reseach groups to caracterize the distribution of the SUMO enzymes/proteases (Bayer et al., 1998; Johnson and Gupta, 2001; Johnson et al., 1997; Matunis et al., 1996; Müller et al., 2004; Okuma et al., 1999; Wohlschlegel et al., 2004). A relevant piece of information obtained from these efforts was that while the distribution of SUMO enzymes differed among eukaryotes, the localization of SUMO proteases was conserved during evolution (Palancade and Doye, 2008).

In budding yeast, the SUMO protease Ulp1 is targeted to the NPC through is the N-terminal domain. While the Ulp1 amino acids residues 1-150 interacts with Kap121, the amino acids residues 150-340 interacts with Kap60-95. (Makhnevych et al., 2007; Palancade and Doye, 2008). Correct Ulp1 tethering to the NPC also requires the nuclear basket proteins the Nup60, Mlp1, and Mlp2 (Zhao et al., 2004). Similar to what was described for mutations in the nuclear basket, deletion of nucleoporins from the Nup84 complex altered Ulp1 ability to interact with NPC, and also reduced its expression levels (Palancade et al., 2007a). Given that NPC interaction with Ulp1 has been implicated in important biological processes, such as DNA repair and replication, mRNA quality control, and nuclear organization, it is likely that Ulp1 interaction with the NPC is mediated by several redundant mechanisms (Galy et al., 2004; Palancade and Doye, 2008; Panse et al., 2006; Zhao et al., 2004). To date, the literature has described NPCs as a hub for deSUMOylation (Strambio-De-Castillia et al., 2010; Texari and Stutz, 2015), however our recent observation that Siz2 purifies with components from the Nup170 complex suggests that NPCs might have a more complex role in SUMOylation. Of note, we only identified interactions between Siz2 with Nups present in the Snup complex. This observation led us to hypothesize that while Ulp1 interaction with the nuclear basket mediates deSUMOylation, the Siz2 interaction with the Snup complex could promote SUMOylation.

5.5 The roles of Siz2 in protein interaction

Previously, Siz2 has been implicated in SUMOylation of the telomeric proteins, Sir4 and yKu70/yKu80. The first study implicating Siz2 and telomere regulation reported that *siz2Δ* mutant impaired telomere tethering by inhibiting the Sir4 interaction with Esc1, and also by inhibiting the yKu70/yKu80 interaction with the telomerase (Ferreira et al., 2011). Since Siz2 purified with Nup170, and both are required for telomere tethering, we investigated whether Nup170 interaction with proteins associated with telomere tethering was dependent on Siz2. The data we obtained using *siz2Δ* mutant suggests that Sir4 interaction with the NE associated proteins Esc1 and Nup170 was not altered (Fig. 3.6 E), an observation that was further supported by the observation that Sir4-eGFP tethering to the NE is not affected in the *siz2Δ* mutant (Fig. 3.7 A). However, while Sir4 association with the NE is SUMO independent, Sir4 loading onto telomeres requires SUMOylation, as the ChIP-on-chip studies showed that Sir4 interaction with chromatin was impaired in SUMO mutants (Wan et al., 2013). Surprisingly, further investigation showed that Esc1 interaction with Nup170 was significantly reduced in the *siz2Δ* mutant, which could partially explain the telomere tethering defects in this mutant (Fig. 3.6 E).

Given the importance of Siz2 in telomere tethering and in mediating the Nup170 interaction with Esc1, we further studied the Siz2 biology. Of

note, we described that Siz2 was evacuated to nuclear periphery during M-phase, in a process mediated by phosphorylation of Siz2 (Fig. 4.1 and 4.2). Moreover, we also observed that phosphorylation is required for the correct role of Siz2 in SUMOylation (Fig. 4-4) and telomere tethering (Fig 4.6). Finally, mutation of the serine residues 522/527 of the Siz2 not only changed the interaction between Siz2 and Nup170, but it also altered the Esc1 interaction with Nup170 (Fig. 4.7 and 4.8).

5.6 The possible functions of Snup complex:

In addition to the nucleocytoplasmic transport, proteins from the NPC have been implicated in several biological processes (Makhnevych et al., 2003; Makhnevych et al., 2007; Palancade et al., 2007a; Stoffler et al., 1999; Suntharalingam and Wente, 2003; Therizols et al., 2006; Wente, 2000). In this dissertation, we observed that Nups forming the core scaffold of the NPC interact with the chromatin silencing protein, Sir4. The Sir4 physical interaction with this group of Nups indicated the potential existence of a new complex formed by nucleoporin that occurred outside the full assembled NPCs. Using microscopy analysis, we further confirmed this initial observation by showing that Sir4-interacting Nups presented a higher degree of colocalization with Sir4 when compared to Nups that did not interact with Sir4. We named this new complex as Snup complex (Sir-Nup complex). The initial identification of the Snup complex not only represent a possibility to reconcile the broad range of biological processes

associated with NPCs, but it also helps explain how Nups that are predicted to be buried inside the NPCs can interact with proteins other than their proposed nucleoporins interacting partners.

Despite our efforts to identify and characterize this new nucleoporin complex, to date, we are still not able to distinguish whether the Snup complex represent a temporal variation of fully assembled NPCs, such as the pre-pores observed in mammalian cells (Gillespie et al., 2007; Walther et al., 2003), or whether this is represent a new population of stably interacting nucleoporins, such as the NPCs lacking the nuclear basket found juxtaposed to the nucleolus (Niepel et al., 2013; Niepel et al., 2005; Strambio-de-Castillia et al., 1999). Functionally, the absence of FG-Nups in the Snup complex would suggest that this structure is not competent to mediate nucleocytoplasmic transport. Instead, the presence of chromatin silencing protein Sir4 led us to hypothesized that Snup complex might function in telomere regulation and gene expression. This hypothesis is further supported by studies showing that nucleoporins from the NPC core scaffold are involved in telomere repair, subtelomeric and telomeric gene expression, and telomere localization (Therizols et al., 2006; Van de Vosse et al., 2013). Another protein present in the Snup complex that also share a role in telomere tethering is the SUMO E3 ligase Siz2. Considering that Ulp1 interacts with the nuclear basket of the NPC and the Siz2 interacts with the Snup, it is possible to imagine those structures

representing a mechanism to regulate the overall SUMOylation (Lewis et al., 2007).

6. References

Ahmed, S., and J.H. Brickner. 2007. Regulation and epigenetic control of transcription at the nuclear periphery. *Trends Genet*. 23:396-402.

Aitchison, J.D., and M.P. Rout. 2012. The yeast nuclear pore complex and transport through it. *Genetics*. 190:855-883.

Aitchison, J.D., M.P. Rout, M. Marelli, G. Blobel, and R.W. Wozniak. 1995. Two novel related yeast nucleoporins Nup170p and Nup157p: complementation with the vertebrate homologue Nup155p and functional interactions with the yeast nuclear pore-membrane protein Pom152p. *J Cell Biol*. 131:1133-1148.

Alber, F., S. Dokudovskaya, L.M. Veenhoff, W. Zhang, J. Kipper, D. Devos, A. Suprapto, O. Karni-Schmidt, R. Williams, B.T. Chait, M.P. Rout, and A. Sali. 2007a. Determining the architectures of macromolecular assemblies. *Nature*. 450:683-694.

Alber, F., S. Dokudovskaya, L.M. Veenhoff, W. Zhang, J. Kipper, D. Devos, A. Suprapto, O. Karni-Schmidt, R. Williams, B.T. Chait, A. Sali, and M.P. Rout. 2007b. The molecular architecture of the nuclear pore complex. *Nature*. 450:695-701.

Albuquerque, C.P., M.B. Smolka, S.H. Payne, V. Bafna, J. Eng, and H. Zhou. 2008. A multidimensional chromatography technology for in-depth phosphoproteome analysis. *Mol Cell Proteomics*. 7:1389-1396.

Amlacher, S., P. Sarges, D. Flemming, V. van Noort, R. Kunze, D.P. Devos, M. Arumugam, P. Bork, and E. Hurt. 2011. Insight into structure and assembly of the nuclear pore complex by utilizing the genome of a eukaryotic thermophile. *Cell*. 146:277-289.

Andrulis, E.D., D.C. Zappulla, A. Ansari, S. Perrod, C.V. Laiosa, M.R. Gartenberg, and R. Sternglanz. 2002. Esc1, a nuclear periphery protein required for Sir4-based plasmid anchoring and partitioning. *Mol Cell Biol*. 22:8292-8301.

Antonin, W., J. Ellenberg, and E. Dultz. 2008. Nuclear pore complex assembly through the cell cycle: regulation and membrane organization. *FEBS Lett*. 582:2004-2016.

Bayer, P., A. Arndt, S. Metzger, R. Mahajan, F. Melchior, R. Jaenicke, and J. Becker. 1998. Structure determination of the small ubiquitin-related modifier SUMO-1. *J Mol Biol*. 280:275-286.

Beck, M., and E. Hurt. 2017. The nuclear pore complex: understanding its function through structural insight. *Nat Rev Mol Cell Biol*. 18:73-89.

Bettermann, K., M. Benesch, S. Weis, and J. Haybaeck. 2011. SUMOylation in carcinogenesis. *Cancer Lett*.

Bolger, A.M., M. Lohse, and B. Usadel. 2014. Trimmomatic: a flexible trimmer for Illumina sequence data. *Bioinformatics*. 30:2114-2120.

Breuer, M., and H. Ohkura. 2015. A negative loop within the nuclear pore complex controls global chromatin organization. *Genes Dev*. 29:1789-1794.

Brickner, D.G., I. Cajigas, Y. Fondufe-Mittendorf, S. Ahmed, P.C. Lee, J. Widom, and J.H. Brickner. 2007. H2A.Z-mediated localization of

genes at the nuclear periphery confers epigenetic memory of previous transcriptional state. *PLoS Biol*. 5:e81.
Buck, S.W., and D. Shore. 1995. Action of a RAP1 carboxy-terminal silencing domain reveals an underlying competition between HMR and telomeres in yeast. *Genes Dev*. 9:370-384.
Bupp, J.M., A.E. Martin, E.S. Stensrud, and S.L. Jaspersen. 2007. Telomere anchoring at the nuclear periphery requires the budding yeast Sad1-UNC-84 domain protein Mps3. *J Cell Biol*. 179:845-854.
Burke, B., and J. Ellenberg. 2002. Remodelling the walls of the nucleus. *Nat Rev Mol Cell Biol*. 3:487-497.
Cairo, L.V., C. Ptak, and R.W. Wozniak. 2013a. Dual personality of Mad1: regulation of nuclear import by a spindle assembly checkpoint protein. *Nucleus*. 4:367-373.
Cairo, L.V., C. Ptak, and R.W. Wozniak. 2013b. Mitosis-specific regulation of nuclear transport by the spindle assembly checkpoint protein Mad1p. *Mol Cell*. 49:109-120.
CALLAN, H.G., and S.G. TOMLIN. 1950. Experimental studies on amphibian oocyte nuclei. I. Investigation of the structure of the nuclear membrane by means of the electron microscope. *Proc R Soc Lond B Biol Sci*. 137:367-378.
Calo, E., and J. Wysocka. 2013. Modification of enhancer chromatin: what, how, and why? *Mol Cell*. 49:825-837.
Capitanio, J.S. 2016. Github - ImageJ Script, https://github.com/jucapitanio/Software/tree/master/ImageJ%20macros/smFISH.
Chadrin, A., B. Hess, M. San Roman, X. Gatti, B. Lombard, D. Loew, Y. Barral, B. Palancade, and V. Doye. 2010. Pom33, a novel transmembrane nucleoporin required for proper nuclear pore complex distribution. *J Cell Biol*. 189:795-811.
Chi, P., C.D. Allis, and G.G. Wang. 2010. Covalent histone modifications--miswritten, misinterpreted and mis-erased in human cancers. *Nat Rev Cancer*. 10:457-469.
Chook, Y.M., and K.E. Süel. 2011. Nuclear import by karyopherin-βs: recognition and inhibition. *Biochim Biophys Acta*. 1813:1593-1606.
Chung, I., and X. Zhao. 2015. DNA break-induced sumoylation is enabled by collaboration between a SUMO ligase and the ssDNA-binding complex RPA. *Genes Dev*. 29:1593-1598.
Corbett, A.H., and P.A. Silver. 1997. Nucleocytoplasmic transport of macromolecules. *Microbiol Mol Biol Rev*. 61:193-211.
Cremona, C.A., P. Sarangi, and X. Zhao. 2012. Sumoylation and the DNA damage response. *Biomolecules*. 2:376-388.
Cubeñas-Potts, C., and M.J. Matunis. 2013. SUMO: a multifaceted modifier of chromatin structure and function. *Dev Cell*. 24:1-12.
Czapiewski, R., M.I. Robson, and E.C. Schirmer. 2016. Anchoring a Leviathan: How the Nuclear Membrane Tethers the Genome. *Front Genet*. 7:82.

D'Angelo, M.A., D.J. Anderson, E. Richard, and M.W. Hetzer. 2006. Nuclear pores form de novo from both sides of the nuclear envelope. *Science*. 312:440-443.

D'Angelo, M.A., J.S. Gomez-Cavazos, A. Mei, D.H. Lackner, and M.W. Hetzer. 2012. A change in nuclear pore complex composition regulates cell differentiation. *Dev Cell*. 22:446-458.

D'Angelo, M.A., and M.W. Hetzer. 2008. Structure, dynamics and function of nuclear pore complexes. *Trends Cell Biol*. 18:456-466.

D'Angelo, M.A., M. Raices, S.H. Panowski, and M.W. Hetzer. 2009. Age-dependent deterioration of nuclear pore complexes causes a loss of nuclear integrity in postmitotic cells. *Cell*. 136:284-295.

David, R. 2010. Sumoylation: Targeting SUMO. *Nat Rev Mol Cell Biol*. 11:387.

Dechat, T., K. Pfleghaar, K. Sengupta, T. Shimi, D.K. Shumaker, L. Solimando, and R.D. Goldman. 2008. Nuclear lamins: major factors in the structural organization and function of the nucleus and chromatin. *Genes Dev*. 22:832-853.

DeGrasse, J.A., K.N. DuBois, D. Devos, T.N. Siegel, A. Sali, M.C. Field, M.P. Rout, and B.T. Chait. 2009. Evidence for a shared nuclear pore complex architecture that is conserved from the last common eukaryotic ancestor. *Mol Cell Proteomics*. 8:2119-2130.

Denison, C., A.D. Rudner, S.A. Gerber, C.E. Bakalarski, D. Moazed, and S.P. Gygi. 2005. A proteomic strategy for gaining insights into protein sumoylation in yeast. *Mol Cell Proteomics*. 4:246-254.

Devos, D., S. Dokudovskaya, R. Williams, F. Alber, N. Eswar, B.T. Chait, M.P. Rout, and A. Sali. 2006. Simple fold composition and modular architecture of the nuclear pore complex. *Proc Natl Acad Sci U S A*. 103:2172-2177.

Doye, V., and E. Hurt. 1997. From nucleoporins to nuclear pore complexes. *Curr Opin Cell Biol*. 9:401-411.

Doye, V., R. Wepf, and E.C. Hurt. 1994. A novel nuclear pore protein Nup133p with distinct roles in poly(A)+ RNA transport and nuclear pore distribution. *EMBO J*. 13:6062-6075.

Duina, A.A., M.E. Miller, and J.B. Keeney. 2014. Budding yeast for budding geneticists: a primer on the Saccharomyces cerevisiae model system. *Genetics*. 197:33-48.

Dultz, E., E. Zanin, C. Wurzenberger, M. Braun, G. Rabut, L. Sironi, and J. Ellenberg. 2008. Systematic kinetic analysis of mitotic dis- and reassembly of the nuclear pore in living cells. *J Cell Biol*. 180:857-865.

Ellahi, A., D.M. Thurtle, and J. Rine. 2015. The Chromatin and Transcriptional Landscape of Native Saccharomyces cerevisiae Telomeres and Subtelomeric Domains. *Genetics*. 200:505-521.

Enomoto, S., M.S. Longtine, and J. Berman. 1994. Enhancement of telomere-plasmid segregation by the X-telomere associated

sequence in Saccharomyces cerevisiae involves SIR2, SIR3, SIR4 and ABF1. *Genetics*. 136:757-767.
Fernandez-Martinez, J., and M.P. Rout. 2009. Nuclear pore complex biogenesis. *Curr Opin Cell Biol*. 21:603-612.
Ferreira, H.C., B. Luke, H. Schober, V. Kalck, J. Lingner, and S.M. Gasser. 2011. The PIAS homologue Siz2 regulates perinuclear telomere position and telomerase activity in budding yeast. *Nat Cell Biol*. 13:867-874.
Feuerbach, F., V. Galy, E. Trelles-Sticken, M. Fromont-Racine, A. Jacquier, E. Gilson, J.C. Olivo-Marin, H. Scherthan, and U. Nehrbass. 2002. Nuclear architecture and spatial positioning help establish transcriptional states of telomeres in yeast. *Nat Cell Biol*. 4:214-221.
Fichtman, B., C. Ramos, B. Rasala, A. Harel, and D.J. Forbes. 2010. Inner/Outer nuclear membrane fusion in nuclear pore assembly: biochemical demonstration and molecular analysis. *Mol Biol Cell*. 21:4197-4211.
Floch, A.G., B. Palancade, and V. Doye. 2014. Fifty years of nuclear pores and nucleocytoplasmic transport studies: multiple tools revealing complex rules. *Methods Cell Biol*. 122:1-40.
Franz, C., R. Walczak, S. Yavuz, R. Santarella, M. Gentzel, P. Askjaer, V. Galy, M. Hetzer, I.W. Mattaj, and W. Antonin. 2007. MEL-28/ELYS is required for the recruitment of nucleoporins to chromatin and postmitotic nuclear pore complex assembly. *EMBO Rep*. 8:165-172.
Frey, S., and D. Görlich. 2007. A saturated FG-repeat hydrogel can reproduce the permeability properties of nuclear pore complexes. *Cell*. 130:512-523.
Gaik, M., D. Flemming, A. von Appen, P. Kastritis, N. Mücke, J. Fischer, P. Stelter, A. Ori, K.H. Bui, J. Baßler, E. Barbar, M. Beck, and E. Hurt. 2015. Structural basis for assembly and function of the Nup82 complex in the nuclear pore scaffold. *J Cell Biol*. 208:283-297.
Galy, V., O. Gadal, M. Fromont-Racine, A. Romano, A. Jacquier, and U. Nehrbass. 2004. Nuclear retention of unspliced mRNAs in yeast is mediated by perinuclear Mlp1. *Cell*. 116:63-73.
Galy, V., J.C. Olivo-Marin, H. Scherthan, V. Doye, N. Rascalou, and U. Nehrbass. 2000. Nuclear pore complexes in the organization of silent telomeric chromatin. *Nature*. 403:108-112.
García-Oliver, E., V. García-Molinero, and S. Rodríguez-Navarro. 2012. mRNA export and gene expression: the SAGA-TREX-2 connection. *Biochim Biophys Acta*. 1819:555-565.
Gareau, J.R., and C.D. Lima. 2010. The SUMO pathway: emerging mechanisms that shape specificity, conjugation and recognition. *Nat Rev Mol Cell Biol*. 11:861-871.
Geiss-Friedlander, R., and F. Melchior. 2007. Concepts in sumoylation: a decade on. *Nat Rev Mol Cell Biol*. 8:947-956.

Gietz, R.D., and R.A. Woods. 2002. Transformation of yeast by lithium acetate/single-stranded carrier DNA/polyethylene glycol method. *Methods Enzymol*. 350:87-96.

Gilbert, S.F. 1978. The embryological origins of the gene theory. *J Hist Biol*. 11:307-351.

Gillespie, P.J., G.A. Khoudoli, G. Stewart, J.R. Swedlow, and J.J. Blow. 2007. ELYS/MEL-28 chromatin association coordinates nuclear pore complex assembly and replication licensing. *Curr Biol*. 17:1657-1662.

Gilson, E., and V. Géli. 2007. How telomeres are replicated. *Nat Rev Mol Cell Biol*. 8:825-838.

Gilson, E., T. Laroche, and S.M. Gasser. 1993. Telomeres and the functional architecture of the nucleus. *Trends Cell Biol*. 3:128-134.

Gong, L., B. Li, S. Millas, and E.T. Yeh. 1999. Molecular cloning and characterization of human AOS1 and UBA2, components of the sentrin-activating enzyme complex. *FEBS Lett*. 448:185-189.

Gotta, M., T. Laroche, A. Formenton, L. Maillet, H. Scherthan, and S.M. Gasser. 1996. The clustering of telomeres and colocalization with Rap1, Sir3, and Sir4 proteins in wild-type Saccharomyces cerevisiae. *J Cell Biol*. 134:1349-1363.

Güttinger, S., E. Laurell, and U. Kutay. 2009. Orchestrating nuclear envelope disassembly and reassembly during mitosis. *Nat Rev Mol Cell Biol*. 10:178-191.

Hannan, A., N.M. Abraham, S. Goyal, I. Jamir, U.D. Priyakumar, and K. Mishra. 2015. Sumoylation of Sir2 differentially regulates transcriptional silencing in yeast. *Nucleic Acids Res*. 43:10213-10226.

Hannich, J.T., A. Lewis, M.B. Kroetz, S.J. Li, H. Heide, A. Emili, and M. Hochstrasser. 2005. Defining the SUMO-modified proteome by multiple approaches in Saccharomyces cerevisiae. *J Biol Chem*. 280:4102-4110.

Hardy, C.F., L. Sussel, and D. Shore. 1992. A RAP1-interacting protein involved in transcriptional silencing and telomere length regulation. *Genes Dev*. 6:801-814.

Hay, R.T. 2007. SUMO-specific proteases: a twist in the tail. *Trends Cell Biol*. 17:370-376.

Hediger, F., K. Dubrana, and S.M. Gasser. 2002. Myosin-like proteins 1 and 2 are not required for silencing or telomere anchoring, but act in the Tel1 pathway of telomere length control. *J Struct Biol*. 140:79-91.

Heichman, K.A., and J.M. Roberts. 1996. The yeast CDC16 and CDC27 genes restrict DNA replication to once per cell cycle. *Cell*. 85:39-48.

Hetzer, M.W. 2010. The nuclear envelope. *Cold Spring Harb Perspect Biol*. 2:a000539.

Hetzer, M.W., T.C. Walther, and I.W. Mattaj. 2005. Pushing the envelope: structure, function, and dynamics of the nuclear periphery. *Annu Rev Cell Dev Biol*. 21:347-380.

Hetzer, M.W., and S.R. Wente. 2009. Border control at the nucleus: biogenesis and organization of the nuclear membrane and pore complexes. *Dev Cell*. 17:606-616.

Hickey, C.M., N.R. Wilson, and M. Hochstrasser. 2012. Function and regulation of SUMO proteases. *Nat Rev Mol Cell Biol*. 13:755-766.

Hochstrasser, M. 2000. Evolution and function of ubiquitin-like protein-conjugation systems. *Nat Cell Biol*. 2:E153-157.

Hochstrasser, M. 2001. SP-RING for SUMO: new functions bloom for a ubiquitin-like protein. *Cell*. 107:5-8.

Hochstrasser, M. 2009. Origin and function of ubiquitin-like proteins. *Nature*. 458:422-429.

Hoelz, A., E.W. Debler, and G. Blobel. 2011. The structure of the nuclear pore complex. *Annu Rev Biochem*. 80:613-643.

Holt, L.J., B.B. Tuch, J. Villén, A.D. Johnson, S.P. Gygi, and D.O. Morgan. 2009. Global analysis of Cdk1 substrate phosphorylation sites provides insights into evolution. *Science*. 325:1682-1686.

Horigome, C., T. Okada, K. Shimazu, S.M. Gasser, and K. Mizuta. 2011. Ribosome biogenesis factors bind a nuclear envelope SUN domain protein to cluster yeast telomeres. *EMBO J*. 30:3799-3811.

Huh, W.K., J.V. Falvo, L.C. Gerke, A.S. Carroll, R.W. Howson, J.S. Weissman, and E.K. O'Shea. 2003. Global analysis of protein localization in budding yeast. *Nature*. 425:686-691.

Hwang, K.W., T.J. Won, H. Kim, H.J. Chun, T. Chun, and Y. Park. 2011. Characterization of the regulatory roles of the SUMO. *Diabetes Metab Res Rev*. 27:854-861.

Ibarra, A., and M.W. Hetzer. 2015. Nuclear pore proteins and the control of genome functions. *Genes Dev*. 29:337-349.

Impens, F., L. Radoshevich, P. Cossart, and D. Ribet. 2014. Mapping of SUMO sites and analysis of SUMOylation changes induced by external stimuli. *Proc Natl Acad Sci U S A*. 111:12432-12437.

Jadhav, T., and M.W. Wooten. 2009. Defining an Embedded Code for Protein Ubiquitination. *J Proteomics Bioinform*. 2:316.

Jahed, Z., M. Soheilypour, M. Peyro, and M.R. Mofrad. 2016. The LINC and NPC relationship - it's complicated! *J Cell Sci*. 129:3219-3229.

Jin, J., Y. Cai, T. Yao, A.J. Gottschalk, L. Florens, S.K. Swanson, J.L. Gutiérrez, M.K. Coleman, J.L. Workman, A. Mushegian, M.P. Washburn, R.C. Conaway, and J.W. Conaway. 2005. A mammalian chromatin remodeling complex with similarities to the yeast INO80 complex. *J Biol Chem*. 280:41207-41212.

Johnson, E.S., and A.A. Gupta. 2001. An E3-like factor that promotes SUMO conjugation to the yeast septins. *Cell*. 106:735-744.

Johnson, E.S., I. Schwienhorst, R.J. Dohmen, and G. Blobel. 1997. The ubiquitin-like protein Smt3p is activated for conjugation to other proteins by an Aos1p/Uba2p heterodimer. *EMBO J*. 16:5509-5519.
Kabachinski, G., and T.U. Schwartz. 2015. The nuclear pore complex--structure and function at a glance. *J Cell Sci*. 128:423-429.
Kalab, P., and R. Heald. 2008. The RanGTP gradient - a GPS for the mitotic spindle. *J Cell Sci*. 121:1577-1586.
Kampmann, M., and G. Blobel. 2009. Three-dimensional structure and flexibility of a membrane-coating module of the nuclear pore complex. *Nat Struct Mol Biol*. 16:782-788.
Kelley, K., K.E. Knockenhauer, G. Kabachinski, and T.U. Schwartz. 2015. Atomic structure of the Y complex of the nuclear pore. *Nat Struct Mol Biol*. 22:425-431.
Knipscheer, P., A. Flotho, H. Klug, J.V. Olsen, W.J. van Dijk, A. Fish, E.S. Johnson, M. Mann, T.K. Sixma, and A. Pichler. 2008. Ubc9 sumoylation regulates SUMO target discrimination. *Mol Cell*. 31:371-382.
Knockenhauer, K.E., and T.U. Schwartz. 2016. The Nuclear Pore Complex as a Flexible and Dynamic Gate. *Cell*. 164:1162-1171.
Kobayashi, J., and Y. Matsuura. 2013. Structural basis for cell-cycle-dependent nuclear import mediated by the karyopherin Kap121p. *J Mol Biol*. 425:1852-1868.
Kupiec, M. 2014. Biology of telomeres: lessons from budding yeast. *FEMS Microbiol Rev*. 38:144-171.
Kvam, E., and D.S. Goldfarb. 2006. Structure and function of nucleus-vacuole junctions: outer-nuclear-membrane targeting of Nvj1p and a role in tryptophan uptake. *J Cell Sci*. 119:3622-3633.
Langmead, B., and S.L. Salzberg. 2012. Fast gapped-read alignment with Bowtie 2. *Nat Methods*. 9:357-359.
Laroche, T., S.G. Martin, M. Tsai-Pflugfelder, and S.M. Gasser. 2000. The dynamics of yeast telomeres and silencing proteins through the cell cycle. *J Struct Biol*. 129:159-174.
Laurell, E., K. Beck, K. Krupina, G. Theerthagiri, B. Bodenmiller, P. Horvath, R. Aebersold, W. Antonin, and U. Kutay. 2011. Phosphorylation of Nup98 by multiple kinases is crucial for NPC disassembly during mitotic entry. *Cell*. 144:539-550.
Lee, S., W.A. Lim, and K.S. Thorn. 2013. Improved blue, green, and red fluorescent protein tagging vectors for S. cerevisiae. *PLoS One*. 8:e67902.
Lewis, A., R. Felberbaum, and M. Hochstrasser. 2007. A nuclear envelope protein linking nuclear pore basket assembly, SUMO protease regulation, and mRNA surveillance. *J Cell Biol*. 178:813-827.
Lezon, T.R., A. Sali, and I. Bahar. 2009. Global motions of the nuclear pore complex: insights from elastic network models. *PLoS Comput Biol*. 5:e1000496.

Li, C., A. Goryaynov, and W. Yang. 2016. The selective permeability barrier in the nuclear pore complex. *Nucleus*. 7:430-446.

Light, W.H., D.G. Brickner, V.R. Brand, and J.H. Brickner. 2010. Interaction of a DNA zip code with the nuclear pore complex promotes H2A.Z incorporation and INO1 transcriptional memory. *Mol Cell*. 40:112-125.

Lin, D.H., T. Stuwe, S. Schilbach, E.J. Rundlet, T. Perriches, G. Mobbs, Y. Fan, K. Thierbach, F.M. Huber, L.N. Collins, A.M. Davenport, Y.E. Jeon, and A. Hoelz. 2016. Architecture of the symmetric core of the nuclear pore. *Science*. 352:aaf1015.

Lombardi, M.L., and J. Lammerding. 2011. Keeping the LINC: the importance of nucleocytoskeletal coupling in intracellular force transmission and cellular function. *Biochem Soc Trans*. 39:1729-1734.

Longtine, M.S., A. McKenzie, D.J. Demarini, N.G. Shah, A. Wach, A. Brachat, P. Philippsen, and J.R. Pringle. 1998. Additional modules for versatile and economical PCR-based gene deletion and modification in Saccharomyces cerevisiae. *Yeast*. 14:953-961.

Lukas, J., C. Lukas, and J. Bartek. 2011. More than just a focus: The chromatin response to DNA damage and its role in genome integrity maintenance. *Nat Cell Biol*. 13:1161-1169.

Luo, K., M.A. Vega-Palas, and M. Grunstein. 2002. Rap1-Sir4 binding independent of other Sir, yKu, or histone interactions initiates the assembly of telomeric heterochromatin in yeast. *Genes Dev*. 16:1528-1539.

Lusk, C.P., T. Makhnevych, M. Marelli, J.D. Aitchison, and R.W. Wozniak. 2002. Karyopherins in nuclear pore biogenesis: a role for Kap121p in the assembly of Nup53p into nuclear pore complexes. *J Cell Biol*. 159:267-278.

Luthra, R., S.C. Kerr, M.T. Harreman, L.H. Apponi, M.B. Fasken, S. Ramineni, S. Chaurasia, S.R. Valentini, and A.H. Corbett. 2007. Actively transcribed GAL genes can be physically linked to the nuclear pore by the SAGA chromatin modifying complex. *J Biol Chem*. 282:3042-3049.

Ma, J., A. Goryaynov, A. Sarma, and W. Yang. 2012. Self-regulated viscous channel in the nuclear pore complex. *Proc Natl Acad Sci U S A*. 109:7326-7331.

Macara, I.G. 2001. Transport into and out of the nucleus. *Microbiol Mol Biol Rev*. 65:570-594, table of contents.

Maeshima, K., H. Iino, S. Hihara, and N. Imamoto. 2011. Nuclear size, nuclear pore number and cell cycle. *Nucleus*. 2:113-118.

Mahajan, R., C. Delphin, T. Guan, L. Gerace, and F. Melchior. 1997. A small ubiquitin-related polypeptide involved in targeting RanGAP1 to nuclear pore complex protein RanBP2. *Cell*. 88:97-107.

Makhnevych, T., C.P. Lusk, A.M. Anderson, J.D. Aitchison, and R.W. Wozniak. 2003. Cell cycle regulated transport controlled by alterations in the nuclear pore complex. *Cell*. 115:813-823.

Makhnevych, T., C. Ptak, C.P. Lusk, J.D. Aitchison, and R.W. Wozniak. 2007. The role of karyopherins in the regulated sumoylation of septins. *J Cell Biol*. 177:39-49.

Makhnevych, T., Y. Sydorskyy, X. Xin, T. Srikumar, F.J. Vizeacoumar, S.M. Jeram, Z. Li, S. Bahr, B.J. Andrews, C. Boone, and B. Raught. 2009. Global map of SUMO function revealed by protein-protein interaction and genetic networks. *Mol Cell*. 33:124-135.

Makio, T., D.L. Lapetina, and R.W. Wozniak. 2013. Inheritance of yeast nuclear pore complexes requires the Nsp1p subcomplex. *J Cell Biol*. 203:187-196.

Makio, T., L.H. Stanton, C.C. Lin, D.S. Goldfarb, K. Weis, and R.W. Wozniak. 2009. The nucleoporins Nup170p and Nup157p are essential for nuclear pore complex assembly. *J Cell Biol*. 185:459-473.

Marcomini, I., and S.M. Gasser. 2015. Nuclear organization in DNA end processing: Telomeres vs double-strand breaks. *DNA Repair (Amst)*. 32:134-140.

Matunis, M.J., E. Coutavas, and G. Blobel. 1996. A novel ubiquitin-like modification modulates the partitioning of the Ran-GTPase-activating protein RanGAP1 between the cytosol and the nuclear pore complex. *J Cell Biol*. 135:1457-1470.

Maul, G.G. 1977. Nuclear pore complexes. Elimination and reconstruction during mitosis. *J Cell Biol*. 74:492-500.

Meister, P., L.R. Gehlen, E. Varela, V. Kalck, and S.M. Gasser. 2010. Visualizing yeast chromosomes and nuclear architecture. *Methods Enzymol*. 470:535-567.

Melchior, F. 2001. Ran GTPase cycle: oOne mechanism -- two functions. *Curr Biol*. 11:R257-260.

Menon, B.B., N.J. Sarma, S. Pasula, S.J. Deminoff, K.A. Willis, K.E. Barbara, B. Andrews, and G.M. Santangelo. 2005. Reverse recruitment: the Nup84 nuclear pore subcomplex mediates Rap1/Gcr1/Gcr2 transcriptional activation. *Proc Natl Acad Sci U S A*. 102:5749-5754.

Meseroll, R.A., and O. Cohen-Fix. 2016. The Malleable Nature of the Budding Yeast Nuclear Envelope: Flares, Fusion, and Fenestrations. *J Cell Physiol*. 231:2353-2360.

Mi, L., A. Goryaynov, A. Lindquist, M. Rexach, and W. Yang. 2015. Quantifying nucleoporin stoichiometry inside single nuclear pore complexes in vivo. *Sci Rep*. 5:9372.

Miteva, M., K. Keusekotten, K. Hofmann, G.J. Praefcke, and R.J. Dohmen. 2010. Sumoylation as a signal for polyubiquitylation and proteasomal degradation. *Subcell Biochem*. 54:195-214.

Moretti, P., K. Freeman, L. Coodly, and D. Shore. 1994. Evidence that a complex of SIR proteins interacts with the silencer and telomere-binding protein RAP1. *Genes Dev*. 8:2257-2269.

Moretti, P., and D. Shore. 2001. Multiple interactions in Sir protein recruitment by Rap1p at silencers and telomeres in yeast. *Mol Cell Biol*. 21:8082-8094.

Morrison, A.J., and X. Shen. 2009. Chromatin remodelling beyond transcription: the INO80 and SWR1 complexes. *Nat Rev Mol Cell Biol*. 10:373-384.

Moussavi-Baygi, R., Y. Jamali, R. Karimi, and M.R. Mofrad. 2011. Biophysical coarse-grained modeling provides insights into transport through the nuclear pore complex. *Biophys J*. 100:1410-1419.

Mukhopadhyay, D., and M. Dasso. 2007. Modification in reverse: the SUMO proteases. *Trends Biochem Sci*. 32:286-295.

Mullen, J.R., M. Das, and S.J. Brill. 2011. Genetic evidence that polysumoylation bypasses the need for a SUMO-targeted Ub ligase. *Genetics*. 187:73-87.

Müller, S., A. Ledl, and D. Schmidt. 2004. SUMO: a regulator of gene expression and genome integrity. *Oncogene*. 23:1998-2008.

Nagai, S., K. Dubrana, M. Tsai-Pflugfelder, M.B. Davidson, T.M. Roberts, G.W. Brown, E. Varela, F. Hediger, S.M. Gasser, and N.J. Krogan. 2008. Functional targeting of DNA damage to a nuclear pore-associated SUMO-dependent ubiquitin ligase. *Science*. 322:597-602.

Niepel, M., K.R. Molloy, R. Williams, J.C. Farr, A.C. Meinema, N. Vecchietti, I.M. Cristea, B.T. Chait, M.P. Rout, and C. Strambio-De-Castillia. 2013. The nuclear basket proteins Mlp1p and Mlp2p are part of a dynamic interactome including Esc1p and the proteasome. *Mol Biol Cell*. 24:3920-3938.

Niepel, M., C. Strambio-de-Castillia, J. Fasolo, B.T. Chait, and M.P. Rout. 2005. The nuclear pore complex-associated protein, Mlp2p, binds to the yeast spindle pole body and promotes its efficient assembly. *J Cell Biol*. 170:225-235.

Oeffinger, M., and D. Zenklusen. 2012. To the pore and through the pore: a story of mRNA export kinetics. *Biochim Biophys Acta*. 1819:494-506.

Okuma, T., R. Honda, G. Ichikawa, N. Tsumagari, and H. Yasuda. 1999. In vitro SUMO-1 modification requires two enzymatic steps, E1 and E2. *Biochem Biophys Res Commun*. 254:693-698.

Olins, D.E., and A.L. Olins. 2003. Chromatin history: our view from the bridge. *Nat Rev Mol Cell Biol*. 4:809-814.

Onischenko, E., L.H. Stanton, A.S. Madrid, T. Kieselbach, and K. Weis. 2009. Role of the Ndc1 interaction network in yeast nuclear pore complex assembly and maintenance. *J Cell Biol*. 185:475-491.

Ori, A., N. Banterle, M. Iskar, A. Andrés-Pons, C. Escher, H. Khanh Bui, L. Sparks, V. Solis-Mezarino, O. Rinner, P. Bork, E.A. Lemke, and M. Beck. 2013. Cell type-specific nuclear pores: a case in point for context-dependent stoichiometry of molecular machines. *Mol Syst Biol*. 9:648.

Osterhage, J.L., and K.L. Friedman. 2009. Chromosome end maintenance by telomerase. *J Biol Chem*. 284:16061-16065.

Palancade, B., and V. Doye. 2008. Sumoylating and desumoylating enzymes at nuclear pores: underpinning their unexpected duties? *Trends Cell Biol*. 18:174-183.

Palancade, B., X. Liu, M. Garcia-Rubio, A. Aguilera, X. Zhao, and V. Doye. 2007a. Nucleoporins prevent DNA damage accumulation by modulating Ulp1-dependent sumoylation processes. *Mol Biol Cell*. 18:2912-2923.

Palancade, B., X. Liu, M. Garcia-Rubio, A. Aguilera, X. Zhao, and V. Doye. 2007b. Nucleoporins prevent DNA damage accumulation by modulating Ulp1-dependent sumoylation processes. *Mol Biol Cell*. 18:2912-2923.

Palladino, F., T. Laroche, E. Gilson, A. Axelrod, L. Pillus, and S.M. Gasser. 1993. SIR3 and SIR4 proteins are required for the positioning and integrity of yeast telomeres. *Cell*. 75:543-555.

Panse, V.G., D. Kressler, A. Pauli, E. Petfalski, M. Gnädig, D. Tollervey, and E. Hurt. 2006. Formation and nuclear export of preribosomes are functionally linked to the small-ubiquitin-related modifier pathway. *Traffic*. 7:1311-1321.

Panté, N., and M. Kann. 2002. Nuclear pore complex is able to transport macromolecules with diameters of about 39 nm. *Mol Biol Cell*. 13:425-434.

Passarge, E. 1979. Emil Heitz and the concept of heterochromatin: longitudinal chromosome differentiation was recognized fifty years ago. *Am J Hum Genet*. 31:106-115.

Pasupala, N., S. Easwaran, A. Hannan, D. Shore, and K. Mishra. 2012. The SUMO E3 ligase Siz2 exerts a locus-dependent effect on gene silencing in Saccharomyces cerevisiae. *Eukaryot Cell*. 11:452-462.

Patel, S.S., B.J. Belmont, J.M. Sante, and M.F. Rexach. 2007. Natively unfolded nucleoporins gate protein diffusion across the nuclear pore complex. *Cell*. 129:83-96.

Pemberton, L.F., J.S. Rosenblum, and G. Blobel. 1999. Nuclear import of the TATA-binding protein: mediation by the karyopherin Kap114p and a possible mechanism for intranuclear targeting. *J Cell Biol*. 145:1407-1417.

Powers, M.A., and D.J. Forbes. 2012. Nuclear transport: beginning to gel? *Curr Biol*. 22:R1006-1009.

Praefcke, G.J., K. Hofmann, and R.J. Dohmen. 2011. SUMO playing tag with ubiquitin. *Trends Biochem Sci*.

Ptak, C., J.D. Aitchison, and R.W. Wozniak. 2014. The multifunctional nuclear pore complex: a platform for controlling gene expression. *Curr Opin Cell Biol*. 28:46-53.

Ptak, C., and R.W. Wozniak. 2016. Nucleoporins and chromatin metabolism. *Curr Opin Cell Biol*. 40:153-160.

Ramírez, F., D.P. Ryan, B. Grüning, V. Bhardwaj, F. Kilpert, A.S. Richter, S. Heyne, F. Dündar, and T. Manke. 2016. deepTools2: a next generation web server for deep-sequencing data analysis. *Nucleic Acids Res*. 44:W160-165.

Reindle, A., I. Belichenko, G.R. Bylebyl, X.L. Chen, N. Gandhi, and E.S. Johnson. 2006. Multiple domains in Siz SUMO ligases contribute to substrate selectivity. *J Cell Sci*. 119:4749-4757.

Ribbeck, K., and D. Görlich. 2001. Kinetic analysis of translocation through nuclear pore complexes. *EMBO J*. 20:1320-1330.

Rice, C., and E. Skordalakes. 2016. Structure and function of the telomeric CST complex. *Comput Struct Biotechnol J*. 14:161-167.

Rine, J., and I. Herskowitz. 1987. Four genes responsible for a position effect on expression from HML and HMR in Saccharomyces cerevisiae. *Genetics*. 116:9-22.

Rodríguez-Navarro, S., and E. Hurt. 2011. Linking gene regulation to mRNA production and export. *Curr Opin Cell Biol*. 23:302-309.

Rohner, S., S.M. Gasser, and P. Meister. 2008. Modules for cloning-free chromatin tagging in Saccharomyces cerevisae. *Yeast*. 25:235-239.

Rossetto, D., N. Avvakumov, and J. Côté. 2012. Histone phosphorylation: a chromatin modification involved in diverse nuclear events. *Epigenetics*. 7:1098-1108.

Rothbart, S.B., and B.D. Strahl. 2014. Interpreting the language of histone and DNA modifications. *Biochim Biophys Acta*. 1839:627-643.

Rout, M.P., J.D. Aitchison, M.O. Magnasco, and B.T. Chait. 2003. Virtual gating and nuclear transport: the hole picture. *Trends Cell Biol*. 13:622-628.

Rout, M.P., J.D. Aitchison, A. Suprapto, K. Hjertaas, Y. Zhao, and B.T. Chait. 2000. The yeast nuclear pore complex: composition, architecture, and transport mechanism. *J Cell Biol*. 148:635-651.

Rudner, A.D., B.E. Hall, T. Ellenberger, and D. Moazed. 2005. A nonhistone protein-protein interaction required for assembly of the SIR complex and silent chromatin. *Mol Cell Biol*. 25:4514-4528.

Ryan, K.J., Y. Zhou, and S.R. Wente. 2007. The karyopherin Kap95 regulates nuclear pore complex assembly into intact nuclear envelopes in vivo. *Mol Biol Cell*. 18:886-898.

Sampathkumar, P., S.J. Kim, P. Upla, W.J. Rice, J. Phillips, B.L. Timney, U. Pieper, J.B. Bonanno, J. Fernandez-Martinez, Z. Hakhverdyan, N.E. Ketaren, T. Matsui, T.M. Weiss, D.L. Stokes, J.M. Sauder, S.K. Burley, A. Sali, M.P. Rout, and S.C. Almo. 2013. Structure, dynamics, evolution, and function of a major scaffold component in the nuclear pore complex. *Structure*. 21:560-571.

Schober, H., H. Ferreira, V. Kalck, L.R. Gehlen, and S.M. Gasser. 2009. Yeast telomerase and the SUN domain protein Mps3 anchor telomeres and repress subtelomeric recombination. *Genes Dev*. 23:928-938.

Shampay, J., and E.H. Blackburn. 1988. Generation of telomere-length heterogeneity in Saccharomyces cerevisiae. *Proc Natl Acad Sci U S A*. 85:534-538.

Sharma, P., S. Yamada, M. Lualdi, M. Dasso, and M.R. Kuehn. 2013. Senp1 is essential for desumoylating Sumo1-modified proteins but dispensable for Sumo2 and Sumo3 deconjugation in the mouse embryo. *Cell Rep*. 3:1640-1650.

Sikorski, R.S., and P. Hieter. 1989. A system of shuttle vectors and yeast host strains designed for efficient manipulation of DNA in Saccharomyces cerevisiae. *Genetics*. 122:19-27.

Song, J., L.K. Durrin, T.A. Wilkinson, T.G. Krontiris, and Y. Chen. 2004. Identification of a SUMO-binding motif that recognizes SUMO-modified proteins. *Proc Natl Acad Sci U S A*. 101:14373-14378.

Spellman, P.T., G. Sherlock, M.Q. Zhang, V.R. Iyer, K. Anders, M.B. Eisen, P.O. Brown, D. Botstein, and B. Futcher. 1998. Comprehensive identification of cell cycle-regulated genes of the yeast Saccharomyces cerevisiae by microarray hybridization. *Mol Biol Cell*. 9:3273-3297.

Stade, K., F. Vogel, I. Schwienhorst, B. Meusser, C. Volkwein, B. Nentwig, R.J. Dohmen, and T. Sommer. 2002. A lack of SUMO conjugation affects cNLS-dependent nuclear protein import in yeast. *J Biol Chem*. 277:49554-49561.

Stewart, M. 2007. Molecular mechanism of the nuclear protein import cycle. *Nat Rev Mol Cell Biol*. 8:195-208.

Stoffler, D., B. Fahrenkrog, and U. Aebi. 1999. The nuclear pore complex: from molecular architecture to functional dynamics. *Curr Opin Cell Biol*. 11:391-401.

Strahl-Bolsinger, S., A. Hecht, K. Luo, and M. Grunstein. 1997. SIR2 and SIR4 interactions differ in core and extended telomeric heterochromatin in yeast. *Genes Dev*. 11:83-93.

Strambio-de-Castillia, C., G. Blobel, and M.P. Rout. 1999. Proteins connecting the nuclear pore complex with the nuclear interior. *J Cell Biol*. 144:839-855.

Strambio-De-Castillia, C., M. Niepel, and M.P. Rout. 2010. The nuclear pore complex: bridging nuclear transport and gene regulation. *Nat Rev Mol Cell Biol*. 11:490-501.

Strambio-de-Castillia, C., and M.P. Rout. 2002. The structure and composition of the yeast NPC. *Results Probl Cell Differ*. 35:1-23.

Strawn, L.A., T. Shen, N. Shulga, D.S. Goldfarb, and S.R. Wente. 2004. Minimal nuclear pore complexes define FG repeat domains essential for transport. *Nat Cell Biol*. 6:197-206.

Ström, A.C., and K. Weis. 2001. Importin-beta-like nuclear transport receptors. *Genome Biol*. 2:REVIEWS3008.

Stuwe, T., C.J. Bley, K. Thierbach, S. Petrovic, S. Schilbach, D.J. Mayo, T. Perriches, E.J. Rundlet, Y.E. Jeon, L.N. Collins, F.M. Huber, D.H. Lin, M. Paduch, A. Koide, V. Lu, J. Fischer, E. Hurt, S. Koide, A.A. Kossiakoff, and A. Hoelz. 2015. Architecture of the fungal nuclear pore inner ring complex. *Science*. 350:56-64.

Sun, J.Q., A. Hatanaka, and M. Oki. 2011. Boundaries of transcriptionally silent chromatin in Saccharomyces cerevisiae. *Genes Genet Syst*. 86:73-81.

Suntharalingam, M., and S.R. Wente. 2003. Peering through the pore: nuclear pore complex structure, assembly, and function. *Dev Cell*. 4:775-789.

Sydorskyy, Y., D.J. Dilworth, B. Halloran, E.C. Yi, T. Makhnevych, R.W. Wozniak, and J.D. Aitchison. 2005. Nop53p is a novel nucleolar 60S ribosomal subunit biogenesis protein. *Biochem J*. 388:819-826.

Taddei, A., and S.M. Gasser. 2012. Structure and function in the budding yeast nucleus. *Genetics*. 192:107-129.

Taddei, A., F. Hediger, F.R. Neumann, C. Bauer, and S.M. Gasser. 2004a. Separation of silencing from perinuclear anchoring functions in yeast Ku80, Sir4 and Esc1 proteins. *EMBO J*. 23:1301-1312.

Taddei, A., F. Hediger, F.R. Neumann, C. Bauer, and S.M. Gasser. 2004b. Separation of silencing from perinuclear anchoring functions in yeast Ku80, Sir4 and Esc1 proteins. *EMBO J*. 23:1301-1312.

Taddei, A., H. Schober, and S.M. Gasser. 2010a. The budding yeast nucleus. *Cold Spring Harb Perspect Biol*. 2:a000612.

Taddei, A., H. Schober, and S.M. Gasser. 2010b. The budding yeast nucleus. *Cold Spring Harb Perspect Biol*. 2:a000612.

Takahashi, Y., T. Kahyo, A. Toh-E, H. Yasuda, and Y. Kikuchi. 2001. Yeast Ull1/Siz1 is a novel SUMO1/Smt3 ligase for septin components and functions as an adaptor between conjugating enzyme and substrates. *J Biol Chem*. 276:48973-48977.

Takahashi, Y., A. Toh-E, and Y. Kikuchi. 2003. Comparative analysis of yeast PIAS-type SUMO ligases in vivo and in vitro. *J Biochem*. 133:415-422.

Tatham, M.H., M.S. Rodriguez, D.P. Xirodimas, and R.T. Hay. 2009. Detection of protein SUMOylation in vivo. *Nat Protoc*. 4:1363-1371.

Tetenbaum-Novatt, J., L.E. Hough, R. Mironska, A.S. McKenney, and M.P. Rout. 2012. Nucleocytoplasmic transport: a role for nonspecific competition in karyopherin-nucleoporin interactions. *Mol Cell Proteomics*. 11:31-46.

Texari, L., and F. Stutz. 2015. Sumoylation and transcription regulation at nuclear pores. *Chromosoma*. 124:45-56.

Theerthagiri, G., N. Eisenhardt, H. Schwarz, and W. Antonin. 2010. The nucleoporin Nup188 controls passage of membrane proteins across the nuclear pore complex. *J Cell Biol*. 189:1129-1142.

Therizols, P., C. Fairhead, G.G. Cabal, A. Genovesio, J.C. Olivo-Marin, B. Dujon, and E. Fabre. 2006. Telomere tethering at the nuclear periphery is essential for efficient DNA double strand break repair in subtelomeric region. *J Cell Biol*. 172:189-199.

Toyama, B.H., and M.W. Hetzer. 2013. Protein homeostasis: live long, won't prosper. *Nat Rev Mol Cell Biol*. 14:55-61.

Van de Vosse, D.W., Y. Wan, D.L. Lapetina, W.M. Chen, J.H. Chiang, J.D. Aitchison, and R.W. Wozniak. 2013. A role for the nucleoporin Nup170p in chromatin structure and gene silencing. *Cell*. 152:969-983.

Van de Vosse, D.W., Y. Wan, R.W. Wozniak, and J.D. Aitchison. 2011. Role of the nuclear envelope in genome organization and gene expression. *Wiley Interdiscip Rev Syst Biol Med*. 3:147-166.

Verdaasdonk, J.S., and K. Bloom. 2011. Centromeres: unique chromatin structures that drive chromosome segregation. *Nat Rev Mol Cell Biol*. 12:320-332.

Walther, T.C., A. Alves, H. Pickersgill, I. Loïodice, M. Hetzer, V. Galy, B.B. Hülsmann, T. Köcher, M. Wilm, T. Allen, I.W. Mattaj, and V. Doye. 2003. The conserved Nup107-160 complex is critical for nuclear pore complex assembly. *Cell*. 113:195-206.

Walther, T.C., H.S. Pickersgill, V.C. Cordes, M.W. Goldberg, T.D. Allen, I.W. Mattaj, and M. Fornerod. 2002. The cytoplasmic filaments of the nuclear pore complex are dispensable for selective nuclear protein import. *J Cell Biol*. 158:63-77.

Wan, Y., X. Zuo, Y. Zhuo, M. Zhu, S.A. Danziger, and Z. Zhou. 2013. The functional role of SUMO E3 ligase Mms21p in the maintenance of subtelomeric silencing in budding yeast. *Biochem Biophys Res Commun*. 438:746-752.

Wang, Y., and M. Dasso. 2009. SUMOylation and deSUMOylation at a glance. *J Cell Sci*. 122:4249-4252.

WATSON, M.L. 1959. Further observations on the nuclear envelope of the animal cell. *J Biophys Biochem Cytol*. 6:147-156.

Weis, K. 2007. The nuclear pore complex: oily spaghetti or gummy bear? *Cell*. 130:405-407.

Wellinger, R.J., and V.A. Zakian. 2012. Everything you ever wanted to know about Saccharomyces cerevisiae telomeres: beginning to end. *Genetics*. 191:1073-1105.

Wente, S.R. 2000. Gatekeepers of the nucleus. *Science*. 288:1374-1377.

Wente, S.R., and M.P. Rout. 2010. The nuclear pore complex and nuclear transport. *Cold Spring Harb Perspect Biol*. 2:a000562.

Wilkinson, K.A., and J.M. Henley. 2010. Mechanisms, regulation and consequences of protein SUMOylation. *Biochem J*. 428:133-145.

Wilson, V.G., and P.R. Heaton. 2008. Ubiquitin proteolytic system: focus on SUMO. *Expert Rev Proteomics*. 5:121-135.

Winey, M., D. Yarar, T.H. Giddings, and D.N. Mastronarde. 1997. Nuclear pore complex number and distribution throughout the

Saccharomyces cerevisiae cell cycle by three-dimensional reconstruction from electron micrographs of nuclear envelopes. *Mol Biol Cell*. 8:2119-2132.

Wohlschlegel, J.A., E.S. Johnson, S.I. Reed, and J.R. Yates. 2004. Global analysis of protein sumoylation in Saccharomyces cerevisiae. *J Biol Chem*. 279:45662-45668.

Woodcock, C.L., and R.P. Ghosh. 2010. Chromatin higher-order structure and dynamics. *Cold Spring Harb Perspect Biol*. 2:a000596.

Wozniak, R.W., G. Blobel, and M.P. Rout. 1994. POM152 is an integral protein of the pore membrane domain of the yeast nuclear envelope. *J Cell Biol*. 125:31-42.

Wu, A.C., and S.A. Rifkin. 2015. Aro: a machine learning approach to identifying single molecules and estimating classification error in fluorescence microscopy images. *BMC Bioinformatics*. 16:102.

Wälde, S., and R.H. Kehlenbach. 2010. The Part and the Whole: functions of nucleoporins in nucleocytoplasmic transport. *Trends Cell Biol*. 20:461-469.

Yang, W. 2011. 'Natively unfolded' nucleoporins in nucleocytoplasmic transport: clustered or evenly distributed? *Nucleus*. 2:10-16.

Yavuz, A.S., and O.U. Sezerman. 2014. Predicting sumoylation sites using support vector machines based on various sequence features, conformational flexibility and disorder. *BMC Genomics*. 15 Suppl 9:S18.

Zeitler, B., and K. Weis. 2004. The FG-repeat asymmetry of the nuclear pore complex is dispensable for bulk nucleocytoplasmic transport in vivo. *J Cell Biol*. 167:583-590.

Zhao, X., and G. Blobel. 2005. A SUMO ligase is part of a nuclear multiprotein complex that affects DNA repair and chromosomal organization. *Proc Natl Acad Sci U S A*. 102:4777-4782.

Zhao, X., C.Y. Wu, and G. Blobel. 2004. Mlp-dependent anchorage and stabilization of a desumoylating enzyme is required to prevent clonal lethality. *J Cell Biol*. 167:605-611.

Zimmer, C., and E. Fabre. 2011. Principles of chromosomal organization: lessons from yeast. *J Cell Biol*. 192:723-733.